Electrodeposition of aluminium in different air and water stable ionic liquids

Dissertation

Zur Erlangung des Grades eines
Doktors der Naturwissenschaften

vorgelegt von M.Sc.

Essam Mohamed Moustafa

aus El-Menoufia / Ägypten

genehmigt von der
Fakultät für Natur- und Materialwissenschaften
der Technischen Universität Clausthal

Tag der mündlichen Prüfung
26 Juni 2007

Moustafa, Essam Mohamed:
Electrodeposition of aluminium in different air and water
stable ionic liquids /
Essam Mohamed Moustafa.- Clausthal-Zellerfeld : Papierflieger 2007
Zugl.: Clausthal, Tech. Univ., Dissertation 2007

ISBN 3-89720-909-8

Bibliografische Information Der Deutschen Bibliothek
Die Deutsche Bibliothek verzeichnet diese Publikation in der Deutschen Nationalbibliografie; detaillierte bibliografische Daten sind im Internet über http://dnb.ddb.de abrufbar.

Diese Arbeit wurde am Institut für Metallurgie
der Technischen Universität Clausthal angefertigt.

Dekan:	Prof. Dr. rer. nat. W. Schade
Berichterstatter:	Prof. Dr. rer. nat. F. Endres
Berichterstatter:	Prof. Dr. rer. nat. M. Antonietti

D 104

1. Auflage, 2007

ISBN 3-89720-909-8

List of abbreviations of cations and anions from which ionic liquids can be formed.

Name	Abbreviation
1-butyl-1-methylpyrrolidinium	[BMP]
1-ethyl-3-methylimidazolium	[EMIm]
1-butyl-3-methylimidazolium	[BMIm]
Trihexyl-tetradecyl phosphonium	$[P_{14,6,6,6}]$
1-ethyl-3-methylimidazolium chloride	[EMIm]Cl
1-butyl-3-methylimidazolium chloride	[BMIm]Cl
N-butylpyridinium chloride	N-BPC
bis(trifluoromethylsulfonyl) amide	Tf_2N

ABSTRACT

The results presented in this thesis show, for the first time, a comparative study on the electrodeposition of aluminium in three air and water stable ionic liquids namely, 1-butyl-1-methyl-pyrrolidinium bis (trifluoromethylsulfonyl) amide [BMP] Tf_2N, 1-ethyl-3-methylimidazolium bis (trifluoromethylsulfonyl) amide [EMIm] Tf_2N and trihexyl-tetradecyl phosphonium bis (trifluoromethylsulfonyl) amide [$P_{14,6,6,6}$] Tf_2N. The two ionic liquids [BMP] Tf_2N and [EMIm] Tf_2N show biphasic behaviour in the concentrations of $AlCl_3$ range from 1.6 to 2.5 M and 2.5 to 5.5 M, respectively. The biphasic mixtures become monophasic at temperatures ≥ 80 ^oC. It was found that nanocrystalline aluminium can be electrodeposited in the ionic liquid [BMP] Tf_2N saturated with $AlCl_3$. The deposits obtained are generally uniform, dense, shining and adherent with very fine crystallites of sizes in the nanometer regime. However, coarse cubic-shaped aluminium particles of sizes in the micrometer range were obtained in the ionic liquid [EMIm] Tf_2N. The particle size significantly increases as the temperature rises. A very thin, mirror-like aluminium film containing very fine crystallites of sizes about 20 nm was obtained in the ionic liquid [$P_{14,6,6,6}$] Tf_2N at room temperature. At 150 ^oC, the average grain size was found to be 35 nm. The electrodeposition of Al on flame annealed Au (111) substrates in three mentioned air and water stable ionic liquids has been investigated by in situ scanning tunneling microscopy (STM) and cyclic voltammetry. The cyclic voltammogram of aluminium deposition and stripping on Au (111) in the upper phase of the biphasic mixture of $AlCl_3$ / [EMIm] Tf_2N at room temperature (25 ^oC) shows that the electrodeposition process is completely reversible as also evidenced by in situ STM studies. Additionally, a cathodic peak at an electrode potential of about 0.55 V *vs.* Al/Al (III) is correlated to the aluminium underpotential deposition (UPD) process that was evidenced by in situ STM results. A surface alloying of Al with Au at the early stage of deposition occurs. It has been found that the Au (111) surface is subject to a restructuring / reconstruction in the upper phase of the biphasic mixture of $AlCl_3$ / [BMP] Tf_2N at room temperature (25 ^oC) and that the deposition is not fully reversible. Furthermore the underpotential deposition (UPD) of Al is not as clear as in [EMIm] Tf_2N ionic liquid. At –2.0 V *vs.* Al/Al (III), a bulk aluminium deposition sets in. Also, the initial stages of aluminium deposition onto Au (111) substrate in the mixture of $AlCl_3$ / [$P_{14,6,6,6}$] Tf_2N ionic liquid at 25 ^oC was investigated by in situ

scanning tunnelling microscopy (STM). Au (111) surface is also subject to restructuring in the mixture of $AlCl_3$ / $[P_{14,6,6,6}]$ Tf_2N at room temperature (25 °C).

Acknowledgement

I would like to express my sincere thanks to Prof. Dr. F. Endres, the main supervisor for this work. I am greatly indebted to him for giving me the opportunity to perform my Ph.D. research under his supervision in his group on a highly interesting topic. Furthermore, I thank him for fruitful discussions and for offering me all research facilities to carry out this work.

Also, I wish to express my deep thanks to Ass. Prof. Dr. S. Zein El Abedin as a co-supervisor for his continued guiding, kind help, very interesting discussions and for his encouragement to pursue my investigations on both electrochemistry and electrochemical scanning tunnelling microscopy (EC-STM).

Many thanks to all our colleagues in the group for their kind help and warm feelings. Really, we have worked together as a family in an ideal working atmosphere.

I would like to thank also Deutsche Forschungsgemeinschaft (DFG) for financial support of this work.

Of course, I wish to thank Prof. Dr. M. Antonietti as a co-referee and for his participating in the final examination committee.

Thanks also to the Egyptian Ministry of High Education and National Research Centre (NRC) for their interest and great help.

Finally, I am very grateful to my parents for their love, kindness, support and great assistances, I hope that they will be proud of me. Also, I would like to thank my wife for her assistance and taking care of our children Dina and Malak.

Clausthal, June 2007

Essam Mohamed Moustafa

CONTENTS

1. Introduction

1.1 Ionic liquids

1.1.1 Definition

Generally, the term “ionic liquids” denotes liquids composed entirely of ions. As a consequence, ionic liquids are different to traditional solvents (e.g., water, ethanol, acetone, benzene etc.), which can be described as molecular liquids. Ionic liquids are usually defined as ionic melts with melting points below 100 °C.

1.1.2 Short history

The early history of ionic liquids began in 1914 when Walden succeeded in synthesising the first low temperature molten salt, ethylammonium nitrate, with a melting point of 12 ^{o}C **[1]**. In 1951, Hurley and Wier **[2]** developed low melting salts with chloroaluminate ions for low-temperature electroplating of aluminum. Popular examples of ionic liquids include the chloroaluminates, which are prepared by combining anhydrous aluminum chloride with a suitable organic chloride salt such as 1-ethyl-3-methylimidazolium chloride ([EMIm]Cl). This kind of ionic liquids, which is based on $AlCl_3$, can be considered as the first generation of ionic liquids. During the 1970s and 1980s, these liquids were studied mainly for electrochemical applications **[3-7]**. In the mid 1980s, low melting point ionic liquids were proposed as solvents for organic synthesis by Fry and Pienta **[8]** and Boon et al. **[9]**. Unfortunately these ionic liquids can be handled only under inert gas atmosphere due to the hygroscopic nature of $AlCl_3$. For this reason, the synthesis of air and water stable ionic liquids, which are considered as the second generation of ionic liquids, attracted much interest for their use in various fields. The first air and water stable ionic liquids were reported by Wilkes and Zaworotko in 1992 **[10]**. These ionic liquids consist of 1-ethyl-3-methylimidazolium as a cation and either tetrafluoroborate (BF_4^-) or hexafluorophosphate (PF_6^-) as anions. The main advantage is that they can be made and handled under air. Later it was found that exposure to moisture for a long time can cause some changes in their physical and chemical properties as in the presence of water (especially at elevated temperatures) a decomposition of the anions liberating HF occurs **[11]**. Therefore, ionic liquids based on more hydrophobic and more stable anions such as trifluoromethylsulfonate (CF_3SO_3), bis(trifluoromethylsulfonyl) amide [$(CF_3SO_2)_2N^-$] and tris(trifluoromethylsulfonyl) methide [$(CF_3SO_2)_3C^-$] and many

others have been developed **[12–14]**. These rather novel ionic liquids represent an interesting class of solvents due to their extraordinary physical properties **[15]**. These ionic liquids have attracted the interest of many researchers as they have high chemical, thermal and electrochemical stability. The molecular structures of some cations and anions from which ionic liquids can be formed are illustrated in the following table (1.1)

Cations	**Discrete anions**
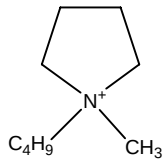 [BMP]	Cl^- (Chloride)
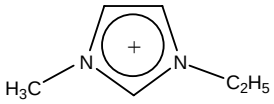 [EMIm]	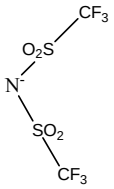 $[Tf_2N]$
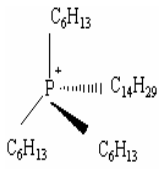 $[P_{14,6,6,6}]$	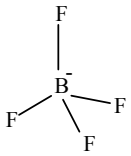 Tertrafluoroborate (BF_4^-)
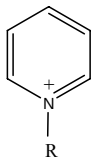 N-Alkyl pyridinium	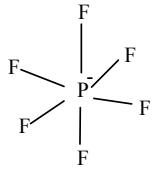 Hexafluorophosphate (PF_6^-)

Table 1.1. A selection of cations and anions used to make ionic liquids.

1.1.3 Importance

During the last few years, the interest in ionic liquids has rosen considerably. Currently, the number of RTILs synthesized exceeds 500 and the research in this area is expanding rapidly. Endres and Zein El Abedin **[16]** reviewed that the average number of publications in the last decade is about 40 papers per year while in 2004 about 1000 papers and in 2006 about 2400 papers were published as shown in figure (1). This reflects the increased interest in ionic liquids in general. Only, theoretically there is a limit in the number of salts with low melting points. Earle and Seddon **[17]** have estimated this number to be of the order of 10^{12}-10^{18}.

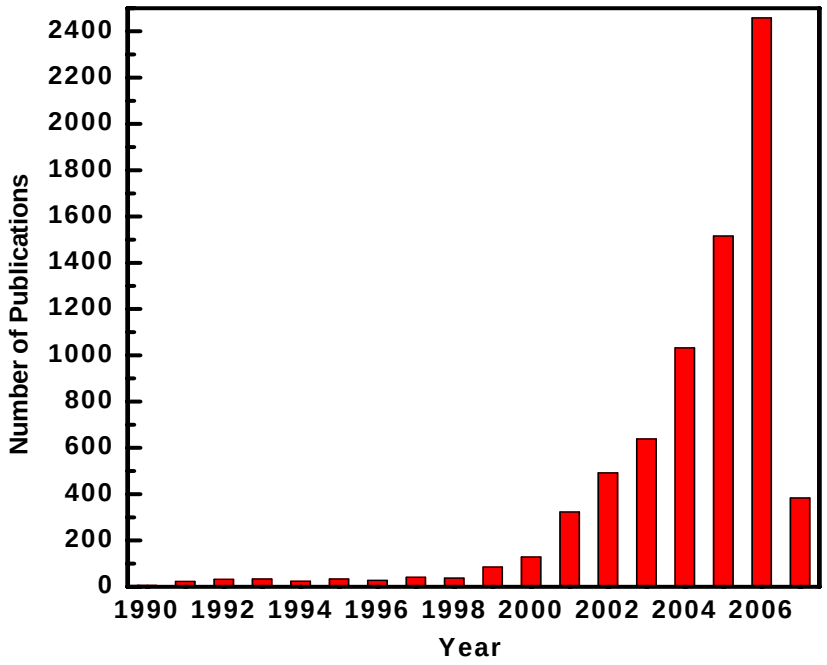

Fig. 1.1. *Publications containing the phrase ''ionic liquid or ionic liquids'' in the title; abstract and key words; determined by ISI web of science; as a function of time.*

1.2 Properties of ionic liquids

As solvents, these liquids exhibit many attractive properties, including low melting points, insignificant vapor pressures at or near room temperature in many cases, good chemical and thermal stabilities, good conductivities, and large electrochemical potential windows. Ionic liquids are currently employed in a wide range of fields in chemistry. Ionic liquids have attracted much interest for their use as non-aqueous electrolytes in electrochemical applications because of their conductivity range (1.0 mS/cm to 10.0 mS/cm) **[18]** as well as their wide electrochemical windows

(> 4 V), which is a measure for their electrochemical stability against reduction and oxidation process.

The electrochemical window is sensitive to impurities and depends on the type of the substrate, too. Together with other interesting properties they appear to be ideal electrolytes for many interesting applications as already shown in a large number of publications **[19]**.

In the following, the properties of ionic liquids are briefly discussed.

1.2.1 Low melting points

Conventional molten salts exhibit a high melting point (i.e., 801 ºC for sodium chloride and 614 ºC for lithium chloride) [18], which greatly limits their use as solvents in most applications. Ionic liquids, however, remain liquids at or below room temperature. These low melting points are a result of the chemical composition of ionic liquids, which contain large asymmetric organic cations compared to their inorganic counterparts of molten salts. In some cases, even the anions are relatively large and play a role in lowering the melting point [20, 21].

1.2.2 Viscosity

Generally, ionic liquids are more viscous than common molecular solvents and their viscosities range from 10 mPa s to about 500 mPa s at room temperature. The viscosity of an ionic liquid plays an important role in electrochemical studies due to its strong effect on the rate of mass transport within solution. The anion has a large effect on the viscosity of an ionic liquid, in particular through their relative basicity and ability to participate in hydrogen bonding. For example, the perfluorinated BF_4^- and PF_6^- anions form much more viscous ionic liquids (containing strong H….F interactions) **[22]** than those formed by the weakly basic Tf_2N^- anion, in which the negative charge is extensively delocalised over the two sulfoxide groups **[12]**. Altering the organic cation causes a more subtle change in viscosity, and this is attributed to the influence of van der Waals interactions; viscosity generally increases with increasing cationic size (for example, by increasing alkyl chain length) **[12]**. The viscosities of room temperature ionic liquids are extremely temperature dependent and can be described both by Arrhenius and by Vogel-Tammann-Fulcher equations:

$$\eta = A\, e^{Ea/RT}$$

where Ea is the activation energy for viscous flow, although slight deviations from this behaviour at temperatures close to the freezing point have been reported, attributed to the onset of ion association and aggregation **[12,23]**.

1.2.3 Conductivity

As with any solvent employed in an electrochemical process, the conductivity of an ionic liquid is of vital importance. Being composed entirely of ions, room temperature ionic liquids possess an abundance of charge carriers and so, based on this consideration alone, a large conductivity might be predicted. Overall, however, the conductivity of any solution depends on both the number of charge carriers and their mobility. For ionic liquids, the ion mobility is usually low and as a consequence ionic liquids at room temperature have usually conductivities below those of concentrated aqueous solutions. For a given anion with a range of cations, conductivity generally decreases in the order 1-alkyl-3-methylimidazolium> N,N dialkylpyrrolidinium>tetra-alkylammonium, and this has been identified with an decrease in planarity of the cationic core; the flatness of the imidazolium ring seems to give a higher conductivity than the tetrahedral arrangement of alkyl groups displayed by the ammonium salts, with the pyrrolidinium- based room temperature ionic liquids adopting an intermediate geometry and conductivity **[14]**. The variation of ionic liquid conductivity with temperature typically gives a distinctly curved Arrhenius plot at low temperatures **[23,24]** and the empirical equation developed for liquids that form glass phases is:

$$k = AT^{-1/2}\exp\left[-B(T-T_0)\right]$$

where, k is conductivity, A and B are empirically determined constants and T_0 is the ideal glass temperature (at which the conductivity drops to zero). At temperatures above $2T_0$, the more simple Arrhenius equation is sufficient to characterise the observed temperature dependence.

1.2.4 Electrochemical Window

Any solvent is only suitable for electrochemical experiments if the species dissolved are more easily oxidised or reduced than the solvent itself. In room temperature ionic liquids, it is in many cases found in practice that the constituent anions are oxidised at sufficiently large potentials, and that at sufficiently low ones, the organic cations undergo reduction. The potentials at which these bulk processes

are initiated determine the accessible electrochemical window for each liquid. The electrodeposition of elements and compounds in water is limited by its low electrochemical window of only about 1.2 V from thermodynamic considerations. In contrast, ionic liquids have significantly larger electrochemical windows, e.g., 4.15 V for [BMIm] PF_6 at a platinum electrode, **[25]** 4.10 V for [BMIm] BF_4 **[25]** and 5.5 V for [BMP] Tf_2N at a glassy carbon electrode **[14]**. The wide electrochemical windows of ionic liquids have opened the door to electrodeposit metals and semiconductors at room temperature, which were formerly obtained only from high temperature molten salts. For example, Al, Mg, Ti, Si, Ge, and rare earth elements can be obtained from room temperature ionic liquids at least in ultra thin layers. A detailed comparison of the various potential windows reported in the literature is not straightforward for some reasons. First, if the purity of an ionic liquid is uncertain, the presence of electroactive impurities can cause an apparent narrowing of the true potential window; second, the potential of solvent breakdown may vary slightly on different electrode surfaces; third, data are often reported against different reference and quasi-reference systems which are not always stable in the course of the experiments. Most voltammetric measurements carried out in ionic liquids have employed quasi-reference electrodes, often silver or platinum wires, **[26-32]** quite simply as there are not yet well defined reference electrodes available. Bond et al. have investigated the use of the metallocene derivatives as voltammetric reference standards for ionic liquids **[26]**. When tested in [BMIm] PF_6, a reversible, one-electron reduction process was observed for cobaltocene with a potential independent of electrode composition, concentration and scan rate. Ferrocene was found to be poorly soluble in this medium, but may function as a less expensive alternative for other ionic liquids. Nevertheless ferrocene can be employed as an internal standard for many ionic liquids.

1.2.5 Thermal stability

Ionic liquids can - on a short time scale- be thermally stable up to temperatures of 450 °C. The thermal stability of ionic liquids is limited by the strength of their heteroatom–carbon and their heteroatom– hydrogen bonds, respectively **[33]**. Wilkes et al. **[34]** reported that the ionic liquids 1-ethyl-3-methyl-imidazolium tetrafluoroborate, 1-butyl-3-methyl-imdazolium tetrafluoroborate and 1,2-dimethyl-3-propyl imidazolium bis (trifluoromethylsulfonyl) amide are stable up to temperatures of 445, 423 and 457 °C, respectively, at least on a short time scale. Endres et al. **[16]**

reviewed that such high temperatures are only tolerated by most liquids for a short time. Long time exposure to such high temperatures inevitably leads to decomposition. Most of the ionic liquids have extremely low vapour pressures, which allows to remove water by simple heating under vacuum. Water contents below 1 ppm are quite easy to achieve with most of the liquids. The thermal stability of ionic liquids allows to electrodeposit Ta, Nb, V, Se and presumably many other ones where kinetic barriers have to be overcomed at elevated temperatures.

1.2.6 Double-layer capacitance

Room temperature ionic liquids can be used for electrochemical capacitor applications. Thus, it is important to measure the double-layer capacitance (C_{dl}) and its variation with potential from which the structure of the interfacial region between an electrode and the adjacent layer of ionic liquid can be determined. There are only few reports that deal with such studies **[35-37]**. The obtained data suggests that ionic liquids have double layer capacitances comparable to those of nonaqueous solvent/ electrolyte systems. For example, Nanjundiah et al. reported that double-layer capacitance (C_{dl}) has values of 10 to 15 $mFcm^{-2}$ at potentials close to the potential of zero charge (PZC) for $[EMIm]^+$ salts of the anions $(CF_3SO_2)_3C^-$, $CF_3SO_3^-$, and BF_4^- at a dropping mercury electrode **[35]**.

1.2.7 Solubility and Solvating properties

It is both for fundamental and applied studies important to know the relative solvating ability of ionic liquids. It was reported that ionic liquids seem to behave most like dipolar, aprotic organic solvents and short-chain alcohols in their interaction with organic solutes **[38-40]**. Clearly, solvating properties will vary depending on the exact nature of the ionic liquid constituent ions; anions with high charge density and organic cations with short alkyl chains rather stabilise polar molecules, whereas a more lipophilic ionic liquid for unpolar solutes may be generated by employing charge-diffuse anions and/or increasing alkyl substitution in the cation. The first generation $AlCl_3$ based ionic liquids are particularly noted for their flexible solvating ability: in these binary mixtures, adding an excess of the organic salt would render the mixture Lewis basic, owing to the presence of free halide ions, whereas addition of extra $AlCl_3$ would create an overall Lewis acidic melt due to the presence of coordinately unsaturated aluminium cluster species. The solvating properties at each

extreme are considerably different, thus by tailoring the proportions accordingly; these ionic liquids are able to dissolve a wide range of inorganic and organometallic compounds. Non-haloaluminate ionic liquids on the other hand have a fixed acidity/basicity and are mostly virtually Lewis neutral due to the very weak acidic and basic donor properties of the ions that comprise them. Identifying this problem, Chen et al. explored the possibility of adding [EMIm]Cl to the ionic liquid [EMIm]BF_4 to give a Lewis basic melt, which facilitated the dissolution and stabilisation of Cu (I) in this medium **[41]**.

1.2.8 Effect of impurities

The presence of some impurities such as halide ions or molecular solvents can greatly influence electrochemical experiments. Thus, it is important to identify and remove these impurities. Halide impurities are generally introduced during the synthesis of ionic liquids. From an electrochemical point of view, halide impurities are likely to manifest themselves predominantly through their effect on the viscosity and electrochemical window. In the former case, a report by Seddon and co-workers observed that even relatively low concentrations of chloride caused a substantial increase in the viscosity of several imidazolium tetrafluoroborate and hexafluorophosphate ionic liquids **[42]**. As chloride and bromide ions are electroactive at potentials below those required to oxidise the heavily fluorinated constituent anions of ionic liquids, the effect of their presence on the solvent window is to narrow it at the anodic extreme or at the very least generate additional background signals which may interfere with the electrochemical process under investigation.

The most prevalent impurity affecting ionic liquids is undoubtedly water. Irrespective of their miscibility with H_2O, all ionic liquids will absorb atmospheric moisture to some extent. Furthermore, Schröder and co-workers have demonstrated that even the presence of relatively low amounts of water can lead to a strong change in the ionic liquid's properties **[43]**. As with halide impurities, a narrowing of the accessible potential window is observed, in this case at both the cathodic and anodic limit, likely due to the electrolysis of water. Whereas halide addition lead to an increase in viscosity however, the presence of water was found to have the opposite effect, as evidenced by an increase in the rate of diffusion for the neutral molecule N,N,N′,N′-tetramethylphenylenediamine **[43]**. While the diffusion coefficient for this

molecule was found to double upon water saturation of a formerly anhydrous ionic liquid solution, the effect on charged solutes was much more pronounced with the diffusion coefficients increasing by an order of magnitude. These findings led to some discussion on the presence of an inhomogeneous "nanostructure" in the wet ionic liquid whereby ionic species were able to undergo faster diffusion in water containing regions while neutral species remained in relatively water-free "dry" locations. Seddon et al. studied the effect of the addition of a range of molecular cosolvents, including water, and discovered that the reduction in viscosity followed essentially the same exponential relationship with mole fraction of added solvent, irrespective of which particular solvent was added **[42]**. When performing experiments involving ionic liquids, water may have to be removed completely prior to use. As mentioned above heating of the ionic liquid under vacuum for several hours removes water down to the few ppm - regime **[29-31,44-47]**. Other reported methods include performing the entire experiment under vacuum conditions **[27,43,48,49]** or employing molecular sieves **[50]**.

In many applications, the presence of water may not have a significant effect. However, the amount of water present should always be measured (Karl Fischer titration is a commonly employed technique) and reported so as to facilitate the accurate comparison of various literature data.

1.3 Applications of ionic liquids

Due to their unique chemical and physical properties, ionic liquids are currently considered as environmentally benign solvents. They have been widely employed in different applications, for example, in catalysis, chemical synthesis, liquid/liquid extractions, photochemistry and nuclear fuel cycle **[51-59]** as well as in electroanalytical applications. The potential of ionic liquids as electrolytes in electroanalytical applications such as photoelectrochemical solar cells, double-layer capacitors and electrodeposition has been discussed by several authors **[60–67]**.

In the following a short review on the use of ionic liquids in electrodeposition of semiconductors, metals and alloys is given.

1.3.1 Electrodeposition of semiconductors

Semiconductors are widely used in many fields, e.g. in electronic devices and in solar cells **[16]**. Ionic liquids were employed successfully to get semiconductors,

which cannot be obtained from aqueous solutions due to hydrogen evolution, which sets in before semiconductor electrodeposition. Endres et al. reported that the elemental semiconductor germanium can be electrodeposited in 1-butyl-3 methylimidazolium hexaflurophosphate ionic liquid that was saturated with germanium iodide (GeI_4) **[11]**, germanium bromide ($GeBr_4$) **[68]** or germanium chloride ($GeCl_4$) **[69, 70]**, respectively and they stated that the reduction of elemental germanium from Ge(IV) halides occurs via Ge(II) species. As germanium, silicon can also not be obtained from aqueous media. Zein El Abedin et al. reported that nanocrystalline silicon of 50-150 nm diameter can be electrodeposited in the room temperature ionic liquid 1-butyl-1-methylpyrrolidinium bis (trifluoromethylsulfonyl) amide **[71, 72]**.

Ionic liquids are not only employed to get elemental semiconductors, they can also be employed to get compound semiconductors such as indium antimonide (InSb) **[73]** and cadmium telluride (CdTe) **[74]** by electrodeposition in 1-ethyl-3-methyl-imidazolium chloride / tetrafluroborate ionic liquid. These two compound semiconductors are of relevance in electronics and solar cells industries.

1.3.2 Electrodeposition of metals and alloys

Room temperature ionic liquids can be employed as solvents for the electrodeposition of metals and alloys. For example, silver can be electrodeposited in 1-ethyl-3 methylimidazolium tetrafluoroborate ($[EMIm]BF_4$) ionic liquid. The ionic liquid $[EMIm]BF_4$ is superior to the chloroaluminate systems since the electrodeposition of silver can be performed without the risk of aluminium codeposition. Also, the electrochemical deposition of silver was investigated at a glassy carbon electrode in hydrophobic 1-n-butyl-3-methylimidazolium hexafluorophosphate ($[BMIm]PF_6$) and hydrophilic 1-n butyl-3-methylimidazolium tetrafluoroborate ($[BMIm]BF_4$) ionic liquids. **[75]**. Tai *et al*. **[76]** studied the electrodeposition of Pd–Ag alloys from the basic $[EMIm]Cl\text{-}BF_4$ ionic liquid in solutions containing Pd(II) and Ag(I) within a temperature range from 35 to 120 ^oC. Scanning electron micrographs of the electrodeposits showed that the Pd–Ag alloys were nodular and become more compact upon increasing the temperature up to 120 ^oC. It was furthermore stated that copper **[77]** can be electrodeposited in a mixture of 1-ethyl-3-methyl imidazolium tetrafluoroborate ($[EMIm]BF_4$) and [EMIm]Cl and the deposits obtained are red brown in appearance with good adhesion. Chen *et al*. **[78]**

reported that copper and copper-Zinc alloys can be electrodeposited on tungsten and nickel electrodes in a Lewis acidic 50-50 mol % $ZnCl_2$–[EMIm]Cl molten salt containing Cu (I). The copper content in the Cu-Zn alloys increases as the Cu (I) concentration in the plating bath and/or the deposition temperature increases and decreases as the deposition overpotential increases. Cadmium **[79]** also can be electrodeposited in basic 1-ethyl-3 methylimidazolium chloride / tetrafluoroborate. The electrochemistry and electrodeposition of antimony were investigated on glassy carbon and nickel electrodes in basic 1-ethyl-3-methylimidazolium chloride tetrafluoroborate. Bulk Sb electrodeposits were prepared on nickel substrates at 30, 80 and 120 ^{o}C **[80]**.

Electrodeposition of palladium–indium alloys is of interest **[81]** because the incorporation of indium into palladium provides higher microhardness and wear-resistance than pure palladium without sacrificing the low contact resistance of the palladium. Thus, the Pd–In coatings can be used as replacement for pure gold, silver and palladium coatings in various applications. Several examples of the electrodeposition of Pd–In in aqueous baths are also available nowadays **[82–86]**. The general difficulties associated with the electrodeposition of Pd–In from aqueous baths are the considerable difference between the deposition potentials of palladium and indium, the low hydrogen overvoltage and the large hydrogen solubility in the Pd metal. Therefore, efforts have been made to minimize these problems. One approach is to replace the aqueous bath with aprotic solvents. The Pd-In coatings were electrodeposited successfully in the [EMIm]Cl-BF_4 ionic liquids and the obtained deposits are smooth and compact **[87]**.

The electrodeposition of Zn and its alloys is possible in the Lewis acidic $ZnCl_2$–[EMIm]Cl ionic liquids. It was shown that Lewis acidic $ZnCl_2$–[EMIm]Cl (in which the molar percentage of $ZnCl_2$ is higher than 33 mol%) are potentially useful for the electrodeposition of zinc and zinc containing alloys **[88–90]**. Huang and Sun have reported that Pt–Zn alloy, **[91]** iron and Zn–Fe alloy, **[92]** tin and Sn–Zn alloy, **[93]** cadmium and Cd–Zn alloy **[94]** can be electrodeposited in Lewis acidic $ZnCl_2$–[EMIm]Cl ionic liquids. In addition, Zinc can be electrodeposited from Lewis basic 1-ethyl-3-methylimidazolium bromide – zinc bromide molten salts with and without dihydric alcohols (ethylene glycol, 1,2-propandiol, 1,2-butanediol) at 120 ^{o}C **[95]**. The addition of the dihydric alcohols to the bath improved the cathodic current

efficiency, the smoothness and colour of the deposit (metallic silver-coloured deposits).

The study of nanoparticles of catalytically active material has attracted intensive interest in recent years because of the important role of nanoparticles in catalysis. Platinium film/nanoparticle is of particular interest, as it is known to be one of the most important catalysts for many chemical reactions, for example, production of hydrogen from methane, conversion of automobile exhaust gas, and especially oxygen reduction and methanol oxidation in a fuel cell **[96]**. Ping He *et al.* **[97]** reported that platinum can be electrodeposited in [BMIm]BF_4 and [BMIm]PF_6 ionic liquids at glassy carbon electrodes, and the electrocatalysis effect of nanostructured platinum films obtained in these ionic liquids on the methanol electrooxidation was also investigated. The obtained platinum deposits were uniform, shiny and fairly dense and the separate spherical nanoclusters were less than 100 nm, obviously different from those of far more than 100 nm prepared in $HClO_4$ aqueous solution. Based on the observed size of platinum nanoclusters, it was reasonable that the catalytic performance and utilization efficiency of the platinum film prepared in [BMIm]BF_4 and [BMIm]PF_6 would be much higher than that prepared in $HClO_4$ aqueous solution. Huang and Sun **[98]** reported the formation of nanoporous platinum by selective anodic dissolution of a Pt-Zn surface alloy in a Lewis acidic zinc chloride- 1-ethyl-3-methylimidazolium chloride ionic liquid is possible and they have studied electrocatalysis effect of the fabricated nanostructured platinum electrode on methanol oxidation. Moreover, nanostructures possess unique properties due to size and interface effects and hence find many applications in electronics, catalysis, and material science **[99]**. Therefore many attempts have been done to make nanostructured materials. Electrodeposition is considered as a versatile method to prepare metal nanostructures, as it allows the precise control over grain size by adjusting the electrochemical parameters such as overpotential, current density and the bath composition. As one example the electrodeposition of monodispersed Fe islands up to 2 nm thick, 50 nm wide and 120 nm long could be deposited from the ionic liquid $AlCl_3$–1-butyl-3-methylimidazolium chloride ($AlCl_3$–[BMIm]Cl) at room temperature on Au(111) **[100]** .

Abbott *et al.* **[101]** studied the electrodeposition of aluminum and aluminum/platinum alloys from $AlCl_3$/benzyltrimethylammonium chloride ionic

liquids. Endres and co-workers **[102]** have reported that tantalum can be electrodeposited in 1-butyl-1-methylpyrrolidinium bis(trifluoromethylsulfonyl) amide ([BMP]Tf_2N) ionic liquid at 200 ^oC in addition to the formation of insoluble tantalum compounds on the electrode surface. The quality and the adherence of the electrodeposit were found to be improved upon addition of LiF to the electrolytic bath. There are hints that Ti metal **[103]** and Ti nanowires **[104]** can be electrodeposited in l-butyl-3-methyl-imidazolium bis (trifluoromethylsulfonyl) amide ([BMIm]Tf_2N) ionic liquid on Au(111) and on highly oriented pyrolytic graphite (HOPG) substrates at room temperature, in ultrathin layers, respectively.

Abbott et al. **[16,105]** have reported the synthesis and characterization of new moisture stable, Lewis acidic ionic liquids/deep eutectic solvents made from metal chlorides and quaternary ammonium salts, which are commercially available. They have shown that mixtures of choline (2-hydroxyethyltrimethylammonium) chloride [$(H_3C)_3NC_2H_4OH)Cl$] and MCl_2 (M = Zn, Sn) give conducting and viscous liquids at or around room temperature. These liquids are easy to prepare, they are water and air insensitive and their low costs make their use in large-scale applications likely. Furthermore, they have reported **[106]** that a dark green, viscous liquid can be formed by mixing choline chloride with chromium (III) chloride hexahydrate and the physical properties of this liquid are characteristic of an ionic liquid. The eutectic composition is found to be 1:2 choline chloride/chromium chloride. From this ionic liquid, chromium black can be electrodeposited efficiently to yield a crack-free deposit. **[106]** Addition of LiCl to the choline chloride/$CrCl_3$-$6H_2O$ mixture was found to allow the deposition of nanocrystalline black chromium films **[107]**. The use of this ionic liquid has some potential for an environmentally friendly process for the electrodeposition of chromium instead of the currently used chromic acid based baths.

1.4 Electrodeposition of aluminium

Aluminium coatings play an important role in modern industries as a light material in automotive and planes as well as for decorative purposes, for example. Furthermore, the high corrosion resistance of Al against chemical and atmospheric attack due to the formation of oxide layers, as a result of exposure to air, makes it – for example – an interesting coating material for steel. The coating has good adherence, is very slightly selfcorrosive, silverish in colour, it can be easily polished, shows good adhesion for varnish and has a very high reflectivity of light and heat so it

can be used for solar energy utilization, the thermal insulation of buildings and the development of various optical devices. With the Hall-Héroult process aluminium can be recoverd from ores but this method is not suitable to coat other metals by aluminium because the electrolysis is carried out at 1000 ^{o}C, a temperature at which cryolite (Na_3AlF_6) and aluminium are in the liquid state **[108, 109]**. Currently, there are several methods available for low temperature aluminium plating such as thermal spray coating, hot dipping, cladding, roll binding, physical and chemical vapour deposition and electroplating but all of these methods except electroplating are expensive, performed at elevated temperatures which may damage the specimens, and not suitable to get a thin aluminium films. However, electroplating was employed successfully to get a thin aluminium film with higher purity and lower porosity. It has a good corrosion resistance and the thermal stress can be avoided since electroplating process can be carried out below 180 ^{o}C **[110]**.

Aluminium can not be electrodeposited from an aqueous solution because of its reactivity (E^{o} = –1.7 V *vs.* NHE). The electrodeposition process would be restricted by hydrogen evolution at the cathode surface; consequently, aluminium can only be electrodepositd from non-aqueous aprotic electrolytes such as molten salts and organic solvents. Many of these electrolytes are sensitive to air and moisture so that the electrodeposition process must be carried out in inert atmosphere such as argon or nitrogen.

Before introducing the different baths used for electrodeposition of aluminium, the requirements for aluminium electrodeposition are shortly mentioned.

Requirements for aluminium electrodeposition baths

The baths for aluminium electrodeposition should have the following requirements **[111,112]**: -

a) The electrolyte should consist of a solvent acting as a slight Lewis base and a solute acting as a Lewis acid so that mutual coordination and dissolution of the solute can take place.
b) The solute that is used as an Al source should exhibit a high solubility in the solvent. A stable complex must be formed in the plating solution.
c) For some applications, it is desirable that the composition of the bath remains constant during the operation. This implies that the electrode process has to be

chemically reversible. This permits the long-term operation of the bath without a change in the electrodeposition characteristics.

d) The medium must exhibit reducing and water-consuming properties.

Also a potentially suitable solvent for the preparation of Al-electrodeposition baths must comply with the following criteria **[112]**: -

a) The solvent must be electrochemically stable in order to permit the reduction of an Al (III) compound without electrolysis of the solvent. This requires that the standard potential that characterises the electrochemical equilibrium between metallic aluminium and the aluminium complex in solution lies within the existence regime of the solvent.
b) The electrode reaction has to be kinetically feasible (low overpotential) and mass-transport phenomena have to favour a controllable surface morphology. The free energy of the co-ordination complex of the solvent and aluminium solute, *e.g* aluminium halide, should be sufficiently low to ensure a good solubility of the salt.
c) The dissociated Al complex ion must release Al at a less negative potential than that of possible electrode reactions involving the solvent.

1.5 Aluminium electrodeposition baths

1.5.1 Electrodeposition of Aluminium from organic solvents

The first attempt to electrodeposit aluminium from organic solvents was made by Plotnikov in 1899 **[113, 114]**. He used solutions of aluminium bromide and Alkali bromide in benzene, toluene and xylene.

Till now, there are three classes of organic solvents, which have been successfully used for aluminium electrodeposition **[115]**.

1.5.1.1 Etheric solvents or hydride baths

In these baths the etheric solvents, such as diethyl ether (Et_2O) and tetrahydrofuran (THF), $AlCl_3$ and LiH or $LiAlH_4$ are combined together to form solutions containing the electroactive species from which aluminium can be electrodeposited. These resulting solutions are called hydride baths and they are classified into two baths, NBS (National Bureau of Standards) and THF baths.

i) The NBS baths

In 1952, Brenner and co-workers at the NBS succeeded to electrodeposit aluminium on an industrial scale by using solution made by dissolving aluminium chloride ($AlCl_3$) and lithium hydride (LiH) in diethylether (Et_2O) **[116-119]**. Later, lithium hydride (LiH) was replaced by lithium aluminium hydride ($LiAlH_4$), which can be dissolved in diethylether more easily **[120]**. The addition of $LiAlH_4$ instead of LiH increased the bath lifetime. The obtained cathodic current efficiency at current densities 2-5 A dm^{-2} and ambient temperatures was 90%. The anodic current efficiency was 100% but the anodically dissolved aluminium could not be deposited onto the cathode, therefore the aluminium content of the bath decreased during the electroplating process and $AlCl_3$ had to be added from time to time to increase the bath lifetime.

NBS electrolyte was used on a pilot plant scale at General Electric by Schmidt and coworkers **[121-124]** who electroformed parabolic mirrors. The cathode current densities were 1.5 - 10 A dm^{-2}. Both the micro and the macro throwing powers were reported to be excellent. Adherent aluminium coatings of 300 μm in thickness were deposited on various aluminium alloys, titanium alloys and copper alloys as well as steel in NBS baths **[125]**. The application of the NBS bath to Electro-Optical Systems **[126]** was similar to the application at General Electric, namely the electroforming of solar mirrors. Withers and Abrams **[127]** electroformed composites containing boron filaments. To strengthen the aluminium deposit they added magnesium solution to the NBS bath, probably as ethylmagnesium bromide. By using bare Al anodes, Clay *et al.* **[128]** succeeded in determining the optimum conditions such as agitation, low current densities (up to 2 A dm^{-2}) and somewhat higher temperature (40 ^{o}C) to prolong life-time of the bath. Under these circumstances the anodic current efficiency was found to be 100 %. Levinskas and coworkers **[129]** studied the relation between the geometry of the cell and the pre-treatment of the cathode surface on the one hand and the optimum current density on the other hand. They also studied the influence of additives such as diethylamine, butylamine and piperidine on the deposit and bath quality **[130]**.

The NBS bath possessed several drawbacks such as flammability, limited life-time, variation of the composition and low anodic current efficiency, hydrogen embrittlement due to excessive hydrogen evolution **[131,132]**. Nevertheless the

process has been a commercial reality for a long time, and has also been adopted by NASA **[133]**.

Now the aim of research work is to improve the quality of the aluminium coatings by addition of suitable additives and to reduce the fire hazards of the highly inflammable ether. Therefore, improvements were made with the choice of a less volatile solvent such as tetrahydrofuran (THF).

ii) The THF baths

The use of THF alone or THF in combination with benzene instead of diethylether has been suggested by Ishibashi and Yoshio **[134,13]**. It was not only less inflammable and less volatile, it also showed better anode dissolution and therefore a longer bath lifetime. Ishibashi and Yoshio were able to apply successfully current densities above 10 A dm^{-2} with agitation. The composition of the bath was roughly 60 vol.% THF, 40 vol.% benzene with 0.7 - 1.3 mol/1 $A1C1_3$ and $LiA1H_4$. Excellent deposits were obtained with an $A1C1_3$: $LiA1H_4$ molar ratio of 3:1. Other hydrocarbons were tried in addition to benzene, such as 1,2-dichloroethane and toluene, in these cases the deposit on the cathode was obtained but a white precipitate was observed on the anode. An unsuccessful attempt was made to improve the operation of the NBS electrolyte by adding some aromatic hydrocarbons **[134]**. Yoshio and Ishibashi have suggested a rather complicated pretreatment of the cathode surface prior to the electrolysis but Eckert and Kölling **[136]** have shown it to be less useful. Kurata et al. **[137-139]** have also studied special pre-treatment of iron and steel surfaces in order to obtain purer and adherent deposits.

The THF electrolyte has been utilized by the Nisshin Steel Co. in Japan for the continuous aluminium coating of steel wires and strips used, for example, in integrated circuits **[140]**. Also, It has been used for the electroplating of carbon fibres **[141]**. Graef studied the mechanism of aluminium electrodeposition from solutions of $AlCl_3$ and $LiAlH_4$ in THF **[142]**. Moreover, Al-Mg alloys containing up to 13% Mg could be obtained from THF bath with $MgBr_2$ **[143]**. In 2000, Lefebvre and Conway reported in two papers that aluminium can be electrodeposited from plating baths of varying ratios of $AlCl_3$ and $LiAlH_4$ dissolved in THF. They studied the kinetics, mechanisms, nucleation and surface morphologies in the process of

electrocrystallization of aluminium on smooth gold and glassy-carbon substrates **[144,145]**.

1.5.1.2 Aromatic hydrocarbons baths

These electrolytes are known as bromide baths because $A1Br_3$ is the aluminium-containing compound. The aromatic hydrocarbons used are usually benzene, toluene, xylene and their mixtures and derivatives.

i) $AlBr_3$ +MBr as the electroactive components

Attempts were done to increase the conductivity of $A1Br_3$ solutions by the addition of quaternary ammonium or pyridinium salts such as ethylpyridinium bromide **[146]**, ethylenepyridinium dichloride and ethylenepyridinium dibromide **[147]**. The cathode efficiencies ranged from 80 to 92% and the current densities from 0.2 to 2 Adm^{-2}, the deposit was about 6 um thick. Also, this type of electrolyte has been studied by Simanavicius and Dobrovolskis **[148-150]**. The best deposits were obtained with quaternary pyridinium or dimethylaniline salts in toluene. The anionic species was assumed to be $A1_2Br_7^-$ on the basis of conductivity measurements. These electrolytes are complicated to operate and the results are rather poor. In small amounts, the quaternary salts can improve the brightness of the deposit but higher concentrations lead to the incorporation of the quaternary salt into the deposit and thus to a decrease in its purity and corrosion resistance. Better results were obtained using alkali bromide (MBr), mainly KBr, in combination with $A1Br_3$. Peled and Gileadi **[151,152]** used an electrolyte consisting of 25 - 45 vol.% $A1Br_3$ and 1% - 1 mol/l KBr in a mixture of hydrocarbons. The function of each component of the bath can be characterized as follows. $A1Br_3$ is the aluminium-containing component. The alkali bromide (MBr) has to increase the solution conductivity to the value required for electrolysis, i.e. 1 - 6 mS/cm, and to improve the throwing power of the solution by forming anions of the types $A1_2Br_7^-$ or $A1Br_4^-$. The concentration of the alkali bromide must not exceed 1 mol/l because co-deposition of the alkali metal can occur. The function of the solvent itself, apart from its dissolution properties, consists in its ability to bind protons formed in contact with the surroundings. The stability of the σ complexes of aromatic hydrocarbons with protons increases in the following sequence: benzene < toluene < m-xylene < mesitylene. In general, the longer and more branched the chain or the higher the number of aromatic rings, the better the

reactivity of the hydrocarbon towards protons. The deposits obtained from such electrolytes were smooth, homogeneous and microcrystalline with good adherence. Both the cathode and the anode efficiencies were 100% and the current density was 10 A dm^{-2}. The purity of the deposits was 99.5%. The metals coated were copper, brass and steel and the anode was 99.5% a1uminium. Simanavicius *et al.* gave in one paper comparative studies on the co-deposition of Al with Co, Cr, Zn or Mn from $AlBr_3$-dimethylethylphenylammonium bromide solutions in toluene containing the acetylacetonate of a corresponding metal **[153]**.

Although there are no reports concerning the industrial application of this bath, the results of laboratory experiments regarding plating quality and long-term performance appeared to be very promising. Its use would permit easier and more economical operation than the baths containing lithium aluminium hydride or aluminium organic compounds.

ii) $AlBr_3$ +HBr as the electroactive components

This combination has been used by Capuano and Davenport **[154-157]**. The electrolyte consisted of 36 - 45 vol.% $A1Br_3$ in a 1:1 mixture of ethylbenzene or diethylbenzene and toluene. The solution was prepared as follows. An inert gas saturated with water vapour was passed through the solution prior to dissolution of the $A1Br_3$, and this led to the formation of HBr. The solution thus prepared must be carefully protected against moisture and oxygen by an inert atmosphere. The presence of HBr in the solution ensures the required specific conductivity of 3 - 4 mS cm^{-1}. The coated surfaces were copper and steel and the anode was pure aluminium. At 1 A dm^{-2} the anodic efficiency was 100% and the cathodic efficiency 80%. With increasing current density the cathodic efficiency decreased. The low cathodic efficiency compared with the anodic efficiency caused an enrichment of the solution with aluminium, which successfully formed bonds with Br ions from the HBr. The quality of deposits up to 25 pm thick has been claimed to be very good with regard to mechanical strength and corrosion resistance. The bath life was also excellent, during one year of operation under optimum conditions the bath composition and function remained unchanged. Although Davenport and Capuano **[156]** regard their electrolyte as highly suitable for application, no industrial use is known as yet. The system $A1Br_3$ + HBr in o-, m- and p-xylene has been investigated in detail by Simanavicius and coworkers **[158-161]**. Current efficiencies of 90% were attained. After the aluminium

had been deposited on the cathode, hydrogen evolution and decomposition of the solvent were observed. Some experiments have been performed to electroplate aluminium from an ethylbenzene solution of $A1Br_3$ without the addition of any further components **[162-164]**. The freshly prepared solution was light yellow and had a conductivity that was of the order of 10^{-8} S cm^{-1}. With time the solution became dark brown and the conductivity increased to 10^{-3} S cm^{-1}. These changes, caused by traces of water in the electrolyte, have been ascribed to the formation of well-dissociated complexes of the type $A1_2Br_4OH.C_8H_{10}^+$ **[164]**. In 2003, Shavkunov and Strugova reported that aluminium would not be deposited electrochemically from a benzene solution of aluminium bromide even after a prolonged electrochemical aging. From a toluene solution, aluminium was deposited with a low current efficiency in the form of individual crystals, and the electrolyte required a prolonged electrochemical aging. They succeeded to obtain high-quality aluminium coatings at a current efficiency of 60-80 % from the xylene, ethylbenzene, xylene-durene electrolytes containing aluminium bromide. Also, they studied the aluminium electrodeposition kinetics in such solutions **[165]**.

Capuano did not only electrodeposit aluminium and aluminium alloys, such as Al-Cu, Al-Sn, Al-Zn alloys, from alkylbenzene-HBr electrolytes but also reviewed the theoretical considerations pertaining to the electrodeposition process. He reported that, aluminium bromide produces π complexes when dissolved in alkylbenzenes. When the solvent has a large number of radicals attached or larger chains, a monomeric II complex (Al cation) is produced. A study of the interaction between Al_2Br_6 and alkylbenzenes showed that toluene produces the highest amount of open dimer, m-xylene, the highest quantity of closed dimer, and 1-2-4- trimethylbenzene is the richest in aluminum cations. The open dimer is responsible for the conductivity of the electrolyte. The aluminium cation is responsible for the electrodeposition of aluminium. Hydrobromic acid enhances the conductivity of the electrolyte and the formation of monomeric π complexes. The content of the minor constituents, Cu, Sn, or Zn, in aluminum alloy coating can be controlled by using Al alloy anodes of specified composition if the current density, agitation, and specific conductances are maintained constants. The co-deposition of Cu, Sn, and Zn in the electrodeposition of aluminum alloy was found to be a diffusion-rate controlling process. The use of pulse plating permits to deposit thicker aluminium alloy coatings. Barrel plating of steel and

titanium fasteners was shown to be possible from organic electrolytes. The corrosion resistance of aluminium-plated fasteners was shown to be increased considerably by a chromating treatment **[166]**.

iii) Organoaluminium compounds as the electroactive components

This type of electrolyte was developed by Ziegler and Lehmkuhl **[167-169]**. The bath is based on the compounds: $(C_2H_5)_4NCl/2Al(C_2H_5)_3$, $NaF/2Al(C_2H_5)_3$ and $NaF/2Al(C_2H_5)_3/3.3C_7H_8$. The solvent is toluene. The bath operates at 60 - 90 ^oC with current densities of 1 - 5 A dm^{-2}. The purity of the deposit is 99.9999%, the best obtained so far. The composition of the bath and the influence of additives on the brightness of the deposit have been studied by Dötzer and coworkers **[170-172]**. Electrolytes with organoaluminium compounds are used by SIGAL (Siemens-Galvano-aluminium) in discontinuous operation for manufacturing reflectors as well as light and heat radiators. In principle the electrolytic cell is put in a double-walled chamber filled with inert gas to prevent the influence of air and moisture on the electrodeposition process.

1.5.1.3 Electrodeposition of aluminium from dimethylsulfone ($DMSO_2$)

With a number of attractive features, such as: high conductivity, good thermal stability **[173]**, ability to dissolve numerous metallic cations **[174,175]**, dimethylsulfone ($DMSO_2$) has been considered a promising organic solvent for rechargeable cells **[176]**. Recent investigations **[177,178]** have shown that aluminium can be reversibliy plated and stripped in a mixture (2:1 mole ratio) of $AlCl_3$: LiCl dissolved in $DMSO_2$ while no aluminium plating was observed in that of a 1:1 mole ratio. Analysis of chronoamperograms indicated that the aluminium deposition process at a tungsten electrode from the mixtures of $AlCl_3/LiCl/DMSO_2$ involved progressive nucleation with diffusion-controlled growth of the nuclei **[177]**. SEM observations **[177]** showed that smooth and continuous aluminium deposits could be obtained from the $DMSO_2$ baths by potential step technique. A Raman study **[179]** revealed:

a) $AlCl_4^-$ ion was always the main Al (III) species even in a melt without LiCl,
b) $Al_2Cl_7^-$ was never found even in the more acidic baths, i.e with $AlCl_3$/LiCl mole ratio greater than one,

c) A coordination complex, $Al[(CH_3)_2SO_2]_3^{3+}$ was formed in the acidic melts between $DMSO_2$ and Al (III).

This complex was responsible for aluminium deposition on tungsten electrode from $AlCl_3$/LiCl/$DMSO_2$ bath through the following reactions **[177]**:

$$Al[(CH_3)_2SO_2]_3^{3+} + 3e^- \longrightarrow Al + 3\,(CH_3)_2\,SO_2$$

No aluminium plating process occurred in a mixture (2:1 mole ratio) of $AlCl_3$: LiCl, indicating that as a Lewis base, $DMSO_2$ was weaker than Cl^- but stronger than $AlCl_4^-$, leading to the following equilibrium for $DMSO_2$-based electrolytes:

$$AlCl_3 + Cl^- \longrightarrow AlCl_4^-$$

$$4\,AlCl_3 + 3\,(CH_3)_2SO_2 \longrightarrow Al[(CH_3)_2SO_2]_3^{3+} + 3AlCl_4^-$$

Fransaer *et al.* **[180]** in 2002 has achieved the electrolytic codeposition of micro- and nano-sized particles with aluminum from $DMSO_2$ baths. SiC, SiO_2, Al_2O_3, TiB_2 and hexagonal BN particles were codeposited with aluminium from an $AlCl_3$/ dimethylsulfone ($DMSO_2$) electrolyte. Moreover, he studied the effect of particle concentration and current density on the codeposition rate of SiO_2 with aluminium. Also he found that the codeposition of the various particles with Al from $AlCl_3$:$DMSO_2$ solutions was very high.

The large degree of codeposition of hydrophilic particles (SiO_2 and Al_2O_3) confirms that elimination of the hydration force achieved by using non-aqueous electrolytes can significantly enhance the codeposition of such particles and can avoid the agglomeration that takes place in aqueous electrolytes. This opens new fields of applications for the synthesis of composite coatings containing homogeneously dispersed nanometre-sized particles with compositions that cannot be obtained from aqueous electrolytes.

Unfortunately, the common feature of all organic baths for the electrodeposition of aluminium is the absolute necessity of operating in an inert atmosphere and therefore in closed systems. All the organic solvent baths have many disadvantages: they are inflammable, volatile, hygroscopic and consequently relatively complicated to handle. For example, from the disadvantages of organoaluminium baths, their self-ignition in air and their vigorous reaction with water.

To avoid the disadvantages of organic solvent baths, the investigation of new nonaqueous electrolytic systems for the electrodeposition of aluminium has continued. Of them, ambient temperature chloroaluminate molten salts such as $AlCl_3$-NaCl and related lower melting chloroaluminates based on quaternary ammonium chloride salts (ionic liquids) such as N-butylpyridinium chloride (N-BPC) and 1-ethyl-3-methylimidazolium chloride [EMIm]Cl. These ambient temperature molten salts have received more attention as the most promising aluminium plating baths for industrial applications.

1.5.2 Electrodeposition of aluminium from chloroaluminate molten salts

Electrodeposition in ionic liquids would have many advantages. The low working temperature (120 ^oC and higher) compared with the hot plating process suppresses the formation of brittle intermetallic compounds in the underlayer. The higher electrical conductivity of the electrolyte (by 1 to 2 orders) makes it possible to carry out the electrolysis at higher current densities. There is less toxicity and no danger of explosion and control of the thickness of the Al layer make it potentially attractive for wider application.

Aluminium can be electrodeposited in molten salts (chloroaluminate molten salts), mainly chlorides, where Al can be deposited either by using a soluble aluminium anode or the electrochemical decomposition of the electroactive species, $Al_2Cl_7^-$, which formed in the Lewis acidic molten $AlCl_3$: Alkali metal chloride mixture of molar ratio 2:1. The electrochemical reduction of the electroactive species occurs by the following **[181]**:

$$4\ Al_2Cl_7^- + 3e^- \longrightarrow Al + 7\ AlCl_4^-$$

Extensive work has been reported on the electrodeposition of aluminium from such type. The first paper on the electrolytic aluminium deposition from a molten $AlCl_3$-NaCl mixture was published at the mid of nineteenth century **[182]**.

The first attempt to use this electrolyte for the deposition of aluminium on an iron base was made by Plotnikov and co-workers [**183-185]**. Chittum [**186]** proposed LiCl instead of NaCl. The quality of the Al layers deposited in molten electrolytes containing aluminium and alkali chlorides was examined by Orleva and Lainer **[187]**. Bromides as well as chlorides have been tested as possible electrolytes for the deposition of Al layers **[188-190]**. A systematic investigation of electrolytic

aluminium-plating in molten chlorides was carried out by Delimarskii and co-workers **[191-193]**. Of the different mixtures containing aluminium and alkali chlorides, the binary mixture with a composition corresponding to the compound 2 $AlCl_3$.NaCl was found to be the most suitable electrolyte. As the electrolyte is hygroscopic, electrolysis is carried out in an inert atmosphere, furthermore dehydrating substances, such as silicagel and active coal should be added directly to the electrolyte. This increases the current efficiency of the electrolysis **[194,195]**.

The results of the electrolysis of the binary aluminium chloride - alkali chloride ($AlCl_3$-MCl) mixtures, however, were disappointing as in all cases Al was deposited in the form of a dull, coarse-grained layer with low anticorrosion resistance. Therefore, numerous attempts were made to influence the process of electrocrystallization of aluminium, mainly by addition of different metals, either in the form of compounds (chlorides or oxides), or as auxiliary anodes of respective metals. The influence of Sn, Pb **[191,193,196-198]**, Zn, Sb, Bi **[199]**, Mn **[200]**, Cu, Ag, Cd, Ga, In, Tl, Ge **[201]** and V **[202]** has been studied. It was found that only Sn, Pb and Mn have a favourable influence on the properties of the deposited layer. In all cases, however, instead of pure aluminium the corresponding aluminium alloy was deposited.

Paucirova and Matiasovsky **[203]** in 1975 have succeeded to electroplate iron substrates by a fine-crystalline, silver-bright and non-porous aluminium layer from molten salts based on chlorides. Also, they found that the optimum electrolyte for aluminium electroplating in molten salts was a quaternary mixture of 80 wt.% $AlCl_3$ + 10 wt.% KC1 + 5 wt.% NaCl + 5 wt.% NaI and in the temperature range 150 - 200 ^oC with a cathodic current density of up to 7 A dm^{-2}. G. R. Stafford reported that aluminium, aluminium–manganese and aluminium-titamnium alloys can be electrodeposited from $AlCl_3$-NaCl molten salt at 150 ^oC **[181, 204]**.

The drawbacks of the $AlCl_3$-NaCl molten salt are its high $AlCl_3$ vapour pressure, which may result in explosions at elevated temperatures and the fact that the melt is very corrosive. Therefore ionic liquids might be an alternative.

1.5.3 Electrodeposition of aluminium in ionic liquids

Electrodeposition of aluminium in ionic liquids can be performed at room temperature. The aluminium deposits obtained are usually of good quality, high purity, of low porosity and heat resistant. Popular examples of ionic liquids include the chloroaluminates, which are prepared by mixing anhydrous $AlCl_3$ with a suitable organic halide. This kind of ionic liquids can be considered as the first generation of ionic liquids. Moreover, it is the simplest system from which aluminium can be easily electrodeposited. As the molar ratio of this mixture changes, the melt can be classified as basic, neutral or acidic in the sense of Lewis acidity. In the neutral 1:l melt Al is present almost entirely as $AlCl_4^-$ ions, whereas in the 2:l melt it is present as $Al_2Cl_7^-$. In melts having a molar ratio between 1:l and 2:1, both $Al_2Cl_7^-$and $AlCl_4^-$ ions will be present. The acid-base properties of the melt at ambient temperature may be described by the following equilibrium [**205,206]**:

$$2\ AlCl_4^- \longleftrightarrow Al_2Cl_7^- + Cl^-$$

with an equilibrium constant K = 3.8 x 20^{-13} at 30 ^oC. In acidic melts, $Al_2Cl_7^-$ ion is the only species from which aluminium can be electrodeposited according to the following reaction:

$$4\ Al_2Cl_7^- + 3e^- \longrightarrow Al + 7\ AlCl_4^-$$

In presence of excess of $AlCl_3$, the following reaction is virtually complete:

$$AlCl_4^- + AlCl_3 \longrightarrow Al_2Cl_7^-$$

A lot of work has been done using chloroaluminate ionic liquids to get high quality aluminium deposits by several authors. For example, $AlCl_3$ / 1-ethyl-3-methylimidazolium chloride ($AlCl_3$ / [EMIm]Cl) and the ionic liquids $AlCl_3$ / N-butylpyridinium chloride ($AlCl_3$ / N-BPC) have been widely used in electrodeposition of aluminium and its alloys.

1.5.3.1 Electrodeposition of aluminium in $AlCl_3$ / imidazolium based ionic liquids

The $AlCl_3$ / [EMIm]Cl ionic liquid is specially attractive for the electrodeposition of aluminium and its alloys because it has a very low melting point over a wide range of compositions, high intrinsic electrical conductivity at room temperature, and a low vapour pressure **[207]**. This system was widely used by several authors to electrodeposit aluminium and its alloys.

Hussey and co-workers did intensive studies on the electrodeposition of aluminium and aluminium alloys in $AlCl_3$ / [EMIm]Cl ionic liquid. They succeeded to electrodeposit transition metal-aluminium alloys such as Al-Mo **[208]**, Al-Ti **[209]**, Al-Zr **[210]**, Ag-Al **[211]**, and ternary Al-Mo-Mn **[212]** alloys. These alloys are technologically important because of their corrosion resistance, especially pitting corrosion, and in some cases, their interesting magnetic properties.

Jiang *et al.* **[213]** have studied the electrodeposition, electrochemical nucleation and surface morphology of aluminium on both tungsten and aluminium electrodes from 2:1 molar ratio $AlCl_3$: [EMIm]Cl ionic liquid. The electrodeposits obtained on both tungsten and aluminium electrodes were dense, continuous and well adherent.

The $AlCl_3$ / [EMIm]Cl (60/40 mol.%) ionic liquid was used to electroplate mild steel by well adherent and highly resisted to scratches aluminium coatings **[214]**. However, the quality of the deposit can be greatly improved by utilizing pulse plating techniques **[215,216]** or by addition of some organic solvents such as benzene and methyl t-butyl ether **[216]** that improve the deposit surface morphology. It is possible that the organic molecules play the role of brighteners.

Endres *et al.* reported that nanocrystalline aluminium can be made electrochemically in Lewis acidic ionic liquids based on $AlCl_3$ and [EMIm]Cl under galvanostatic conditions by addition of nicotinic acid **[217]**.

Also the $AlCl_3$ / 1-ethyl-3-methylimidazolium chloride ($AlCl_3$ / [EMIm]Cl) melt is a viscous and transparent liquid at room temperature when the molar composition is in the range of 0.3:1 to 2:1 **[218]**.

Lai **[219]** have electrodeposited aluminium in room temperature $AlCl_3$ / [EMIm]Cl ionic liquid on glassy carbon, platinum and tungsten. Moreover, he has studied the mechanism of the electrodeposition and dissolution processes in such ionic liquid. The obtained results indicated that the aluminium deposition process at the above-mentioned substrates is preceded by a nucleation step and is kinetically complicated. The deposited aluminium was found to be unstable and subject to a slow corrosion process. This is most likely due to impurities and organic cation present in the melt.

Also, aluminum deposition from $AlCl_3$ / [EMIm]Cl ionic liquid was studied employing an inverted optical microscope to perform *in situ* optical observations during the deposition process at tungsten electrode. Thin, continuous aluminum coatings with crystal sizes below optical microscopic resolution are produced from a 1.1:1 $AlCl_3$: [EMIm]Cl molten salt at potentials < -0.2 V *vs.* an Al(III)/Al reference electrode. Analysis of chronoamperograms indicated that the deposition process involves progressive nucleation with diffusion-controlled growth of the three-dimensional nuclei **[220]**.

Liao *et al.* **[221]** have improved the quality of the aluminium deposit obtained in Lewis acidic $AlCl_3$ / [EMIm]Cl ionic liquid by addition of benzene as a cosolvant.

1.5.3.2 Electrodeposition of aluminium in ($AlCl_3$ / N-BPC) system

The $AlCl_3$ / N-butylpyridinium chloride ($AlCl_3$ / N-BPC) system is liquid at ambient temperatures over a wide composition range (molar ratio from 0.75:1 to 2:1 $AlCl_3$ / N-BPC) **[222]**.

Kazacos and co-workers employed different electrodes such as glassy carbon, tungsten **[223]** and platinum **[224]** to investigate the mechanism of aluminium deposition and dissolution reactions in $AlCl_3$ / N-BPC melts at ambient temperature. The results showed that the electrodeposition of aluminium from that liquid at glassy carbon and tungsten electrodes is kinetically complicated and the corrosion rate of aluminium is linearly proportional to the acidity of the melt at 40 °C. Besides impurities, the major reason for the corrosion of the deposited aluminium in that melt was also found to be due to the organic butylpyridinium cation ($BuPy^+$) **[223]** while at platinum electrodes, the results indicated that the aluminium deposition reaction is a quasi-reversible process and there is an evidence for formation of Pt-Al alloy in the initial stages of aluminium deposition **[224]**.

In 1980, Robinson and Osteryoung **[225]** studied the electrodeposition and stripping processes of aluminium in $AlCl_3$ / N-BPC melts with and without benzene at tungsten, platinum and glassy carbon electrodes. In acidic liquids, at all three electrodes, the reduction of $Al_2Cl_7^-$ ions was found to involve a nucleation process while at the tungsten and platinum electrodes under potential deposition was also observed. Studies of the stripping of aluminium from inert substrates showed that aluminium is very slowly corroded in acidic melts, and melt-benzene mixtures, by

traces of oxidizing impurities while in basic systems aluminum reduces the n-butyl pyridinium cation.

Yang **[226]** electrodeposited aluminium from an acidic liquid of this system by using DC constant current and pulse current methods at 30 °C. The quality of as-deposited aluminium layer was improved by applying pulse current; the particle size decreased and the adhesion became much better.

Moreover, alloys such as Co-Al **[227]** and Al-Cr **[228]** alloys can be electrodeposited on different substrates in the acidic melt of this system.

1.6 Scanning tunneling microscopy, STM

The scanning tunneling microscopy was first introduced in 1982 by Gerd Binnig and Heinrich Rohrer **[229]**. They were awarded the Nobel Prize in Physics in 1986. Nowadays, scanning tunneling microscopy (STM) is employed in many fields in academics and industry. The application of the scanning tunneling microscopy (STM) to probe the structure at the electrode/electrolyte interface is one of the most important advances in electrochemistry over the past 2 decades **[230]**. Sonnenfeld and Hansma **[231]** were the first ones to study a surface immersed in a liquid. To achieve this purpose, they combined the normal STM with a potentiostat to be able to perform electrochemical STM measurements. They succeeded to get images of highly oriented pyrolytic graphite (HOPG) in aqueous media. Following these initial efforts in 1986, a rapid series of advances was done to apply in a variety of electrochemical studies in both aqueous **[232-234]** and ionic electrolytes **[70, 72, 235-238]**. STM performed under electrochemical conditions (EC-STM technique) gave an insight into various processes, such as for example the initial stages of electrodeposition. Despite the extensive studies in aqueous media **[232-234]**, in situ STM studies on electrode / electrolyte interface behaviour in chloroaluminate ionic liquids are difficult, as chloroaluminates are strongly hygroscopic and liberate highly aggressive HCl upon reaction with ambient water. Therefore, Endres *et al.* **[239]** developed a new design suited for working under inert-gas atmosphere for several days. Recently, STM was used successfully to investigate the electrodeposition of metals, alloys **[235, 102, 237, 238]** and semiconductors **[70, 72]** in ionic liquids. It is well-known that Au (111) is subject to restructuring/reconstruction under electrochemical control in both aqueous solutions **[234]** and ionic liquids **[72, 236]** and STM helps to show these phenomena. There are few papers dealing with *in situ* STM measurements on electrochemical

deposition of aluminium in chloroaluminate ionic liquids **[237, 238]**. Zell *et al.* performed *in situ* EC-STM studies on the electrodeposition of aluminium in chloroaluminate ionic liquid on Au (111). It was reported that the cyclic voltamograms exhibit underpotential deposition process before the bulk deposition starts in, which was proved by in situ STM studies **[237]**.

1.6.1 Electron tunneling phenomenon

Scanning tunnelling microscopy and spectroscopy rely on electron tunnelling, a phenomenon that is based on quantum mechanics in that it is not allowed in classical mechanics **[240, 241]**.

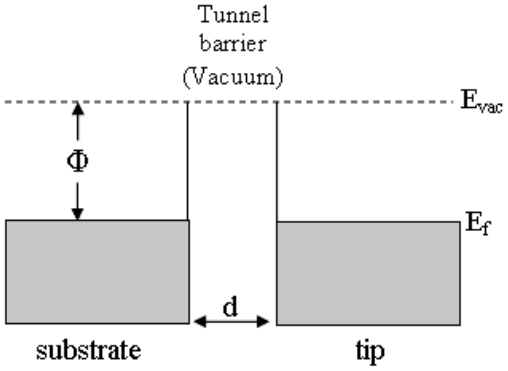

Fig.1.2a. *When the substrate and the tip are brought close to each other, there is only a narrow region of empty space left between them. On either side, the electrons are present up to the Fermi energy. They need to overcome a barrier Φ to travel from the tip to the substrate or vice versa.*

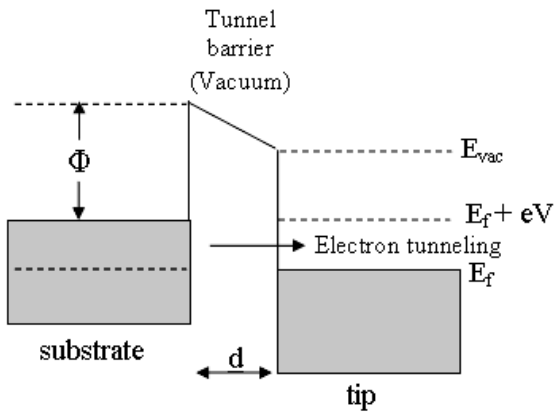

Fig. 1.2b. *If the distance d between the substrate and the tip is small enough, electrons can 'tunnel' through the vacuum barrier. When a voltage V is applied between the substrate and the tip, the tunneling effect results in a net electron current (tunneling current). In this example from the substrate to the tip.*

In a metal or semiconductor, the electrons occupy all available energy levels up to the energy EF (Fermi energy), at which they precisely compensate the positive charge of the metal ions. For an electron to leave the metal, it needs to acquire an extra amount of energy of Φ above the Fermi energy. This brings it up to the vacuum level, at which point it is free to move away from the metal. The energy Φ is known as the work function of the metal. Figure 1.2a shows that the tip and the substrate are close to each other. There is only a narrow region of space between both, but there is

no conductive connection. According to classical mechanics, electrons still need to have an extra energy Φ above the Fermi energy to move across the barrier. However, quantum mechanics allows a finite, albeit small, number of electrons to traverse the barrier if the thickness d is small this process is known as tunnelling (see fig. 1.2b).

When an electrical voltage V is applied between the substrate and the tip, the electron can tunnel from the substrate to the tip and vice versa and this electron tunneling results in a net electrical current (tunneling current). This current depends on the tip-surface distance d, on the voltage V, and on the height of the barrier Φ.

1.6.2 Principle of STM operation under electrochemical conditions

The principle of the STM operation is remarkably simple, and can be compared best with that of an old-fashioned record player. Just like in a record player, the instrument uses a sharp needle, referred to as the 'tip', to interrogate the shape of the surface. But in contrast with a normal record player, the STM tip does not touch the surface.

The simplified STM circuit under electrochemical conditions was interpreted by Endres **[240]**. Figure 1.3 shows the simplified circuit of an electrochemical STM set up.

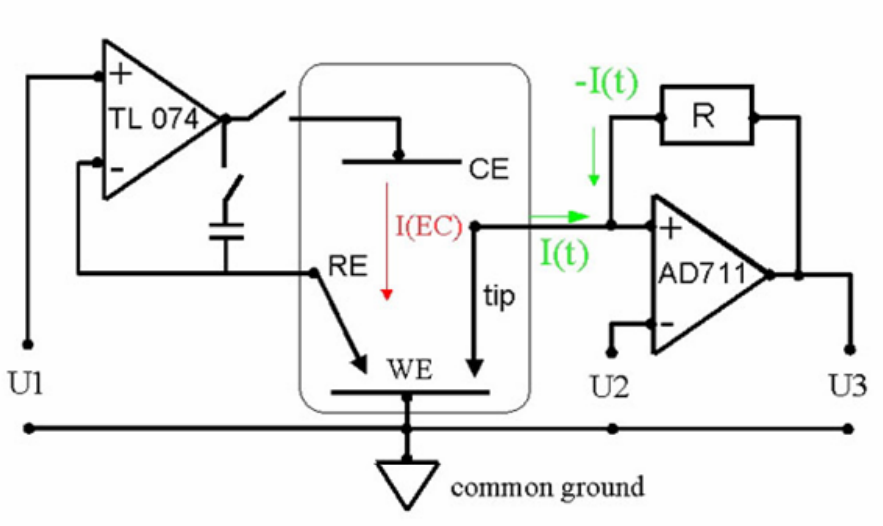

Fig. 1.3. *Simplified circuit of an electrochemical STM set up. In addition to the potentiostat (in the left side), an STM preamplifier is added, to which the tip is connected. U1: potentiostatic stepoint, U2: tunnelling voltage, I(t): tunnelling current, U3 = - R I(t).*

The left side is essentially identical to a potentiostat circuit. The right side is the preamplifier of the STM. The atomically sharp metal tip is located roughly 1 nm over an electronically conductive substrate, here the working electrode (WE) of interest. This is done by computer control, with the help of step motors and micrometer screws as well as piezoelectric elements, to which the tip is connected. If a potential U2 is applied between tip and sample (typically 5-500 mV) a tunnling current I(t) flows, with typical values between 0.1 and 10 nA, depending on the distance. This current is transformed into a voltage U3 (= R* I(t)) that can be further processed. The tunnelling current is an extremely dependent on the distance between tip and surface of sample (d) and is a function of the electronic density of tip D (tip) and sample D (sample). For a strongly simplified case at low tunnelling voltages one obtains to a first approximation the following equation **[241]**.

$$I(\text{tunnel}) = f(U_{\text{bias}}) * D(\text{tip}) * D(\text{sample}) * \exp[-\text{const.} * d]$$

Because of this strong distance dependence, local height changes can in principle be detected in the picometer range. There are two modes of operation.

i) Constant Height Mode

In this mode the tip is scanned over the surface at a constant height and the

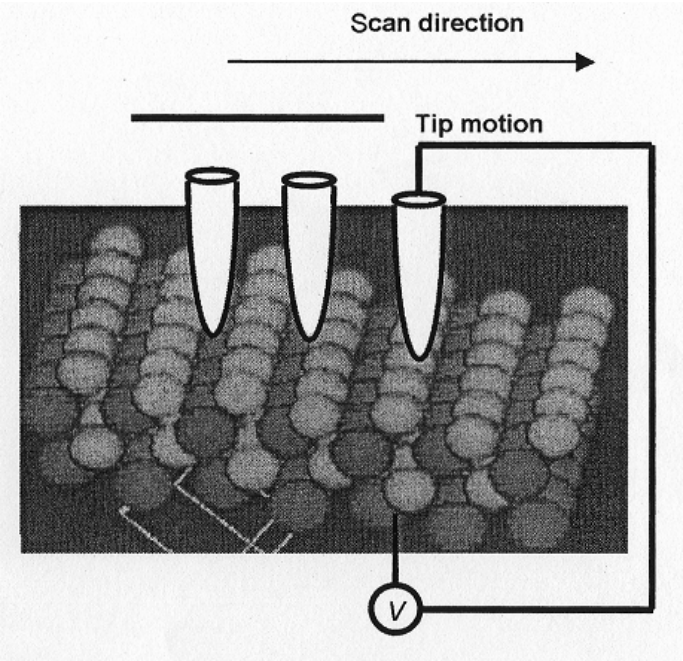

Fig.1.4. Constant height mode, a bias potential is applied between the sample and the tip. During the tip scanning from left to right, the vertical position is held constant and the current varies.

local changes of the tunnelling current are acquired.

A variation in current results as the tip scans the sample surface because the topographic structure varies the sample-tip separation (see Fig.1.4). In this case, the current is the image and be related to charge density. The main advantage of this mode is that it provides for faster scan rates not being limited by the response time of the vertical driver.

ii) Constant Current Mode

In this a feed back electronics holds the current between the tip and the sample constant and consequently keeps the distance constant (see Fig.1.5). As the tip is scanned over the sample, the vertical position of the tip is altered to maintain the distance between the tip and the sample constant. The motion in all three directions (*x, y,* and *z*) is controlled by piezoelectric elements. It works such that U3 in fig. 1.3 is amplified and finally fed back through an adding amplifier to the piezo control. This type of mode is characterized by the advantage that produces contrast directly related to electron charge density profiles.

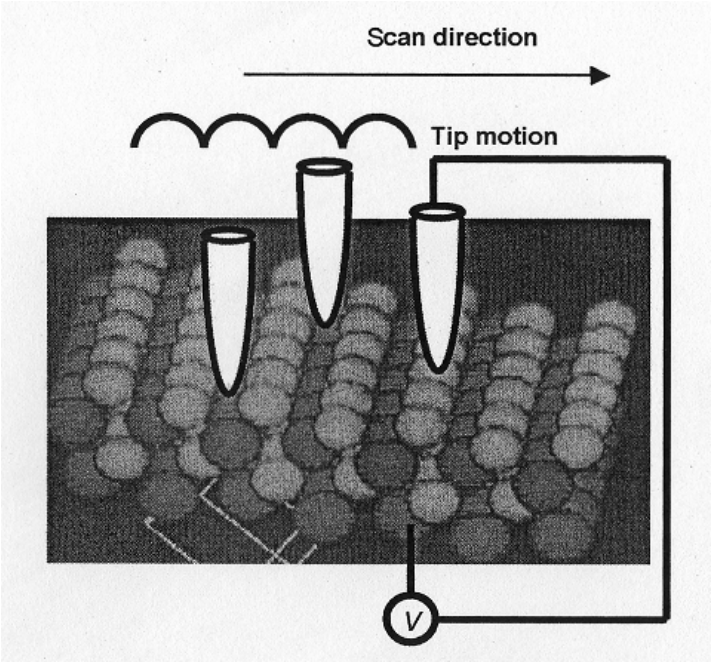

Fig.1.5. *Constant current mode, a bias potential is applied between the sample and the tip. During the tip scanning from left to right, the tip is moved vertically to keep current constant.*

It is also clear that the STM tip acts as an electrode in the electrochemical cell. As soon as a voltage is applied to the tip, a current can flow. Such Faradaic currents (the deposition of metal, or hydrogen or oxygen evolution, for example) can easily reach some hundreds of nanoamperes. Macroscopically this is negligible but, as the tunnelling currents are only some nanoamperes, the tip has to be insulated- with the exception of its very end- by a paint or by glass. Hence, the Faradaic currents can be reduced down to the picoampere range, making stable tunnelling conditions under electrochemical conditions possible.

2. Aim of the work

Aluminium plays an important role in modern industries as a light weight material in automotive and planes as well as for decorative purpose, for example. Furthermore, the high corrosion resistance of Al against chemical and atmospheric attack makes it an interesting coating material for steel. It is known that aluminium can not be electrodeposited in aqueous baths due to its reactivity ($E° = {}^{-}1.7$ V *vs.* NHE). Thus the electrodeposition process can be carried out from organic solvents or ionic liquids. Unfortunately, organic solvents are inflammable, volatile, hygroscopic and relatively complicated to handle. To avoid these disadvantages, new nonaqueous aprotic electrolytic systems for the electrodeposition of aluminium are under development. Of them, chloroaluminate ionic liquids (1^{st} generation of ionic liquids), which are prepared by mixing anhydrous $AlCl_3$ with a suitable organic chloride salt, can be used to electrodeposit aluminium. A lot of work has been done using chloroaluminate ionic liquids to get high quality aluminium and aluminium alloys deposits. A shortcoming is that the choloroaluminate ionic liquids can only be handled under inert gas atmosphere due to the hygroscopic nature of $AlCl_3$. For this reason, air and water stable ionic liquids, which can be considered as 2^{nd} and 3^{rd} generation of ionic liquids, were invented. The 3^{rd} generation ionic liquids have many advantages such as low melting points, insignificant vapour pressures, good chemical and thermal stabilities, high intrinsic conductivities, large electrochemical potential windows and low reactivity with water. In addition, they can be dried until water content below 3 ppm.

The motivations to perform the present study are:-

a) Employment of water free liquids (3^{rd} generation of ionic liquids, for example) and thus to avoid the problems raised by water in the first generation ionic liquids because these ionic liquids can be dried till water content below 3 ppm. Therefore in the present thesis, three different air and water stable ionic liquids namely, 1-butyl-1-methyl-pyrrolidinium bis(trifluoromethylsulfonyl) amide [BMP] Tf_2N, 1-ethyl-3-methyl-imidazolium bis(trifluoromethylsulfonyl) amide [EMIm] Tf_2N and trihexyltetradecyl phosphonium bis(trifluoromethylsulfonyl) amide [$P_{14,6,6,6}$] Tf_2N have been employed for electrodeposition of aluminium.

b) Is there an influence of aromatic / aliphatic cations on Al deposition?

c) Can nanocrystalline Al layers be made in this type of ionic liquids?

To achieve these purposes the following techniques have been employed:

1. Cyclic voltammetry (CV).

2. X-ray diffraction analysis (XRD).

3. Energy dispersive X-ray analysis (EDAX).

4. Scanning electron microscopy (SEM).

5. Scanning tunneling microscopy (STM).

3. Experimental work

3.1 Ionic liquids

In this thesis, three different ionic liquids namely, 1-butyl-1-methylpyrrolidinium bis(trifluoromethylsulfonyl) amide [BMP] Tf_2N, 1-ethyl-3-methylimidazolium bis(trifluoromethylsulfonyl) amide [EMIm] Tf_2N and trihexyl-tetradecyl phosphonium bis(trifluoromethylsulfonyl) amide [$P_{14,6,6,6}$] Tf_2N in ultrapure quality were employed. Prior to use, these ionic liquids were dried under vacuum for 12 hours at a temperature of 100 °C to achieve water contents below 3 ppm (by Karl–Fischer titration).

Ionic liquid	Structure		Melting point (°C)	Viscosity (mm/s)	Density (g/m)	Conductivity (mS cm^{-1})	EC window (V)
	Cation	Anion					
1-butyl-1-methylpyrrolidiniumbis (trifluoromethylsulfonyl) amide ([BMP]Tf_2N).	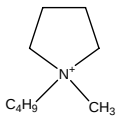	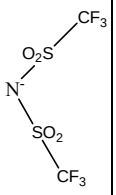	- 50	71	1.4	2.2	≈ 5.5
1-ethyl-3-methylimidazolium bis (trifluoromethylsulfonyl) amide ([EMIm] Tf_2N).	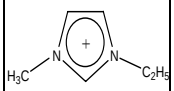	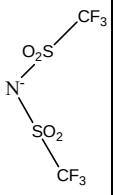	- 17	18	1.52	8.8	≈ 4.1
trihexyl-tetradecyl phosphonium bis (trifluoro-methylsulfonyl) amide ([$P_{14,6,6,6}$] Tf_2N).	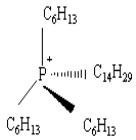	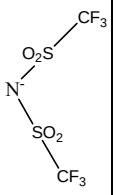	-50	401	1.07		

Table.3.1. *The structures and physical properties of three used ionic liquids (Sigma-Aldrich.com/ionic liquids).*

All liquids were stored in an argon filled glove box with water and oxygen below 1 ppm (OMNI-LAB from Vacuum-Atmospheres). The structures and physical properties of ionic liquids are shown in table (3.1).

3.2 Aluminium Salts

All chemicals were handled under a dry argon atmosphere in a glovebox. The aluminium salt is anhydrous aluminium chloride $AlCl_3$ (Fluka, 99 %) and it was used without further purification as a source of aluminium ions in the ionic liquids.

3.3 Baths

The chemical compositions of the baths used for aluminium deposition in three ionic liquids [BMP] Tf_2N, [EMIm] Tf_2N and [$P_{14,6,6,6}$] Tf_2N are listed in table (3.2).

Ionic liquid	**$AlCl_3$ concentration mol/L (M)**	**Notes**
1) 1-butyl-1-methylpyrrolidinium bis(trifluoromethylsulfonyl) amide [BMP]Tf_2N.	1.6	Two phases
2) 1-ethyl-3-methylimidazolium bis(trifluoromethylsulfonyl) amide [EMIm] Tf_2N.	5.5	Two phases
3) trihexyl-tetradecyl phosphonium bis(trifluoro-methylsulfonyl) amide ([$P_{14,6,6,6}$] Tf_2N)	4.0	One phase

Table 3.2. *The chemical compositions of baths used for aluminium deposition in three air and water stable ionic liquids.*

3.3.1 [BMP] Tf_2N bath

The ionic liquid 1-butyl-1-methylpyrrolidinium bis(trifluoromethylsulfonyl) imide [BMP] Tf_2N shows a biphasic behaviour, above a concentration of $AlCl_3$ of 1.6 M. The lower phase is colourless while the upper one is pale and more viscous. By further addition of $AlCl_3$ the volume of the lower phase decreases till reaching a concentration of 2.7 M, then only one solid phase is formed. The biphasic mixture of $AlCl_3$/ [BMP] Tf_2N becomes monophasic by heating up to a temperature higher than 80 ºC (see figure 3.1). Interestingly, we have found that Al can only be deposited from the upper phase of the biphasic mixture as will be shown in chapter (4).

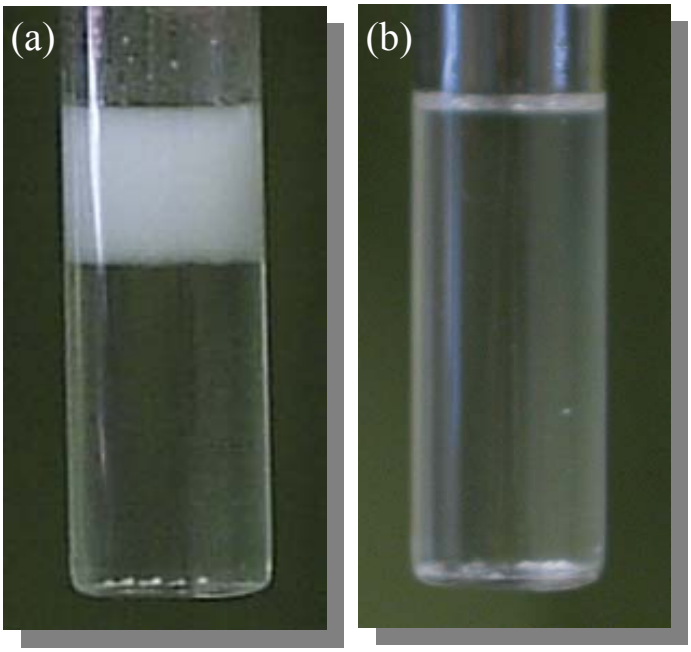

Fig.3.1. *(a) A biphasic mixture of the ionic liquid 1-butyl-1-methyl pyrrolidinium bis(trifluoromethylsulfonyl) amide containing 1.6 M $AlCl_3$ at room temperature. (b) The biphasic mixture becomes monophasic at 80 ^oC.*

3.3.2 [EMIm] Tf_2N bath

Also, the second used ionic liquid 1-ethyl-3-methylimidazolium bis(trifluoro-methylsulfonyl) amide [EMIm] Tf_2N shows a biphasic behaviour with increasing concentration of $AlCl_3$. In this ionic liquid, $AlCl_3$ can be dissolved more easily than that in the above mentioned 1-butyl-1-methylpyrrolidinium bis(trifluoromethylsulfonyl) amide [BMP] Tf_2N ionic liquid. At a concentration of $AlCl_3$ more than 2.5 M, a biphasic

mixture is formed. It is not possible to deposit Al at concentrations below 2.5 M. In contrast to the mixture $AlCl_3$/[BMP] Tf_2N, the upper phase of the mixture $AlCl_3$/ [EMIm] Tf_2N is clear and colourless while the lower one is pale and more viscous. Upon further addition of $AlCl_3$, the viscosity of the lower phase increases and it solidifies at an "added" concentration of a bit more than 5 M. The biphasic mixture also becomes monophasic by heating up to a temperature of about 80 ºC. We tried to electrodeposit Al from both phases at different $AlCl_3$ concentrations and we found that Al can only be electrodeposited from the upper phase, that is, the clear one as shown in chapter (4).

3.3.3 [$P_{14,6,6,6}$] Tf_2N bath

The ionic liquid [(tri-hexyl-tetradecyl) phosphonium] Tf_2N does not form two phases by addition of $AlCl_3$ as noted in the two previous ionic liquids [BMP] Tf_2N and [EMIm] Tf_2N. At room temperature 25 ºC, the $AlCl_3$ dissolves homogeneously up to a concentration of 1.5 M and the colour of the liquid changes by addition of $AlCl_3$ from colourless to yellow and finally to red at a concentration of 1.5 M of $AlCl_3$. Unfortunately, at this concentration (1.5 M), there are no hints for Al deposition. Therefore we have tried to increase the $AlCl_3$ concentration by dissolve more $AlCl_3$ by increasing the temperature to 150 ºC. At a concentration of 4.0 M, a dark red more viscous liquid is formed and it is still liquid after cooling down to room temperature. At this concentration (4.0 M), this mixture allows Al electrodeposition even at room temperature as will be shown in chapter (4).

3.4 Electrodes

For cyclic voltammetric and chronoamperometric techniques, gold substrates from Arrandee (gold films of 200-300 nm thickness deposited on chromium-covered borosilicate glass) and glassy carbon (Alfa) were used as working electrodes (WE), respectively. Directly before use, the gold substrates were heated in a hydrogen flame to slightly red glow for several minutes. Au (111) (gold on mica) substrates, purchased from Molecular Imaging, were used as working electrodes for in situ STM measurements. Prior to each experiment, the working surface of Au (111) was subject to heat in H_2 flame for several minutes to avoid surface contaminants. After plating, the cathode was withdrawn, washed with isopropanol and dried.

Al-wires (Alfa, 99.999%) of 0.5 cm diameter were used as reference (RE) and counter (CE) electrodes, respectively. Prior to use they are mechanically polished to remove the oxide film, rinsed with acetone and finally dried under vacuum.

3.5 Electrochemical cells

The electrochemical cell, shown in figure 3.2, was made of polytetrafluoroethylene and clamped over a Teflon covered Viton o-ring onto the substrate, thus yielding a geometric surface area of 0.3 cm^2. This cell is suitable only for measurements at room temperature. For measurements at higher temperatures, a quartz round flask with a Teflon cap, as shown in figure 3.3, was used as an electrochemical cell. Prior to use, all parts in contact with the solution were thoroughly cleaned in a mixture of 50/50 vol % H_2SO_4/H_2O_2 followed by refluxing in bi-distilled water. For STM experiments, pyrogene free water (aqua destillata ad iniectabilia) was used for refluxing instead of bi-distilled water.

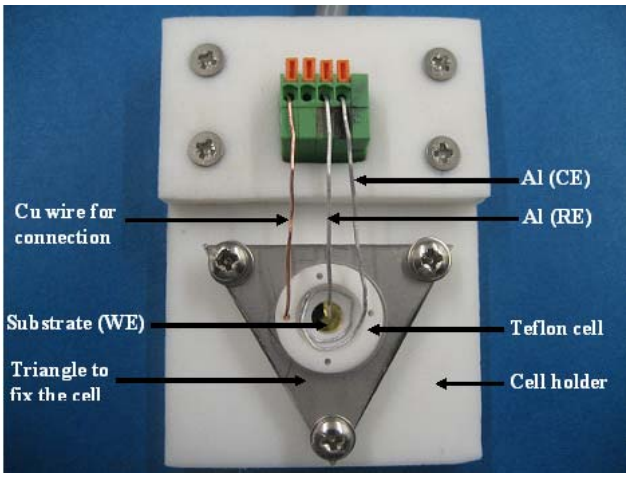

Fig. 3.2. *Electrochemical cell used for Al electrodeposition at room temperature.*

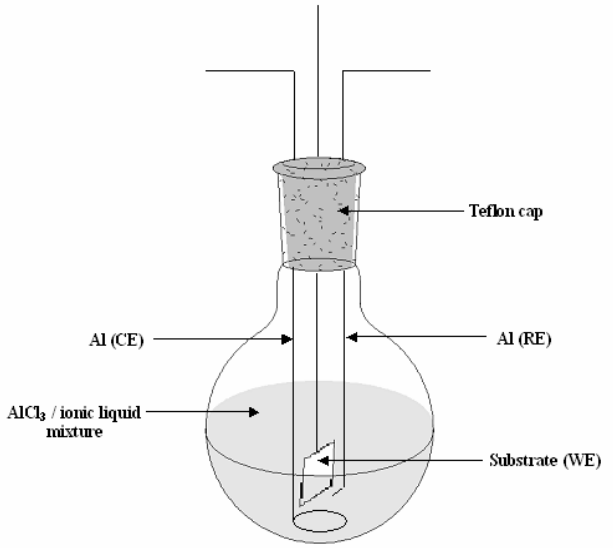

Fig. 3.3. *A schematic diagram shows the electrochemical cell used for Al electrodeposition at higher temperatures.*

3.6 Experimental techniques

3.6.1 Cyclic Voltammetry

Cyclic voltammetry is a standard analytical technique in electrochemistry. It is used for studying the redox properties of chemicals and interfacial structures. For the majority of experiments the electroactive species is dissolved in a solution. A potentiostat requires a three-electrode cell with a reference electrode (RE), a working electrode (WE), and a counter electrode (CE) (also called the secondary or auxiliary electrode). The potentiostat is required to impose on the WE a cyclic linear potential sweep and to ouput the resulting current-potential curve. There are two types of sweep, forward and reverse sweep as described in the following:

$E = E_i + \nu t$ (forward sweep)

$E = E_s - \nu t$ (reverse sweep)

Where E_i, E_s and E, are initial, switching and final potentials in volt, respectively. And ν and t are sweep (or scan) rate in V s^{-1} and time in sec, respectively. The electrochemical reaction of interest takes place at the WE. Electrical current at the WE due to electron transfer is termed *faradaic current*. A counter electrode (CE) is driven by the potentiostatic circuit to balance the faradaic process at the WE with an electron transfer of opposite direction (e.g., if reduction takes place at the WE, oxidation takes place at the CE). The process at the CE is typical not of interest, and in most experiments the small currents observed mean that the electrolytic products at the CE have no influence on the process at the WE. The faradaic current at the WE is transduced to a potential at a selected sensitivity, expressed in amperes per volt, and recorded in a digital or analog form. The CV response is plotted as current versus potential. During the forward sweep the oxidized form is reduced, while on the reverse sweep the reduced form near the electrode is reoxidized. Chemical reaction coupled to the electrode reaction can drastically affect the shape of the CV response. Cyclic voltammetry is very useful because it helps in understanding the nature of electrodeposition process. For this reason, cyclic voltammograms for Al deposition in [BMP] Tf_2N, [EMIm] Tf_2N and [$P_{14,6,6,6}$] Tf_2N ionic liquids were studied. The cyclic voltammetry measurements were performed

in an inert gas glove box using a Parstat 2263 Potentiostat/Galvanostat (Princeton Applied Research) controlled by a PowerCV software. The potential was swept in both cathodic and anodic direction with scan rate of 10 mV s^{-1}.

3.6.2 X-ray diffraction (XRD)

This technique uses Bragg's Law to determine the type and relative amount of crystalline substances in a bulk sample. In addition, the peaks of the XRD pattern can be used to determine the crystallite sizes. The crystallite sizes can be calculated using standard Sherrer's formula **[242]**:

$$D = 0.9\lambda/\beta\cos\theta$$

where D is the crystallite size in nm, λ is the radiation wavelength, θ is the diffraction peak angle, and β is the line width at half peak intensity. β can be calculated using the formula:

$$\beta^2=\beta_m^2-\beta_s^2$$

where β_m is the measured full width at half maxima (FWHM) and β_s is the FWHM of a standard silicon sample.

Therefore, the crystal structures of as deposited aluminium on glassy carbon and Au (111) substrates were examined by X-ray diffraction analysis using a Siemens D-500 diffractometer with CuK_α radiation.

3.6.3 Warren-Averbach method

The Warren-Averbach method **[217, 243]** allows the separation of size and strain effects and enables us to determine the particle size distribution. It was known that, for either distortion broadening or particle size broadening, the shape of the diffraction peak can be represented by the Fourier series.

$$P_{2\theta} = K \Sigma_n A_n (l) \cos 2\pi n h_3 \qquad (1)$$

Where $h_3 = 2 a_3 \sin\theta/\lambda$

For distortion $A_n^D(l) = (\cos 2\pi l Z_n)_{Av}$,

For particle size $A_n^P = 1/N \; \Sigma^{\infty}_{i=/n/+1} (i - /n/) n_i$.

If both types of broadening are present, the measured coefficient is the product of coefficients for each effect.

$A_n(l) = A_n^P A_n^D(l)$ (2)

If measurements are made for several orders of (00*l*), the two effects can be separated, since the distortion coefficient $A_n^D(l)$ depends upon the order, while the particle size coefficient A_n^P is independent of *l*. for small *l*, and small values of n where Z_n is also small, $[\cos 2\pi n l Z_n]$ can be approximated by an exponential.

$A_n^D(l) = [\cos 2\pi n l Z_n]_{Av} . \exp[-2\pi^2 l^2 (Z_n^2)_{Av}]$.

Writing of equation 2 in logarithmic form

$\ln A_n(l) = \ln A_n^P - 2\pi^2 l^2 (Z_n^2)_{Av}$ (3)

For several orders of a particular set of planes, a plot of $\ln A_n(l)$ *vs.* l^2 gives a curve which is a straight line for the small values of *l.* The intercept on the axis of ordinates gives $\ln A_n^P$, and the slope gives $-2\pi^2 l^2 (Z_n^2)_{Av}$ from which the mean square strain can be computed. For orders of the general plane (*hkl*) of a cubic crystal, it convenient to express $A_n^D(l)$ as $\exp[-2\pi^2 l_0^2 (\Delta L^2)/a^2]$, where $l_0^2 = h^2 + k^2 + l^2$, $L = na_3$ and $\Delta L = a_3 Z_n$.

Therefore, the particle size distributions of Al deposits in the nanometer regime on glassy carbon substrates were determined by the Warren-Averbach method.

3.6.4 Energy dispersive X-ray analysis (EDAX)

This technique is used in conjunction with SEM and is not a surface science technique. It can be used for determination of composition of surface films. Therefore, we have used this technique to determine the composition of the films formed on different substrates.

3.6.5 Scanning electron microscopy (SEM)

The surface morphology of some selected samples of the as deposited aluminium on Au (111) surfaces was investigated by using a high-resolution field emission scanning electron microscopy (Carl Zeiss DSM 982 Gemini).

3.6.6 Scanning tunneling microscopy (STM)

The STM experiments were performed with in-house built STM head (see figure 3.4b) and scanner (see figure 3.4c) under inert gas conditions with a Molecular Imaging PicoScan 2500 STM controller in feedback mode (see the principle of STM operation in chapter (1)).

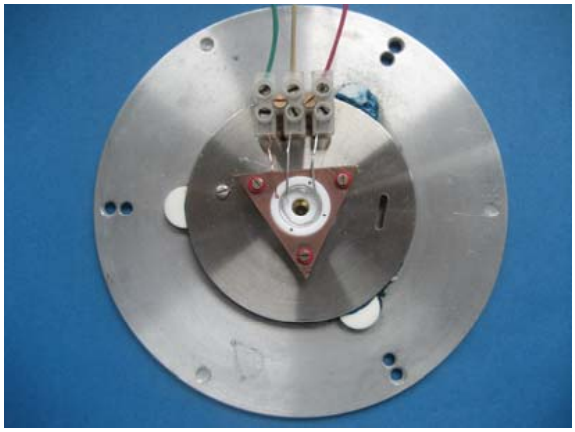

(a)

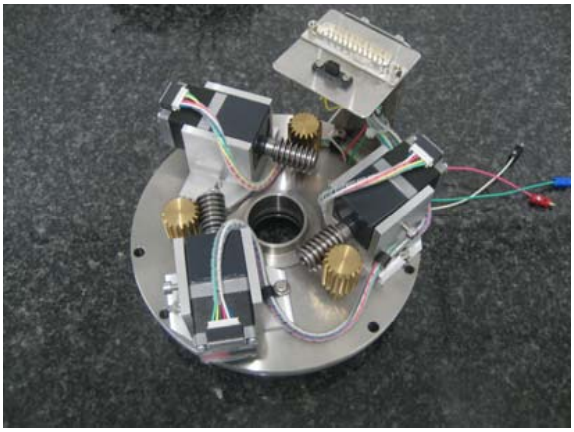

(b)

(c)

Fig. 3.4. *(a) Cell holder containing the teflon cell with electrodes. (b) STM head. (c) Scanner contains piezoelectric elements.*

Assembling of the STM head - containing step motors and micrometer screws as well as scanner, to which the tip is connected - and filling of the electrochemical cell (see figure 3.4a) were performed in argon filled glovebox and subsequently, the STM head was placed inside a vacuum tight stainless steel cylinder which was argon-filled, to be sure that the STM experiment was performed in a clean and inert gas atmosphere,

transferred to the air-conditioned laboratory with a constant temperature of 23 ± 1 °C, and placed onto a vibration-damped table from IDE. During the STM experiments the potential of the working electrode was controlled by the PicoStat from Molecular Imaging. In all experiments, all STM pictures were obtained by scanning from bottom to top with a low scan rate of 2 Hz and a resolution of 512 pixels per line.

3.6.6.1 Preparation of tips

The STM tips were prepared by electrochemical etching of 0.25 mm 90:10 Pt/Ir wires in 4.0 M NaCN solution followed by electrophoretical coating with an electropaint from BASF (ZQ 84-3225 0201) and subsequently heated to 100 ^{o}C and 200 ^{o}C for one hour and 10 minutes, respectively. This coating is sufficiently resistant against the ionic liquids without showing any detectable degradation.

Results and discussion

4. Electrodeposition of Al in different ionic liquids

4.1 Electrodeposition of Al in [BMP] Tf_2N

In this part of the thesis the electrodeposition of aluminium in 1-butyl-1-methylpyrrolidinium bis(trifluoromethylsulfonyl) amide [BMP] Tf_2N ionic liquid is presented. In this study we have used cyclic voltammetery as an electrochemical technique for the determination of the kinetics of electrode reactions during the electrodeposition process. X-ray diffractometry and scanning electron microscopy (SEM) were used to determine the crystal structure and surface morphology of aluminium deposit, respectively.

$AlCl_3$ dissolves well and homogeneously in this ionic liquid up to a concentration of about 1.5 M giving a clear solution, from which Al cannot be deposited. By further increasing of the concentration of $AlCl_3$ a biphasic mixture is obtained similar to the behaviour of several liquids based on the bis(trifluoromethylsulfonyl) amide systems described by Wasserscheid **[244]**. The lower phase is colourless while the upper one is pale and more viscous (see figure 3.1a). By adding more $AlCl_3$ the volume of the lower phase decreases till reaching a concentration of 2.7 M, then only one solid phase is obtained at room temperature. The biphasic mixture $AlCl_3$/IL becomes monophasic by heating up to a temperature of 80 ^oC as shown in figure 3.1b. The electrodeposition of Al was investigated from both phases and it was found that at room temperature Al can only be deposited from the upper phase. This can be interpreted in the light of the work of Wasserscheid **[244]** who reported first results on the biphasic behaviour of new highly acidic ionic liquids based on [cation][$(CF_3SO_2)_2N$] / $AlCl_3$. He assumed that the lower phase is formed by neutral, mixed chloro-[bis(trifluoromethylsulfonyl) amide]-aluminium species. In contrast, the upper phase contains the organic cation and a mixture of chloro [bis(trifluoromethylsulfonyl) amide]-aluminate ions. This means that reducible aluminium containing species only exist in the upper phase of the $AlCl_3$ / ionic liquid mixture and hence the electrodeposition of Al occurs only from the upper phase.

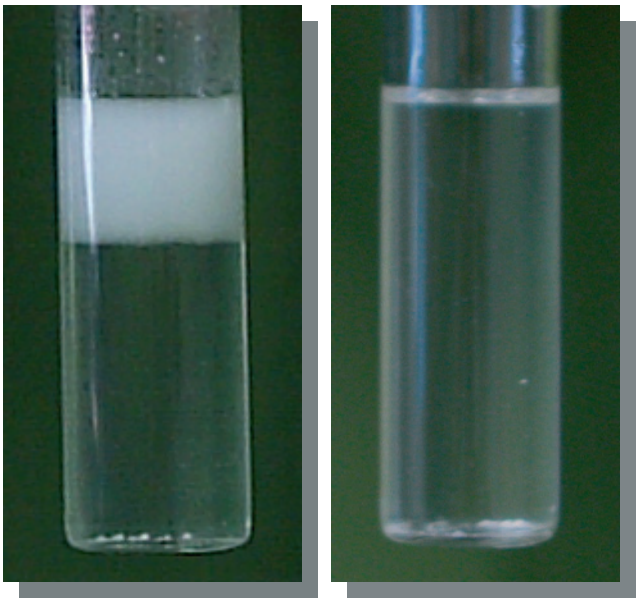

Fig. 3.1. (a) A biphasic mixture of the ionic liquid 1-butyl-1-methyl pyrrolidinium bis(trifluoromethylsulfonyl)imide containing 1.6 M $AlCl_3$ at room temperature. (b) The biphasic mixture becomes monophasic at 80 ^{o}C.

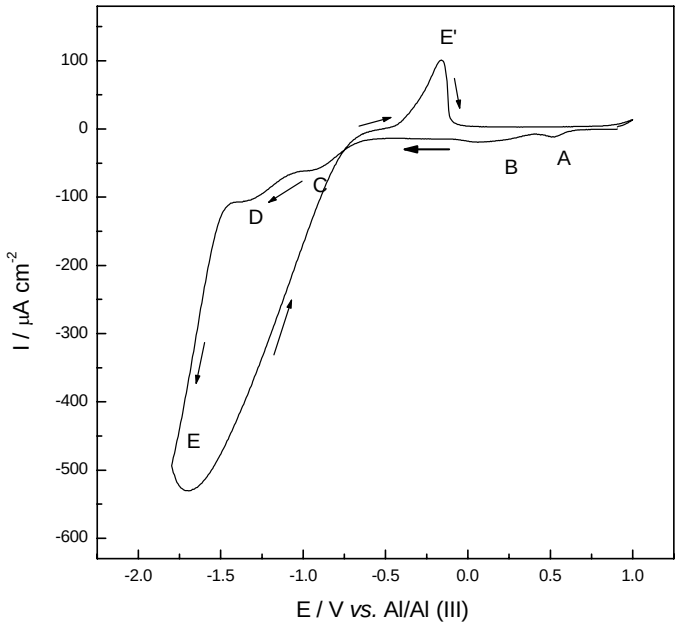

Fig. 4.1. *Cyclic voltammogram recorded at Au (111) substrate in the ionic liquid 1-butyl-1-methyl pyrrolidinium bis(trifluoromethylsulfonyl) amide containing 1.6 M $AlCl_3$ (from the upper phase of the mixture) at room temperature. The scan rate was 10 mVs^{-1}.*

Cyclic voltammetry helps in understanding the nature of the electrodeposition process. For this reason, the cyclic voltammograms for Aluminium deposition in 1-butyl-1-methylpyrrolidinium bis(trifluoromethylsulfonyl) amide [BMP] Tf_2N ionic liquid were studied.

Figure (4.1) shows a typical cyclic voltammogram of Au (111) substrate in the upper phase of the biphasic mixture of $AlCl_3$/1-butyl-1-methylpyrrolidinium bis(trifluoro-methylsulfonyl) amide at room temperature. The electrode potential was scanned cathodically from the open circuit potential to more negative values with a scan rate of 10 mV s^{-1}. All electrode potentials are referred to Al/Al (III). From the cyclic voltammogram, there is a large nucleation overpotential for the deposition of aluminium on Au (111) and the in situ STM does not show a clear aluminium underpotential deposition as is presented in chapter (5). Moreover, this cyclic voltammogram is characterized by the presence of five cathodic peaks A, B, C, D and E at potentials of about 0.4, 0.0, –1.0, –1.3 and –1.5 V, respectively. Without any information from STM one could argue that the small cathodic peaks A and B might be attributed to underpotential deposition of aluminium. At a potential of –0.7 V *vs.* Al/Al (III), the cathodic current rises with two small cathodic steps (C and D) at –1.0 and –1.3 V *vs.* Al/Al (III), respectively, that are presumably correlated to two different processes before a massive bulk growth of Al sets in. It is assumed that the two peaks (C and D) at –1.0 and –1.3 V are due to alloying between Au and Al and / or to Al electrodeposition from different Al (III) ion species in the liquid **[240]**. Furthermore, the decomposition of Tf_2N is possible. One has to take into consideration that during Al deposition, chloride is liberated. This chloride can react with Al (III) ions, diffusing to the electrode, to form other complexes with a different reduction potential. However, as is shown in chapter (5), there is no bulk deposition visible with the in situ STM in this potential regime. At a potential of –1.5 V the bulk aluminium deposition starts (process E). In the reverse scan, the cathodic current continues to flow forming a current loop, which is typical for nucleation processes. A small anodic peak (E`) is recorded on the reverse scan at a potential of about –0.17 V that is correlated to partial stripping of the as-deposited aluminium. Here, stripping seems to be kinetically hindered which is a common phenomenon in ionic liquids. From in situ STM shown in chapter (5) an explanation for the complex electrochemical behaviour is suggested.

Figure (4.2) shows the cyclic voltammograms of the upper phase of the biphasic mixture of $AlCl_3$/1-butyl-1-methylpyrrolidinium bis(trifluoromethylsulfonyl) amide on gold substrate at different temperatures, such as 25, 50, 75 and 100 ^oC. Whereas the employed ionic liquid remains stable up to at least 300 ^oC under inert gas conditions, with $AlCl_3$ a practical temperature limit on a longer timescale might be around 150 ^oC where the evaporation of $AlCl_3$ slowly begins. At a temperature of 180-190 ^oC $AlCl_3$ can be distilled under reduced pressure in such liquids. The electrode potential was scanned from the open circuit potential in the negative direction at a scan rate of 10 mVs^{-1}.

It is interesting and surprising that – reproducibly – the oxidation peak at 25 ^oC occurs at electrode potentials a bit below 0.0 V *vs.* Al/Al (III) whereas in cyclic voltammograms at 50, 75 and 100 ^oC the oxidation of the deposit begins at 0.0 V. In $AlCl_3$-based ionic liquids the Al/Al (III) couple gives, however, a very stable electrode potential at all temperatures above 0.0 ^oC. The Al/Al (III) electrode potential in liquids with the Tf_2N anion (or others) still has to be defined thermodynamically, as the Al (III) species are not yet exactly known. The cyclic voltammograms recorded at 50 and 75 ^oC exhibit a similar behaviour as that one recorded at room temperature, that is, in all cases there is a nucleation loop. At 50 ^oC there is a broad reduction process from –0.6 to –0.9 V. Then the current rises steeply at –0.9 V and less steeply at –1.1 V. These processes are correlated to Al deposition; the reduction of the organic cation begins well below –2.0 V vs. Al/Al (III). There is a slight oxidation peak located at +0.1 V. At 75 ^oC, there is only one reduction shoulder at –0.5 V, followed by a steep increase (Al deposition) beginning at –0.7 V, then by a nucleation loop, before the deposit starts to be oxidized incompletely beginning at 0.0 V. At 100 ^oC there is no evidence for nucleation and there is only one steep rising deposition current beginning at –0.2 V. The incomplete oxidation of the deposit begins at 0.0 V *vs.* Al/Al(III). In all cases the anodic peaks observed on the anodic branch of the cyclic voltammograms are due to the partial stripping of the electrodeposits, as the ratio of anodic/cathodic charge is far below 1. The visibly observable deposition of Al is highly irreversible in this ionic liquid. The oxidation of Al is likely to be hindered for kinetic reasons.

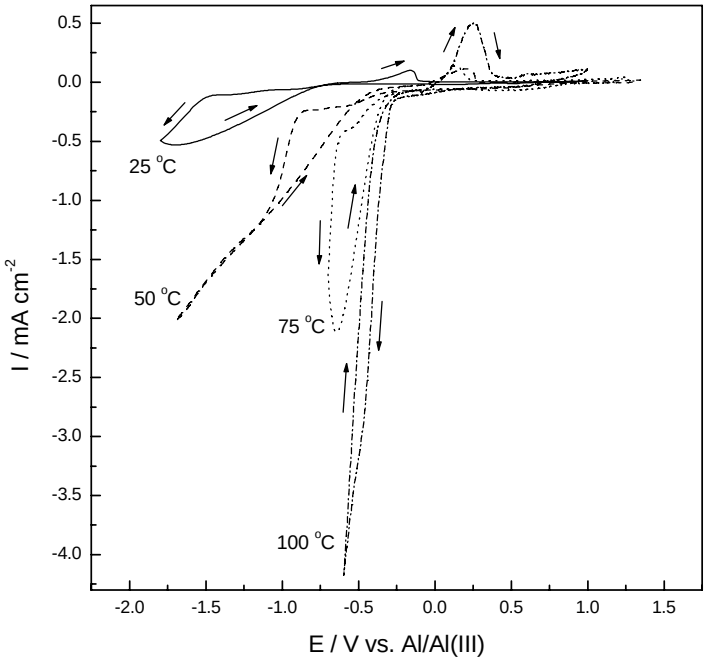

Fig. 4.2. *Cyclic voltammograms recorded at Au substrates in the ionic liquid 1-butyl-1-methyl pyrrolidinium bis (trifluoromethylsulfonyl) amide containing $AlCl_3$ 1.6 M (from the upper phase of the mixture) at different temperatures. The scan rate was 10 mV s^{-1}.*

The available data and experience in Clausthal show that Al (and also Mg) is passivated in ultrapure and well-dried liquids with the Tf_2N anion. The oxidation of Al is dependent on the available anions, which can create a complex or solvate Al (III). However, at 150 °C, where $AlCl_3$ can be dissolved up to 6.0 M in [BMP] Tf_2N, the ratio of anodic to cathodic charge is still below 1. One explanation for this complicated electrochemical behaviour will be given in the STM section (see chapter (5)). The Al electrodeposits obtained at different temperatures were investigated by means of high-resolution field–emission scanning electron microscopy (SEM). Visually, the deposits appear to be thick, shiny and well adhering to the gold substrate. Figure (4.3) shows high resolution SEM micrographs of thick layers of Al on gold substrate electrodeposited potentiostatically at 25, 50, 75 and 100 °C at potentials of – 1.7, –1.0, – 0.8 and – 0.5 V *vs.* Al/Al (III), respectively, for 2 hours. We obtain thickness between 2 and 5 µm. Generally, the electrodeposited layers contain very fine crystallites in the nanometer regime. The electrodeposits obtained at 25, 50 and 75 °C are stressed, as also observed by visual inspection (see Figs.4.3a-c). Occasionally the Al film made at room temperature peeled off, forming a cylinder. This is not too surprising since during the

electrodeposition of metals and alloys, internal or residual stress almost always appears. The stress can originate from intrinsic film stress and from interfacial stress between the deposit and substrate. Generally, this may be attributed to some factors such as coalescence of the crystallites, inclusion of foreign species or generation of structural defects **[245]**. Interestingly, the quality of the deposit obtained at 100 ^{o}C improves enormously and also the crystallites apparently become finer (Fig. 4.3d). Moreover, there is no stress in the electrodeposited Al film.

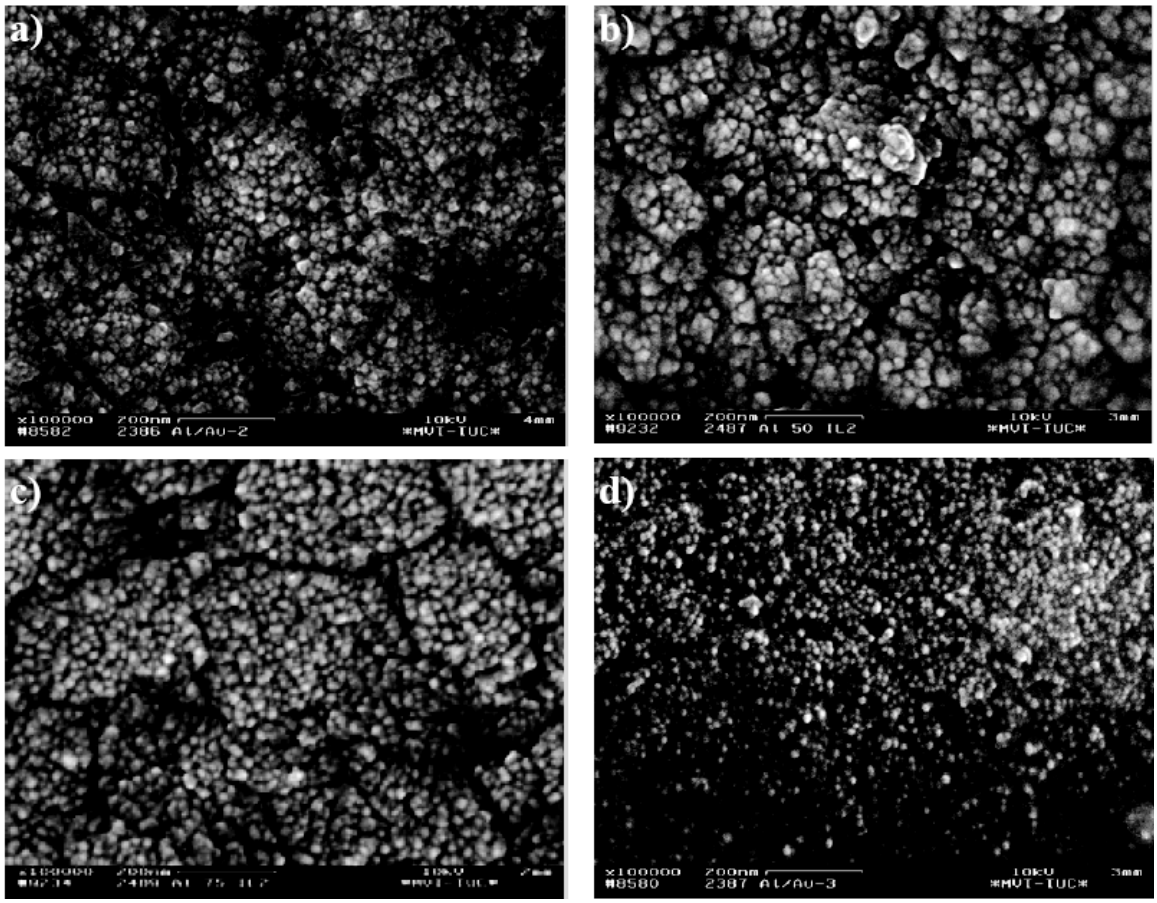

Fig. 4.3. *SEM micrographs of electrodeposited Al films on gold formed in the upper phase of the mixture $AlCl_3$/[BMP] Tf_2N after potentiostatic polarization for 2 hours at a) room temperature (E = –1.7 V, corresponding I = –0.5 mA/cm^2), b) 50 ^{o}C (E = –1.0 V, corresponding I = –1 mA/cm^2), c) 75 ^{o}C (E = –0.75 V, corresponding I = –1.7 mA/cm^2) and d) 100 ^{o}C (E = –0.45 V, corresponding I = –2 mA/cm^2).*

Figure (4.4) shows the XRD patterns of nanocrystalline Al films obtained potentiostatically in the mentioned ionic liquid on glassy carbon substrates at potentials of –1.0 and –0.5 V *vs.* Al/Al (III) at temperatures of 50 ^{o}C and 100 ^{o}C, respectively. For XRD

measurements and analysis of the grain sizes of Al by Scherrer or Warren-Averbach, gold is a less favoured substrate as its XRD patterns overlap with the patterns of Al thus making the analysis of thin films difficult. Therefore we selected glassy carbon as a substrate. At 25 ºC only Al films of less than 100 nm thickness were obtained. The deposition of Al on glassy carbon or highly oriented pyrolytic graphite (HOPG) is strongly hindered at room temperature. With our XRD device, patterns of such thin films cannot be obtained. For the samples made at 50, 75 and 100 ºC, it is clearly seen that the XRD patterns show the characteristic peaks of crystalline Al. The peaks are broad, indicating the small crystal size of the electrodeposited Al and the width of the peaks slightly decreases as the temperature increases upon electrodeposition. The average grain size of Al is determined from the full width at half maximum (FWHM) of the 100 % peak [Al(111)] using Scherrer's equation **[242]** and is 40 and 34 nm at 50 and 100 °C, respectively. It is remarkable that the average grain size is quite similar.

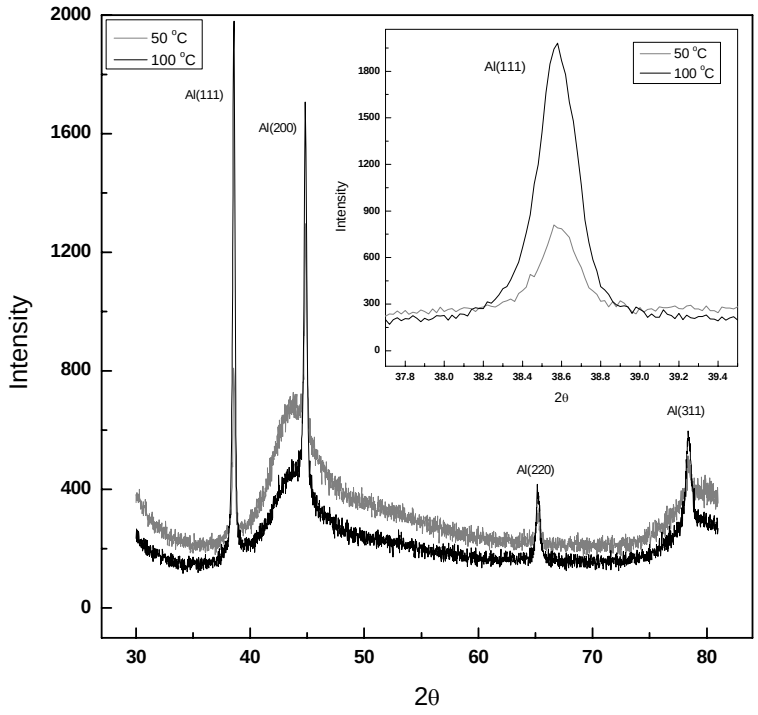

Fig. 4.4. *XRD patterns of electrodeposited Al films on glassy carbon formed in the upper phase of the mixture $AlCl_3$/[BMP] Tf_2N after potentiostatic polarization for 2 hours at 50 ^oC (E = -1.0 V, corresponding I = -2 mA/cm^2) and 100 ^oC (E = -0.5 V, corresponding I = -3 mA/cm^2). Inset: FWHM of Al(111) peak of XRD patterns*

In order to get more information on the size distribution of the nanocrystalline aluminium, a Warren-Averbach analysis was performed, (Fig. 4.5). It is clear from Figure (4.5) that the sizes of Al crystallites prepared at 50 °C range from 5 to 60 nm and most of the crystallites are of about 20 nm. At 100 °C, the average sizes of the crystallites ranges between 20 and 65 nm with a maximum around 40 nm. This analysis shows that the temperature in the electrodeposition does not seem to play a significant role, as the grain size distributions are similar. At 75 °C the particle size distribution is in between those at 50 °C and 100 °C, but it can vary a bit from deposit to deposit.

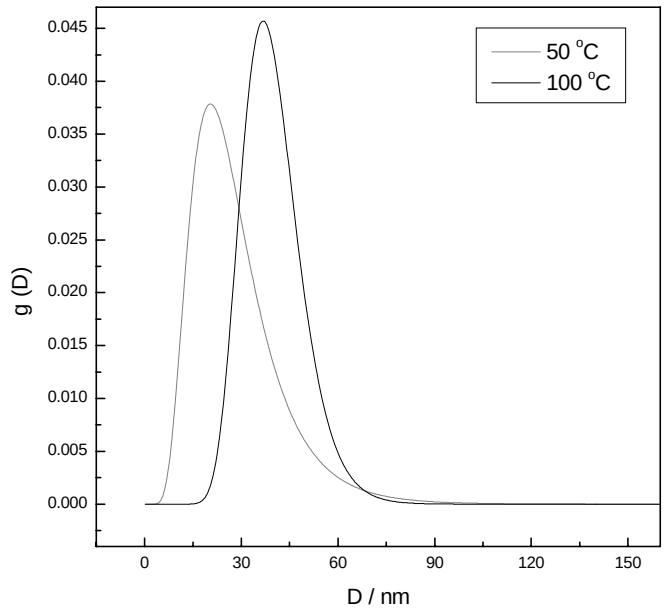

Fig. 4.5 *The size distribution of Al nanoparticles determined from the Warren-Averbach analysis.*

Typical thicknesses of the samples are between 2 and 5 μm. Although the crystal size of aluminium prepared in this way is in an interesting size regime, we were not able to make aluminium deposits with average grain sizes above 100 nm. Nanocrystalline aluminium in the bulk phase or as coating is an interesting material because by decreasing the particle size an increase in hardness is usually observed. A "hard" aluminium coating on reactive substrates such as mild steel is interesting for corrosion protection. Furthermore, nano-Al (or nano aluminium alloys) is a precursor to nano-Al_2O_3.

It can be concluded that under the applied conditions aluminium is deposited as a nanocrystalline metal from $AlCl_3$ in [BMP] Tf_2N.

4.2 Electrodeposition of Al in in [EMIm] Tf_2N

In the present part, attempts were done to electrodeposit dense and adherent aluminium films onto different substrates such as Au and glassy carbon in 1-ethyl-3-methylimidazolium bis(trifluoromethylsulfonyl) amide [EMIm] Tf_2N ionic liquid. As mentioned above an influence of the cation on morphology should be investigated. Therefore, cyclic voltammetery as an electrochemical technique to understand the electrochemical process of aluminium deposition in this ionic liquid was employed. The crystal structure of as-deposited aluminium was examined by X-ray diffraction analysis (XRD) and the surface morphology of some selected samples of the as-deposited aluminium on Au substrates was examined by using scanning electron microscopy (SEM).

Similar to the $AlCl_3$/[BMP] Tf_2N mixture, $AlCl_3$/[EMIm] Tf_2N also shows a biphasic behaviour with increase in the concentration of $AlCl_3$, as found first by Wasserscheid **[244]**. Here, $AlCl_3$ dissolves well in the ionic liquid [EMIm] Tf_2N up to a concentration of about 2.5 M, then a biphasic mixture is obtained on further addition of $AlCl_3$. It is not possible to deposit Al at concentrations below 2.5 M, which implies that the Tf_2N anion reacts with $AlCl_3$ to form a stable complex that is not reduced within the liquid electrochemical window. In contrast to the mixture $AlCl_3$/[BMP] Tf_2N, the upper phase of the mixture $AlCl_3$/[EMIm] Tf_2N is clear and colourless while the lower one is pale and more viscous. Upon further addition of $AlCl_3$, the viscosity of the lower phase increases and it solidifies at a concentration little bit more than 5 M. The biphasic mixture, also, becomes monophasic by heating up to a temperature of about 80 ^oC. We tried to electrodeposit Al from both phases at different $AlCl_3$ concentrations and we found that Al can only be electrodeposited from the upper phase, that is, the clear one. This can be ascribed to the presence of a reducible aluminium containing species only in the upper phase of the biphasic mixture. As discussed before aluminium containing species exist only in the upper phase of the $AlCl_3$/[EMIm]Tf_2N mixture and hence the electrodeposition of Al occurs only from the upper phase. $AlCl_3$ concentrations of, for example, 0.1 or 1.0 M (monophasic) do not allow aluminium electrodeposition. It would be interesting to analyse the phases formed on addition of $AlCl_3$ to the employed ionic

liquids, [BMP] Tf_2N and [EMIm] Tf_2N, e.g. by RAMAN spectroscopy and mass spectroscopy in order to get more information on the chemical structure of the reducible aluminium containing species.

Figure (4.6) shows the cyclic voltammogram of the upper phase of the biphasic mixture of $AlCl_3$ / [EMIm] Tf_2N ($AlCl_3$ concentration : 5 M) on a gold substrate at 25 ^oC. Scans were initially swept cathodically from the open circuit potential (1.1 V *vs.* Al/Al(III)) with a rate of 10 mV/s. The onset of bulk deposition of aluminium starts at a potential of about – 0.2 V *vs.* Al/Al (III) as indicated by the reduction peak (C) observed in the forward scan.

Furthermore the current density at 25 ^oC is quite similar to the current density in [BMP] $Tf_2N/AlCl_3$ at 100 ^oC. This is likely due to the viscosity of the upper phases of [EMIm]$Tf_2N/AlCl_3$ and [BMP]$Tf_2N/AlCl_3$ at 25 and 100 ^oC which are quite similar from simple visual observations. For some more information on the viscosity of ionic liquids and challenges in viscosity measurements we refer to an excellent paper from VanderNoot **[246]**. The anodic peak (C´) recorded on the backward scan is correlated to the stripping of the electrodeposited aluminium. The ratio of anodic to cathodic charge is equal to the unity within the experimental error, suggesting the complete stripping of Al electrodeposits which was evidenced by in situ STM measurements in chapter (5). In figure (4.7) the UPD regime is depicted. The cyclic voltammogram shows distinct features both in the forward and reverse scans. There is a direct correlation between processes A and A` and C and C`. A significant overpotential attributed to nucleation was found for Al bulk deposition (peak C) with a sharp corresponding stripping peak of bulk aluminium, C`, at about 0.05V *vs.* Al/Al (III). The two additional cathodic peaks (A and B) at 0.55 V and – 0.02 V *vs.* Al/Al (III) are correlated to aluminium UPD and 3D aluminium cluster formation in the beginning of the OPD regime, respectively, as evidenced by STM results presented in chapter (5). On the reverse scan, the dissolution peak C` for aluminium bulk deposition is followed by a peak A` at a potential of about 0.55 V which can be assigned to the dissolution of aluminium deposited in the UPD regime.

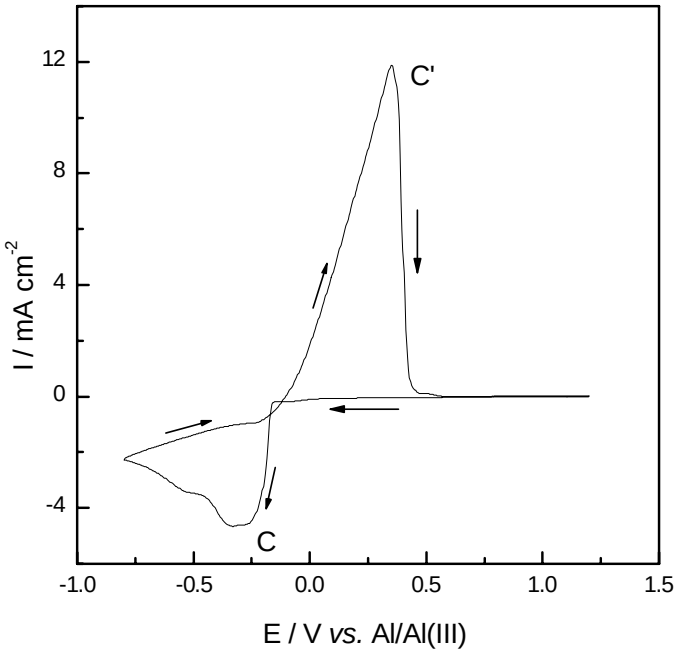

Fig. 4.6. *Cyclic voltammogram recorded at Au substrate in the ionic liquid 1-ethyl-3-methyl imidazolium bis (trifluoromethylsulfonyl) amide saturated with $AlCl_3$ (from the upper phase of the mixture) at room temperature. The scan rate was 10 mV s^{-1}.*

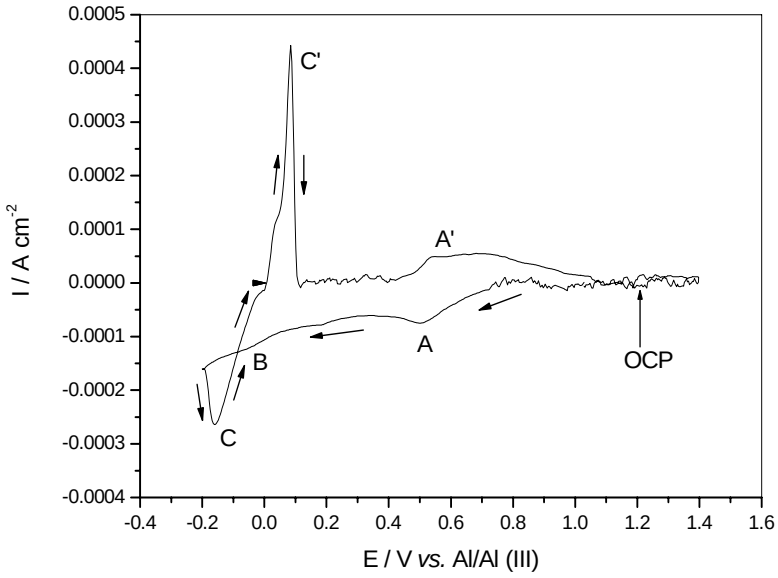

Fig. 4.7 *a typical cyclic voltammogram for aluminium deposition and stripping on Au(111) in the upper phase of the biphasic mixture of $AlCl_3$ / [EMIm] Tf_2N at room temperature (25 ^oC) showing the Al UPD process. Scan rate: 10 mVs^{-1}.*

The effect of increasing temperature, that is, 50, 75 and 100 ^{o}C, on the cyclic voltammograms of the upper phase of the biphasic mixture of $AlCl_3$ / [EMIm] Tf_2N on gold substrate is shown in Figure (4.8). As seen the cyclic voltammograms exhibit the same general feature of the cyclic voltammogram recorded at 25 ^{o}C. The deposition potential slightly shifts to less negative values on increasing the temperature. Furthermore, the peak currents of both deposition and stripping peaks significantly increase with rising temperature. This is ascribed to the increased mobility of the electroactive species towards the electrode surface, which, in turn, leads to accelerating the reaction rate of both reduction and oxidation. It is known that the conductivity and viscosity of such types of ionic liquids are strongly dependent on temperature **[246]**.

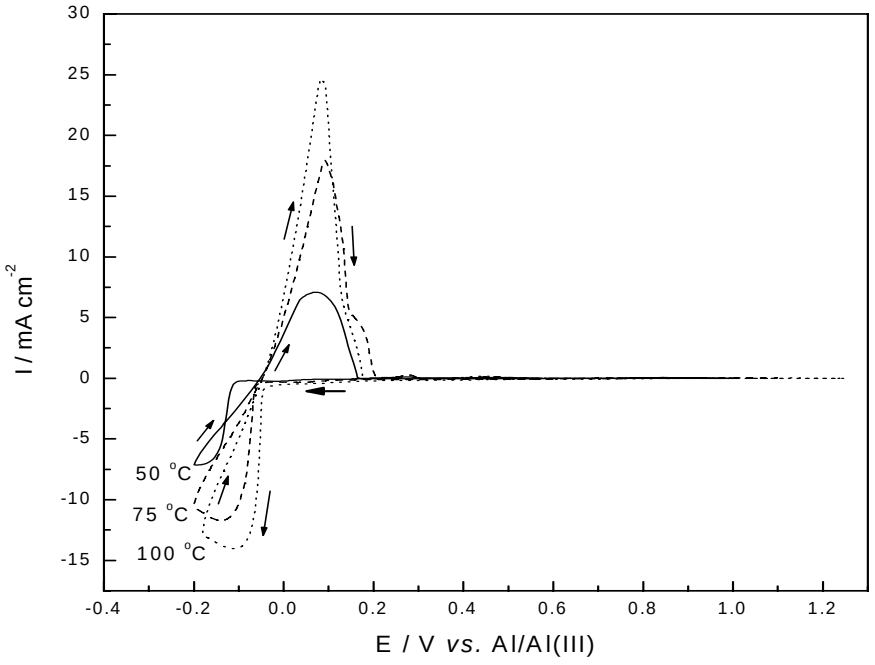

Fig. 4.8. *Cyclic voltammograms recorded at Au substrate in the ionic liquid 1-ethyl-3-methyl imidazolium bis (trifluoromethylsulfonyl) amide saturated with $AlCl_3$ (from the upper phase of the mixture) at different temperatures, 50, 75 and 100 ^{o}C. The scan rate was 10 mV s^{-1}.*

The SEM micrographs of Fig. 4.9 show the effect of increasing temperature, from room temperature up to 100 ^{o}C, on the surface morphology of the electrodeposits. The deposits were obtained potentiostatically at 25, 50, 75 and 100 ^{o}C and at potentials of – 0.3, –0.1, –0.08 and –0.06 V *vs.* Al/Al (III), respectively, for 1 hour on gold substrates.

In all cases the deposits are compact, dense and contain coarse cubic-shaped microcrystallites with film thichness from 1 to 5 μm. As the deposition potentials only slightly differ, this trend is expected due to the grain growth of the deposited crystallites and the increased mass transport in the liquid at high temperatures.

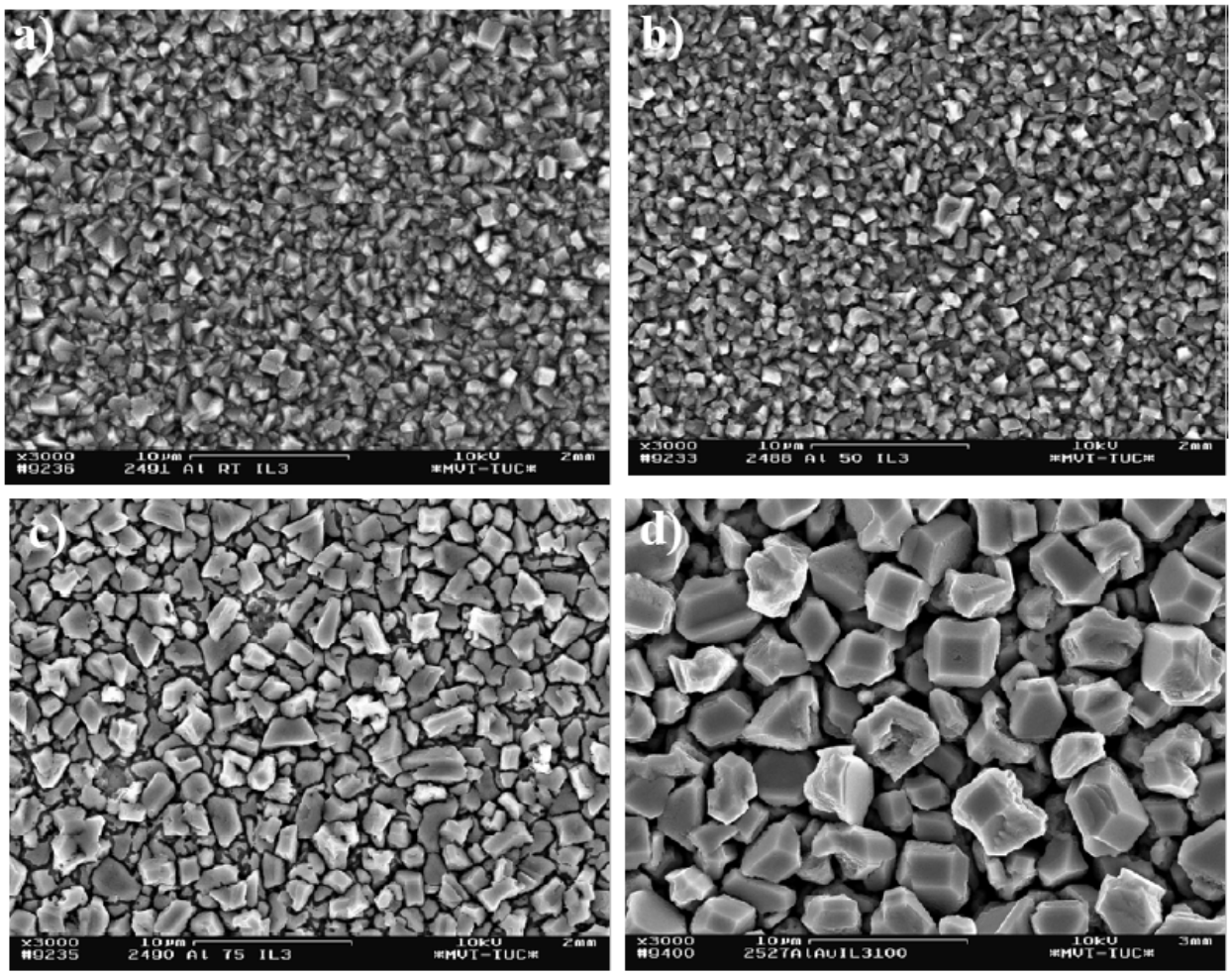

Fig. 4.9. *SEM micrographs of electrodeposited Al films on gold formed after potentiostatic polarization for 1 hour in the upper phase of the mixture $AlCl_3$ / [EMIm] Tf_2N at a) 25 ^oC (E = –0.3 V, corresponding I = –1 mA/cm^2), b) 50 ^oC (E = –0.135 V, corresponding I =–2.5 mA/cm^2), c) 75 ^oC (E = –0.082 V, corresponding I = –3.5 mA/cm^2) and d) 100 ^oC (E = –0.055 V, corresponding I = –4 mA/cm^2).*

The XRD patterns of a thick Al film electrodeposited potentiostatically at – 0.3 V for 2 hours and at 100 ^oC on gold substrates, Au (111), show only one peak of Al (111), (Fig. 4.10). This means that under such experimental conditions, electrodeposited aluminium is textured presumably du to epitaxial growth on the (111) oriented substrate. The peak is sharp indicating the large crystal size of the electrodeposited aluminium. This

is consistent with the SEM results, which show that the crystal size is in the micrometer regime, (Fig. 4.9d). On the other hand, polycrystalline aluminium films have been obtained on glassy carbon substrates at different temperatures, (Fig. 4.11) indicating that the crystal orientation of the substrate plays an important role in the crystallization of the deposits.

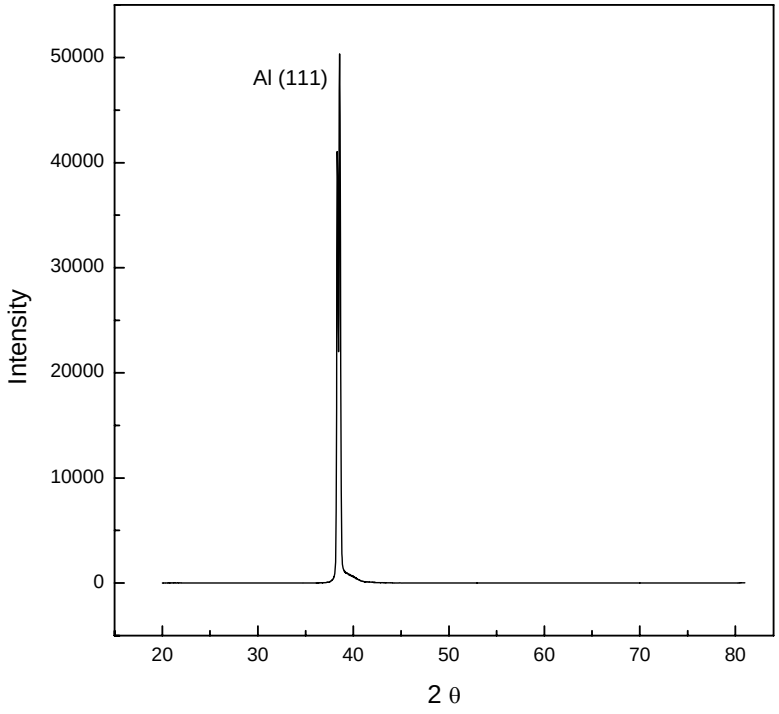

Fig. 4.10. *XRD patterns of an electrodeposited Al layer obtained potentiostatically at – 0.3 V (corresponding I = -4 mA/cm^2) for 2 hours on gold substrate in the upper phase of the mixture $AlCl_3$ / [EMIm]Tf_2N at 100 ^oC.*

In the light of the aforementioned results, it is concluded that in the employed imidazolium based ionic liquid the deposit is always microcrystalline at temperatures between 25 and 100 ^oC, whereas in the pyrrolidinium based liquid in the same temperature range it is preferably nanocrystalline. Furthermore, the reoxidation of the formerly deposited aluminium is complete in the case of [EMIm] Tf_2N and incomplete in the case of [BMP]Tf_2N, a possible further explanation might be that pyrrolidinium ions are adsorbed on the Al deposit thus acting as a grain refiner leading both to a nanocrystalline deposit and to incomplete oxidation. It is well known in aqueous electrochemistry that brighteners such as crystal violet, coumarine, saccharine and others

can hinder metal stripping. We found one reference in the literature where a series of N-alkyl-N-methylpyrrolidinium halides were investigated as a new class of cationic surfactants for variety of applications **[247]**. Viscosity effects alone are rather unlikely as the viscosities of $AlCl_3$/[BMP]Tf_2N at 100 ^oC and of $AlCl_3$ / [EMIm]Tf_2N at 25 ^oC are quite similar. Currently it is an open question why the grain size in [BMP] Tf_2N/$AlCl_3$ and [EMIm]Tf_2N/$AlCl_3$ is so dramatically different.

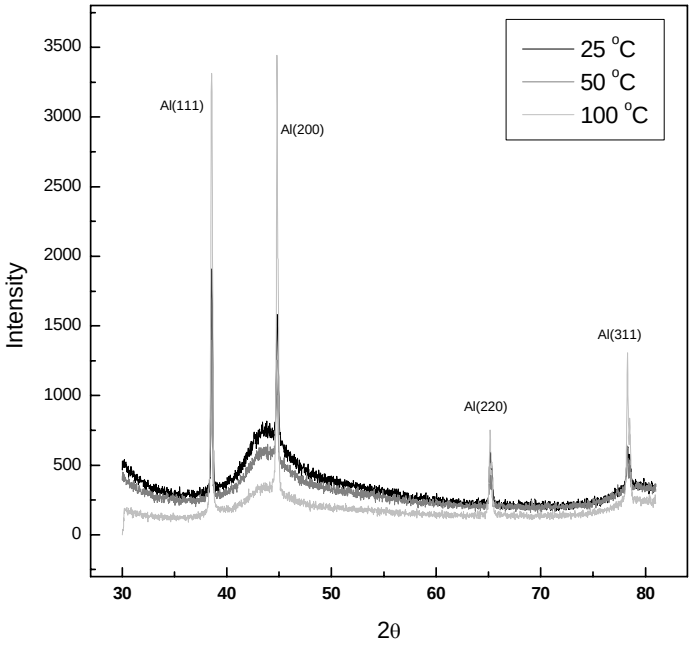

Fig. 4.11. *XRD patterns of electrodeposited Al films on glassy carbon formed after potentiostatic polarization for 2 hours in the upper phase of the mixture AlCl3 / [EMIm] Tf2N at 25 ^oC (E = -0.35 V, corresponding I = -4.5 mA/cm2), 50 ^oC (E = -0.15 V, corresponding I = -18 mA/cm2) and 100 ^oC (E = –0.12 V, corresponding I = -20 mA/cm^2).*

In Situ STM measurements (see chapter (5)) show that in contrast to Al from [BMP] Tf_2N there is clearly an underpotential deposition of Al on Au (111) in [EMIm] Tf_2N.

Also it can be concluded that, microcrystalline Al was deposited from [EMIm] Tf_2N ionic liquid and the particle size was strongly dependent on temperature, the particle size of Al crystallites was increased by increasing temperature.

4.3 Electrodeposition of Al in [(tri-hexyl-tetradecyl) phosphonium] Tf_2N

The objective of the present section, is to investigate Al deposition in trihexyl-tetradecyl phosphonium bis(trifluoromethylsulfonyl) amide ($[P_{14,6,6,6}]$ Tf_2N) ionic liquid which has a bulky cation. We have employed cyclic voltammetery as an electrochemical technique. The crystal structure and the surface morphology of as-deposited aluminium layers were examined by X-ray diffraction analysis (XRD) and scanning electron microscopy (SEM), respectively.

We have employed this ionic liquid, as the polarizability of long chain phosphonium cations should lie in the range between imidazolium and pyrrolidinium cations. If adsorption of the cations to growing Al nuclei plays a role we might see a difference in the grain sizes of the electrodeposits. Unlike in the case of [BMP] Tf_2N and [EMIm] Tf_2N, the ionic liquid [(tri-hexyl-tetradecyl) phosphonium] Tf_2N does not show biphasic behaviour on addition of $AlCl_3$. Here, $AlCl_3$ dissolves homogeneously up to a concentration of 1.5 M at 25 ^oC and the colour of the liquid changes on addition of $AlCl_3$, from colourless to yellow, turning to red at a concentration of 1.5 M $AlCl_3$. This colour change might be due to charge transfer complexes, or may be due to the presence of low amounts of residual organic impurities. The electrodeposition of aluminium is investigated in this ionic liquid with 1.5 M $AlCl_3$ at different temperatures. Unfortunately aluminium cannot be deposited even at elevated temperatures, i.e., up to 150 ^oC as in the previous cases. Further additions of $AlCl_3$, up to a concentration of 4.0 M, can only be dissolved by increasing the temperature up to 150 ^oC forming a dark red more viscous liquid. In this mixture aluminium can then be deposited even if the liquid is cooled down to room temperature.

Figure (4.12) exhibits the cyclic voltammogram of the ionic liquid trihexyl-tetradecyl phosphonium Tf_2N containing 4.0 M $AlCl_3$ made at 150 ^oC and cooled down to 25 ^oC on gold substrate at 25 ^oC. As seen, a small cathodic step is recorded in the cathodic branch of the cyclic voltammogram at a potential of – 0.2 V which maybe due to Au/Al alloying **(see [240])**. At a potential of about – 0.3 V *vs.* Al/Al (III), it is noted that the cathodic current increases gradually, not sharply as in the case of [EMIm] Tf_2N ionic liquid, and this may attributed to the high viscosity of $[P_{14,6,6,6}]$ Tf_2N ionic liquid. The increasing of cathodic current at that potential

(–0.3 V) is due to the bulk Al electrodeposition. The recorded anodic peak is correlated to the complete stripping of the electrodeposited aluminium.

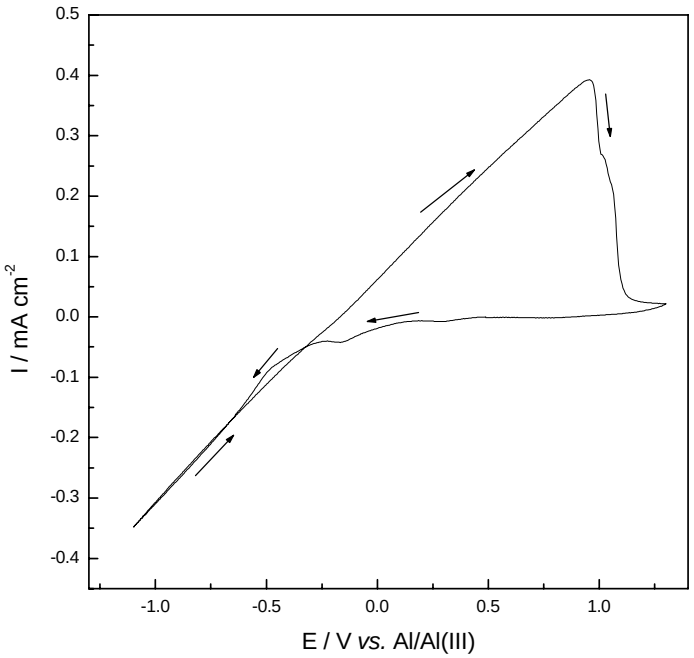

Fig. 4.12. *Cyclic voltammogram of the ionic liquid trihexyl-tetradecyl phosphonium Tf_2N containing 4.0 M $AlCl_3$ on gold substrate at room temperature.*

Fig. 4.13. represents the cyclic voltammograms of the ionic liquid trihexyl-tetradecyl phosphonium Tf_2N containing 4.0 M $AlCl_3$ on gold substrates at different temperatures, 50, 100 and 150 ^oC. As shown from the figure, all cyclic voltammograms are similar to that recorded at 25 ^oC. The onset of aluminium deposition occurs at less negative potentials i.e., the deposition potentials of aluminium decrease as the temperature increases and this is may be attributed to the decrease in the overpotential of aluminium deposition. A rise of temperature also enhances the diffusion rate of reducible aluminium ions species to the cathode surface. The both cathodic and anodic currents increase as the temperature increases. A second anodic peak observed on the anodic branch of the cyclic voltammograms recorded at temperatures of 50 and 100 ^oC is presumably correlated to Au-Al alloys.

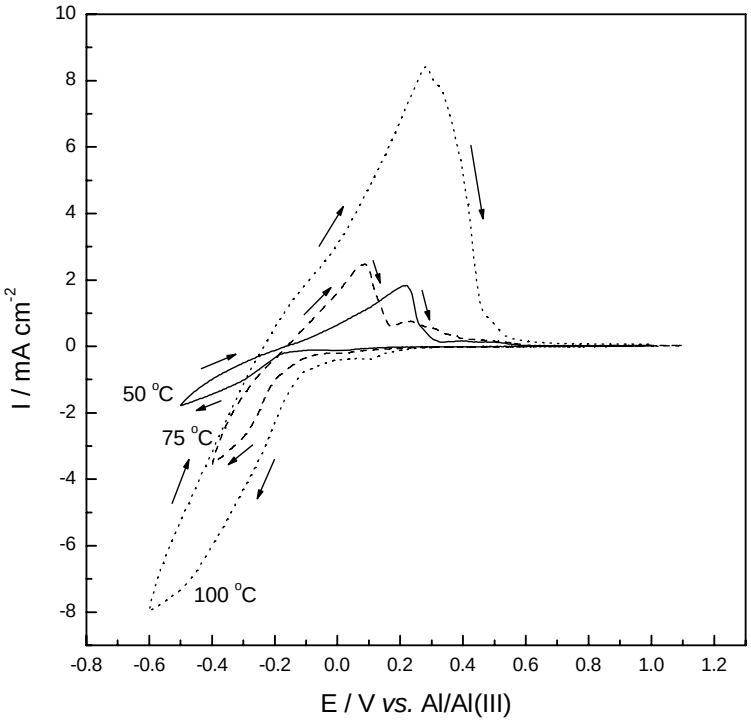

Fig. 4.13. *Cyclic voltammograms of the ionic liquid trihexyl-tetradecyl phosphonium Tf_2N containing 4.0 M $AlCl_3$ on gold substrates at different temperatures.*

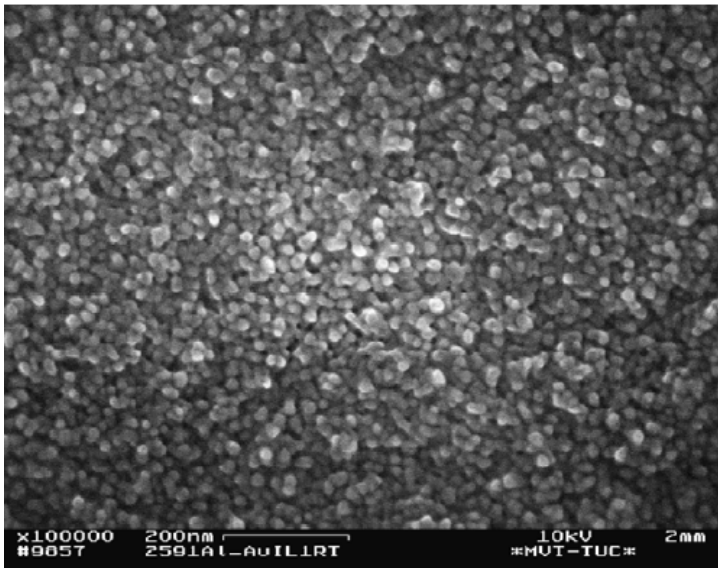

Fig. 4.14. *SEM micrograph of electrodeposited Al on gold formed after potentiostatic polarization at –1.1 V (corresponding I = – 0.3 mA/cm^2) for 1 hour in the ionic liquid trihexyl-tetradecyl phosphonium Tf_2N containing 4.0 M $AlCl_3$.*

Figure 4.14. shows the surface morphology of the as deposited aluminium film produced potentiostatically on Au substrate at –1.1 V (*vs.* Al/$AlCl_3$) for one hour. Visually, a shining, thin aluminium film is formed on the surface with mirror-like appearance. The SEM micrograph of such Al film shows that the layer contains very fine crystallites with an average size of about 20 nm. Figure 4.15. displays the EDAX profile of the film deposited on Au at –1.1 V for one hour in the ionic liquid trihexyl-tetradecyl phosphonium Tf_2N containing 4.0 M $AlCl_3$ and at room temperature. The electrodeposit is analysed as Al with some oxygen, due to the exposure to air.

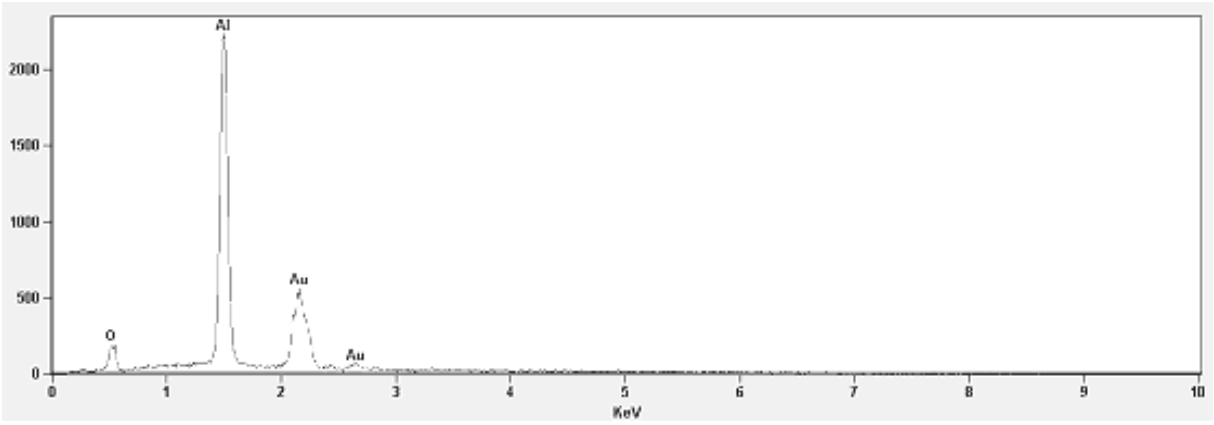

Fig. 4.15. *EDAX profile for the area shown in the SEM micrograph (Fig. 4.14).*

The XRD patterns of electrodeposited Al films obtained potentiostatically at – 0.4 V in the ionic liquid trihexyl-tetradecyl phosphonium Tf_2N containing 4.0 M $AlCl_3$ on glassy carbon substrate at 150 ^oC are shown in Fig. 4.16. The XRD patterns show the characteristic peaks of crystalline Al and the peaks are broad indicating a small crystal size of the electrodeposit. The average grain size from the Scherrer's equation is calculated to be 34 nm. The particle size distribution of such nanocrystalline aluminium film determined by a Warren-Averbach analysis is displayed in Figure (4.17). As manifested, the sizes of Al crystallites range from 10 to 80 nm and most of the crystallites have sizes of about 35 nm.

As a consequence, in this phosphonium cation based ionic liquid we can get nanocrystalline Al even at 150 ^oC. In contrast to ionic liquids based on the pyrrolidinium cation the process is reversible, In a possible future technical process to make nano-Al by electrochemical means, an Al sacrificial anode might be employed. Our results emply

that similar to the observations in [BMP] Tf_2N, the temperature does not play a dominant role on the particle sizes.

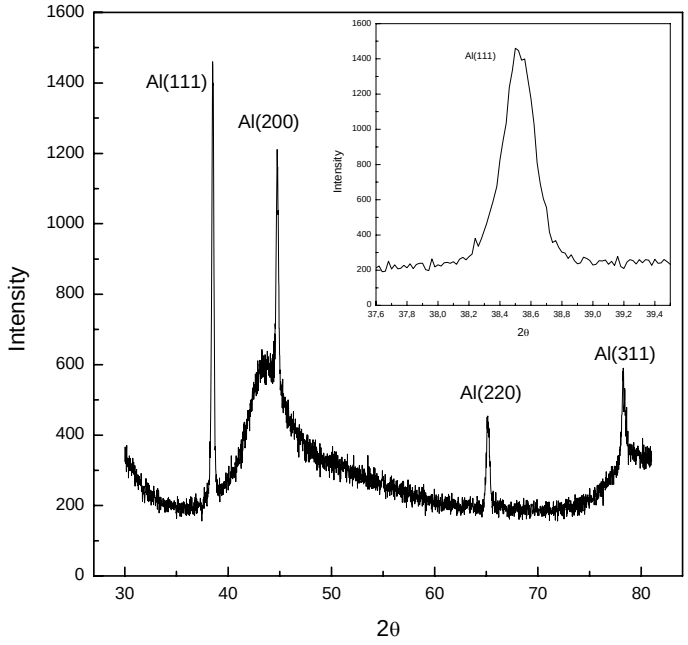

Fig. 4.16. *XRD patterns of electrodeposited Al films on glassy carbon formed after potentiostatic polarization at – 0.4 V (corresponding I = –3 mA/cm^2) for 2 hours in the ionic liquid trihexyl-tetradecyl phosphonium Tf_2N containing 4 M $AlCl_3$ at 150 ^{o} C. Inset: FWHM of Al(111) peak of XRD patterns*

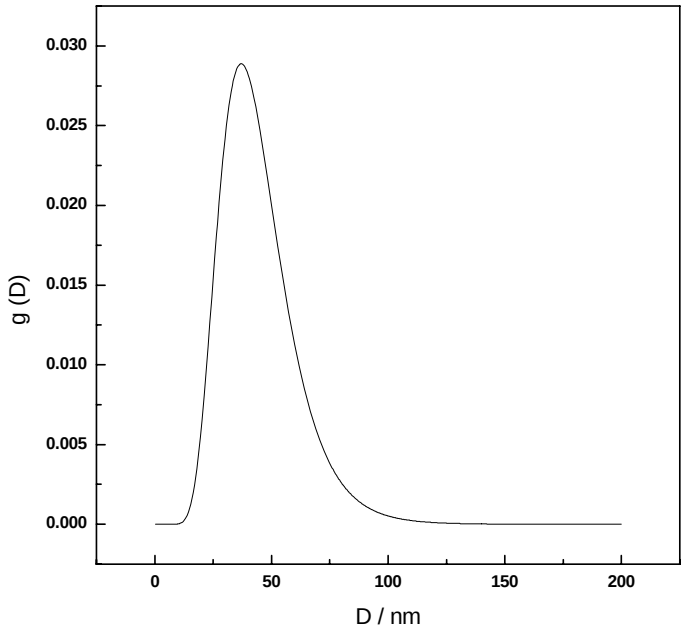

Fig. 4.17. *The size distribution of Al nanoparticles determined from the Warren-Averbach analysis.*

The results presented in this chapter can be summarized as the following. The two ionic liquids [BMP] Tf_2N and [EMIm] Tf_2N exhibit a biphasic behaviour in the $AlCl_3$ concentration range from 1.6 to 2.5 M and from 2.2 to 5.5 M, respectively. The two phases in the two ionic liquids can be changed to one phase by increasing the temperature to 80 ^oC. It was surprising that only the upper phase allows Al electrodeposition due to the presence of reducible aluminium containing species in this phase. In the case of [BMP] Tf_2N ionic liquid, the electrodeposition process is highly irreversible and the obtained deposits are shiny, dense and adherent with very fine crystallites in the nanometer regime. The quality of the Al deposits was improved by increasing the operating temperature to 100 ^oC. The average grain size of Al determined from Scherrer's equation is 40 and 34 nm at 50 and 100 °C, respectively. Warren-Averbach analysis showed that the sizes of Al crystallites prepared at 50 ^{o}C range from 5 to 60 nm and most of the crystallites are of about 20 nm. At 100 ^{o}C, the average sizes of the crystallites range between 20 and 65 nm with a maximum around 40 nm. This analysis shows that the temperature in the electrodeposition does not seem to play a significant role, as the grain size distributions are similar. In contrast, The Al deposits obtained from the second ionic liquid [EMIm] Tf_2N were compact, dense and contained coarse cubic-shaped microcrystallites with thickness ranges from 1 to 5 μm. The electrodeposition process is completely reversible. The sizes of the cystallites are strongly dependent on temperature. The size of the crystallites increases with increasing temperature. Unlikely, the ionic liquid [(tri-hexyl-tetradecyl) phosphonium] Tf_2N does not show a biphasic behaviour on addition of $AlCl_3$. Here, $AlCl_3$ dissolves homogeneously up to a concentration of 1.5 M at 25 ^oC. Unfortunately, aluminium cannot be deposited even at elevated temperatures at this concentration. By increasing the concentration of $AlCl_3$ to 4.0 M, $AlCl_3$ dissolution process was carried out at 150 ^oC forming a dark red more viscous liquid, from which Al can be deposited even if the liquid is cooled down to room temperature. Due to the high viscosity of this mixture, the cathodic current increases gradually at a potential of – 0.3 V indicating to bulk aluminium electrodeposition. The electrodeposition process is completely reversible and the obtained Al deposit at 25 ^oC on gold substrates was very thin, mirror-like and containing very fine crystallites of about 20 nm. The average grain size calculated from the Scherrer's equation is about 34 nm. Warren-Averbach analysis

indicates that the sizes of Al crystallites range from 10 to 80 nm and most of the crystallites have sizes of about 35 nm. Similar to the observations in [BMP] Tf_2N, the temperature does not play a dominant role on the particle sizes.

Therefore it can be concluded that under the applied conditions aluminium is deposited as a nanocrystalline metal from the two ionic liquids [BMP] Tf_2N and [$P_{14,6,6,6}$] Tf_2N without using brighteners or pulse plating technique. However, coarse cubic-shaped aluminium particles in the micrometer regime are obtained in the ionic liquid [EMIm] Tf_2N. Unlikely, these observations are not due to viscosity alone. These results can be interpreted on the basis of cation adsorption on growing Al nuclei.

5. In situ STM measurements

As shown in chapter (4), shiny, dense and adherent Al deposits with very fine crystallites in the nanometer regime can be obtained without any addition of organic brighteners or using pulse plating techniques in two air and water stable ionic liquids, [BMP] Tf_2N and [$P_{14,6,6,6}$] Tf_2N. However, coarse cubic-shaped aluminium particles in the micrometer regime are obtained in the ionic liquid [EMIm] Tf_2N. As the temperature and electrochemical parameters were varied it is unlikely that this observation is due to viscosity effects alone. In accordance to the (not yet fully understood) role of brighteners and grain refiners in aqueous electrochemistry, we interpreted these results on the basis of cation adsorption on growing Al nuclei in the case of [BMP] Tf_2N, which seems to play a role in the liquid with the pyrrolidinium cation. In order to shed more light on this pretty complicated aluminium electrochemistry, we investigated the Al deposition in [BMP]Tf_2N, [EMIm]Tf_2N and [$P_{14,6,6,6}$] Tf_2N ionic liquids by in situ STM in the present chapter to get more information on the initial growth of the deposits.

5.1 In situ STM measurements of electrodeposition of Al in [BMP] Tf_2N

In this section, in-situ scanning tunnling microscopy (STM) was employed to shed more light on the complicated electrochemical process for Al deposition on Au (111) in the upper phase of the biphasic mixture of $AlCl_3$ / [BMP] Tf_2N at 25 °C.

Figure 5.1 shows STM pictures of the Au (111) surface in the upper phase of the mixture of $AlCl_3$ / [BMP] Tf_2N at room temperature (25 ^oC). In the beginning of the STM experiment, a rough Au (111) surface with monoatomically high steps was observed at a potential of 0.3V *vs.* Al/Al(III). The surface is characterized by a large number of tiny pits with a measurable depth range from 230 to 250 pm which is typical for monoatomic defects. Quite similar to what was observed for the pure liquid on Au (111) **[72]** it can be concluded that the Au (111) surface is also restructured in the upper phase of the mixture of $AlCl_3$ / [BMP] Tf_2N. Such effects are known and an adsorption of ions can be responsible for the formation of vacancies and pits as a result of their interaction with Au surface atoms **[248-251]**. On the other hand, the presence of Cl^- ions can weaken the Au-Au bond at the surface and consequently lead to an increased mobility of gold atoms **[234]**. There is only quite a bit of information

available on restructuring / reconstruction of single crystalline metal surfaces in ionic liquids. Thus it is currently an open question to which extent cation / anion adsorption influences the surface electrochemistry.

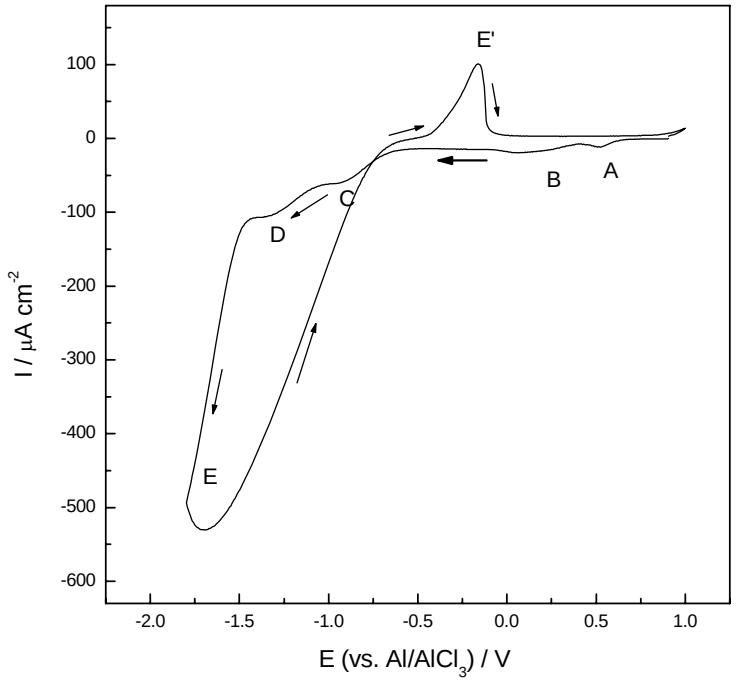

Fig. 4.1. *Cyclic voltammogram recorded at Au (111) substrate in the ionic liquid 1-butyl-1-methyl pyrrolidinium bis(trifluoromethylsulfonyl) amide containing 1.6 M $AlCl_3$ (from the upper phase of the mixture) at room temperature. The scan rate was 10 mVs^{-1}.*

When the electrode potential is set to 0.0 V, the roughness of the surface decreases remarkably (fig. 5.2a – 5.2c). At 0.0 mV we finally observe the typical Au (111) surface with monoatomically high terraces (see fig. 5.2d and the respective height profile). It should be mentioned clearly that in the potential regime from 0.8 to –1.1 V *vs.* Al / Al (III) we do not see clear evidence for the deposition of Al islands. Island formation, which we sometimes observed, was rather correlated to a surface restructuring process.

Figure 5.3 shows the initial stages of aluminium electrodeposition in the upper phase of the biphasic mixture of $AlCl_3$ / [BMP] Tf_2N on Au (111) at room temperature (25 ºC). Figure 5.3a shows a typical Au (111) surface at a potential of – 0.9 V. From the data obtained from the acquired STM pictures, there are no clear hints for aluminium deposition down to a potential of –1.1 V.

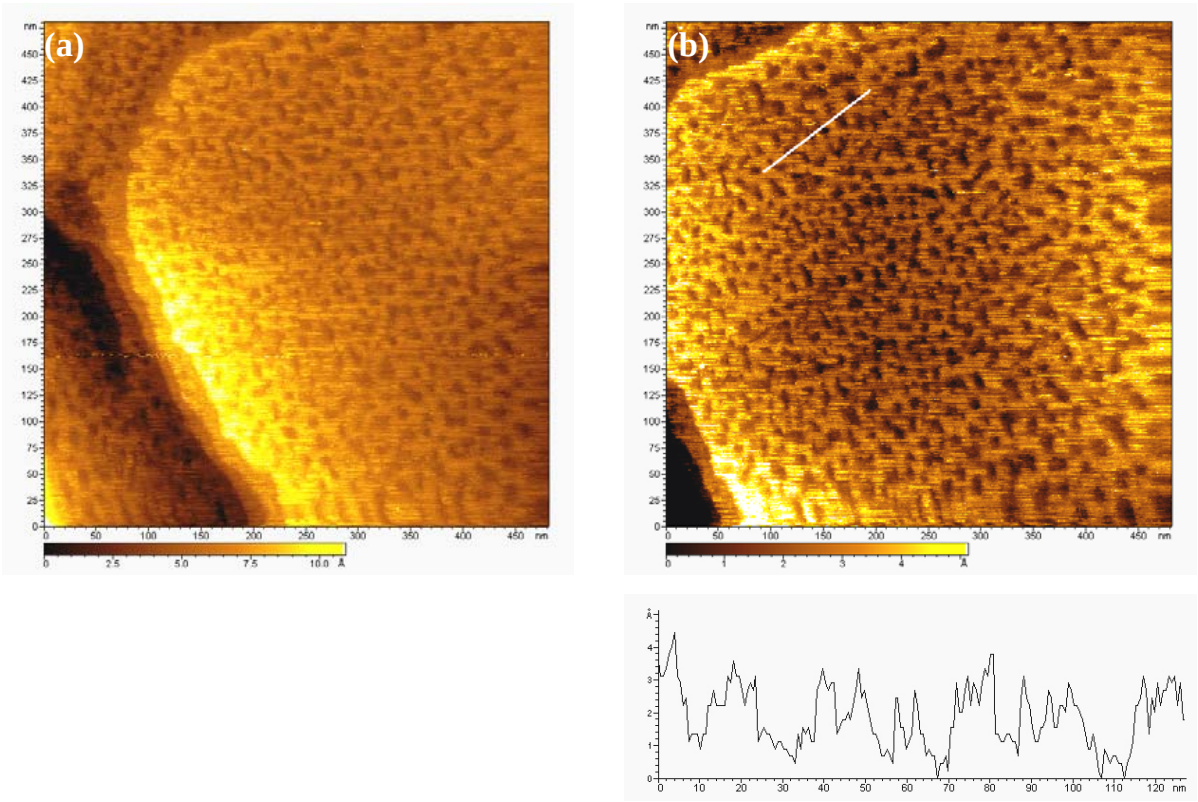

Fig. 5.1. *Two STM images of Au (111) in the upper phase of the biphasic mixture of $AlCl_3$ / [BMP] Tf_2N showing surface restructuring with tiny pits of height of about 250 pm as shown from the typical height profile, E_{tip} = 0.60 V, I_{tun}= 2 nA and 2 Hz scan rate. (a) At E = 0.3 V vs. Al/Al(III). (b) After 8 minutes at the same E = 0.3 V vs. Al/Al(III).*

At this electrode potential 2D aluminium islands of 200 – 250 pm height were formed as shown in fig. 5.3b and in the respective height profile. We have to mention that the gold surface at –1.1 V appears reproducibly noisy, and this noise does not disappear before reaching an electrode potential of –2.0 V at which the bulk aluminium deposition starts. It is likely that in this potential regime the irreversible cathodic breakdown of the Tf_2N anion is observed which is known to occur in 2 – 3 steps (see **[252, 253]**). Thus the peaks C and D in fig. 4.1 are presumably due to Tf_2N breakdown, presumably interfering with or even preventing the underpotential deposition of Al. It is unlikely that the anion breakdown is responsible for the bulk deposition of nanocrystalline Al in this liquid, as at 100 ^{o}C, thus at lower overvoltages, the deposits are still nanocrystalline without clear evidence for anion breakdown. Furthermore the adsorption of the pyrrolidinium ion to the surface might prevent an Al upd. The 2D aluminium islands can be completely removed by switching the potential to 0.5 V. Hence, clear, flat and monoatomically high gold terraces are obtained.

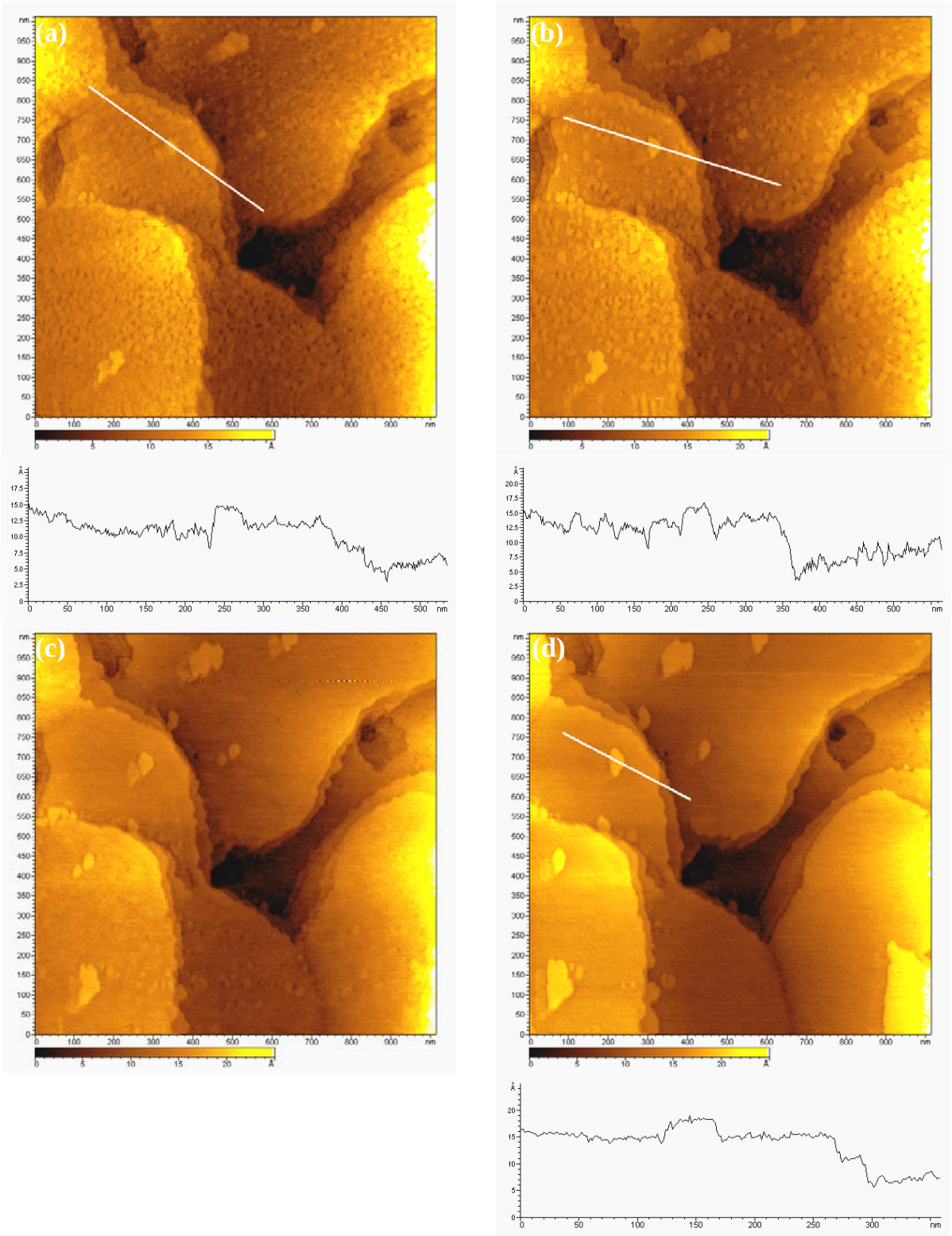

Fig. 5.2. *Sequence of STM images of Au (111) in the upper phase of the biphasic mixture of $AlCl_3$ / [BMP] Tf_2N at E = 0.0 V vs. Al/Al(III), E_{tip} = 0.3 V, I_{tun}= 2 nA and 2 Hz scan rate. (a) A rough surface film of gold. (b) After 6 minutes. (c) After 12 minutes. (d) After 24 minutes, the gold surface is reconstructed showing the typical Au (111) terraces of monoatomic height.*

In the following we demonstrate that already at 0.5 V *vs.* Al / Al (III) the dissolution of the Au (111) surface begins in the upper phase of $AlCl_3$ / [BMP] Tf_2N. The STM images in figure 5.4 were successively recorded in a surface area exhibiting gold terraces with monatomic steps. Figure 5.4a was recorded after the potential was raised to a potential of 0.5 V to remove the as deposited 2D aluminium islands. At this potential, 0.5 V, the gold surface topography changes continuously with time. As can be seen in figure 5.4a and the subsequently recorded image in figure 5.4b, a hole in the center of the picture is formed. This hole continuously increases in size and there is a clear oxidation at the step edges. Hence, the surface dissolution occurs first at step edges.

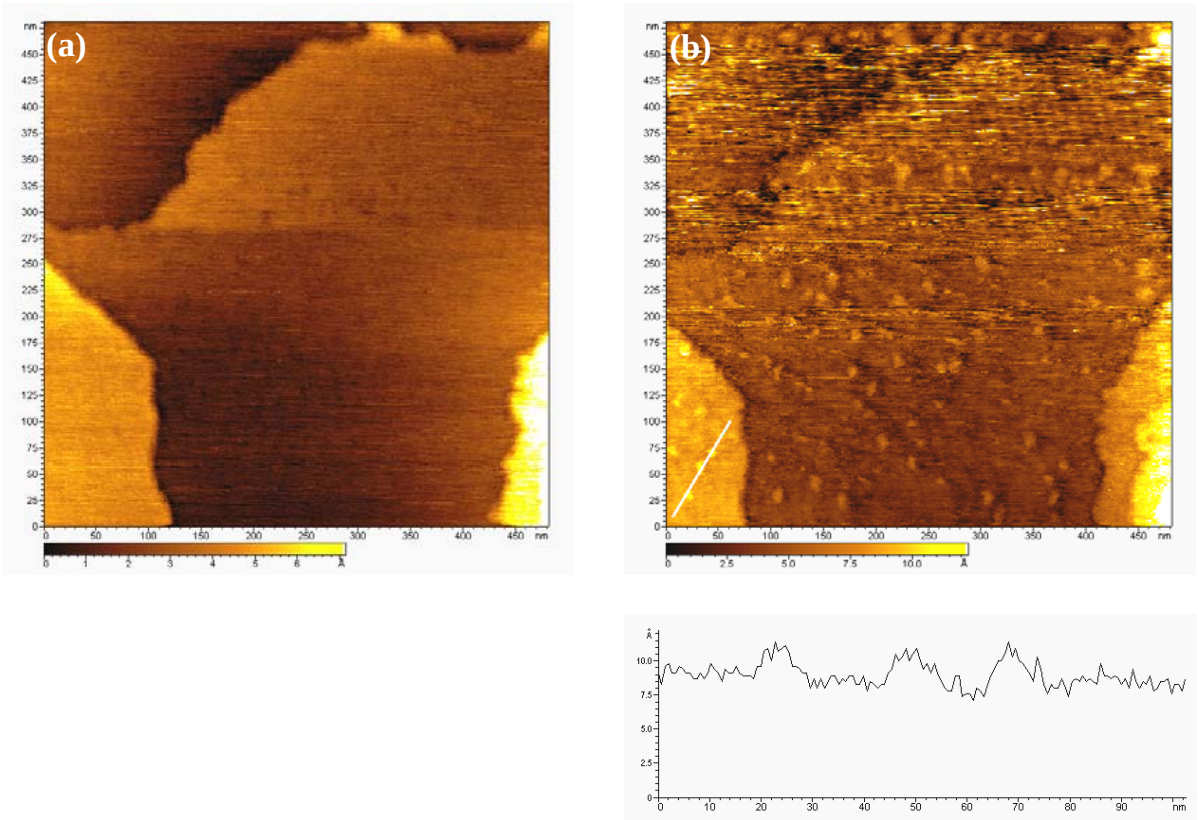

Fig. 5.3. *The initial stages of aluminium electrodeposition in the upper phase of the biphasic mixture of $AlCl_3$ / [BMP] Tf_2N on Au (111) at room temperature (25 ºC). (a) A typical Au (111) surface is obtained at a potential of – 0.9 V vs. Al/Al(III), E_{tip} = – 0.39 V, I_{tun}= 2 nA and 2 Hz scan rate. (b) 2D aluminium islands of 250 pm height are formed as shown from the typical height profile at E = –1.1 V vs. Al/Al(III), E_{tip} = – 0.59 V, I_{tun}= 2 nA and 2 Hz scan rate.*

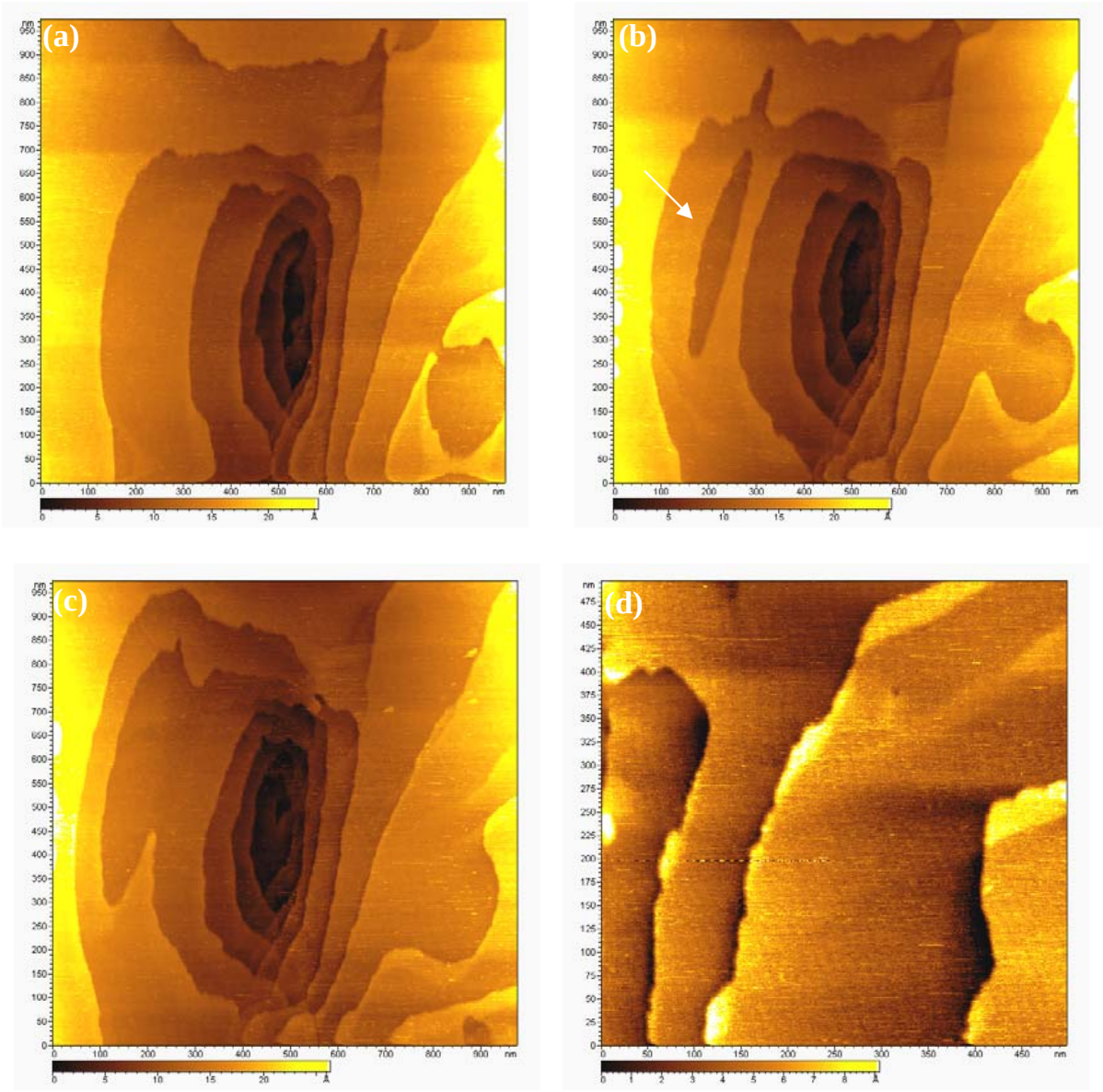

Fig. 5.4. *A sequence of STM images recorded after complete dissolution of 2D aluminium film by switching the potential to E = 0.5 V vs. Al/Al(III), E_{tip} = 1.02 V, I_{tun}= 2 nA and 2 Hz scan rate. (a) STM image shows gold terraces with monatomic steps. (b) the gold surface is oxidized at the step edges (after 4 min.). (c) After 17 minutes. This series of STM images show the redeposition of gold by switching the potential to the cathodic regime. (d) At E = 0.0 V vs. Al/Al(III), E_{tip} = 0.5 V, I_{tun}= 2 nA and 2 Hz scan rate, typical monoatomically high gold terraces are observed.*

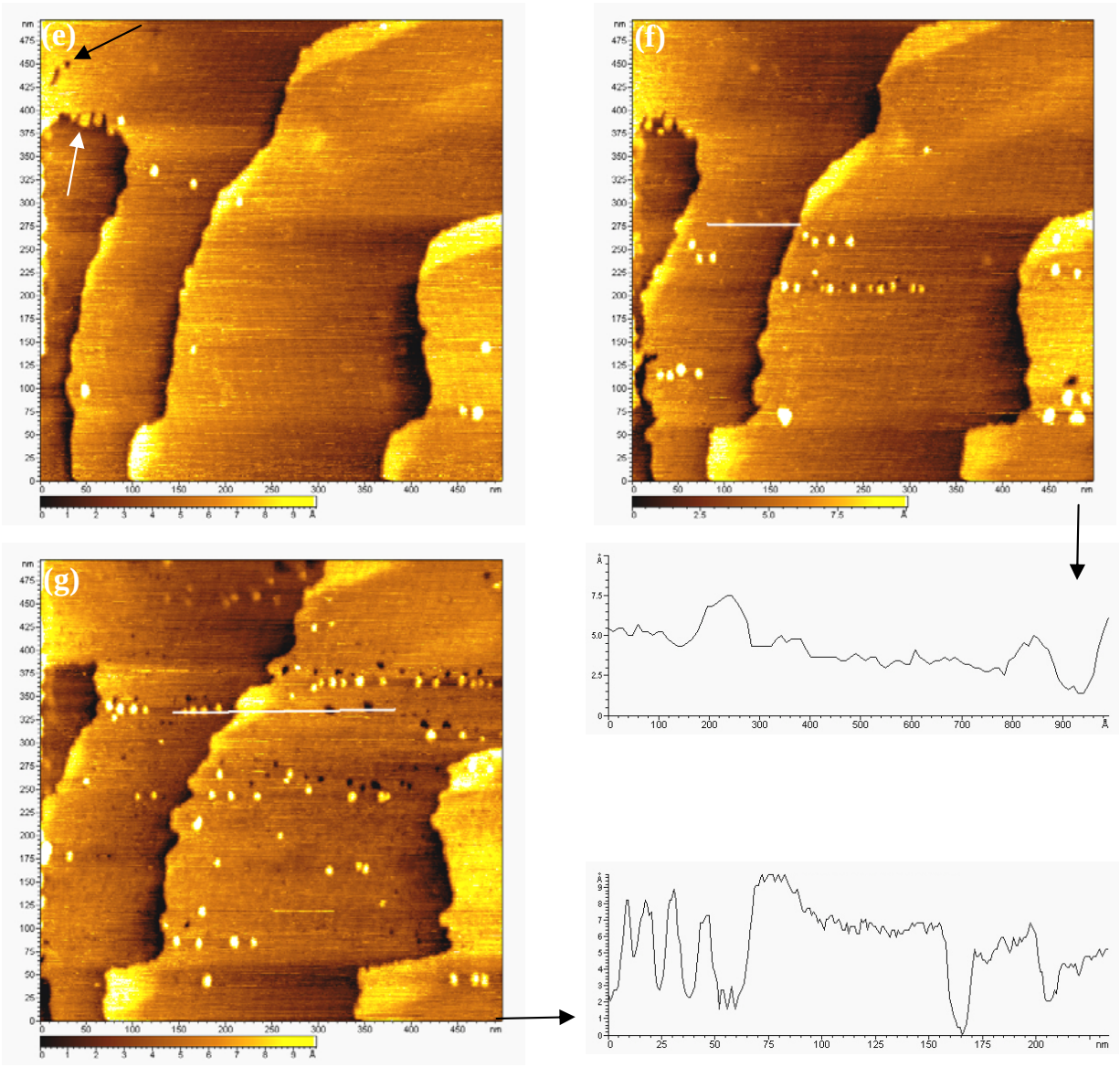

Fig. 5.4 *(continued) (e) At E = – 0.3 V vs. Al/Al(III), E_{tip} = 0.21 V, I_{tun}= 2 nA and 2 Hz scan rate, 2D gold islands of about 15 nm in diameter are formed together with vacancy islands. (f) The number of gold islands and of vacancy islands has increased (about 4 minutes between two fig. 5.4e – 5.4f). (g) At E = – 0.4 V vs. Al/Al (III), E_{tip} = 0.11 V, I_{tun}= 2 nA and 2 Hz, it can be seen that the step edges have grown laterally.*

In the following, the electrode potential was decreased again. Figure 5.4d shows typical gold terraces at a potential of 0.0 V. If the potential is held at this potential or set to – 0.3 V, monoatomically high islands of about 15 nm in diameter are formed. Furthermore some tiny pits or defects, marked with the black arrow in picture 5.4e can be observed. In addition, a deposition at the step edges is obvious (see the white arrow). The number of gold islands increases with ongoing time, see fig. 5.4f (4 minutes between figs. 5.4e and 5.4f). By switching

the electrode potential to – 0.4 V, pits with a width of about 6 nm and more islands were formed as shown in fig 5.4g. As quite obviously the step edges grow two dimensionally and as there is no such process when gold was not subject to oxidation, we might conclude that formerly oxidized gold is redeposited. It is not straightforward to understand why at the same time islands and vacancy islands form on the surface. This might be a hint for a surface film, which has been suggested several times now for metals in the presence of the Tf_2N anion.

At – 2.0 V the bulk deposition of Al occurs, and under these potentiostatic conditions close to equilibrium (slow growth rate) a width of 50 – 100 nm for the crystallites is obtained (see fig. 5.5). However, if bulk deposits of Al are made, we clearly get a nanocrystalline deposit.

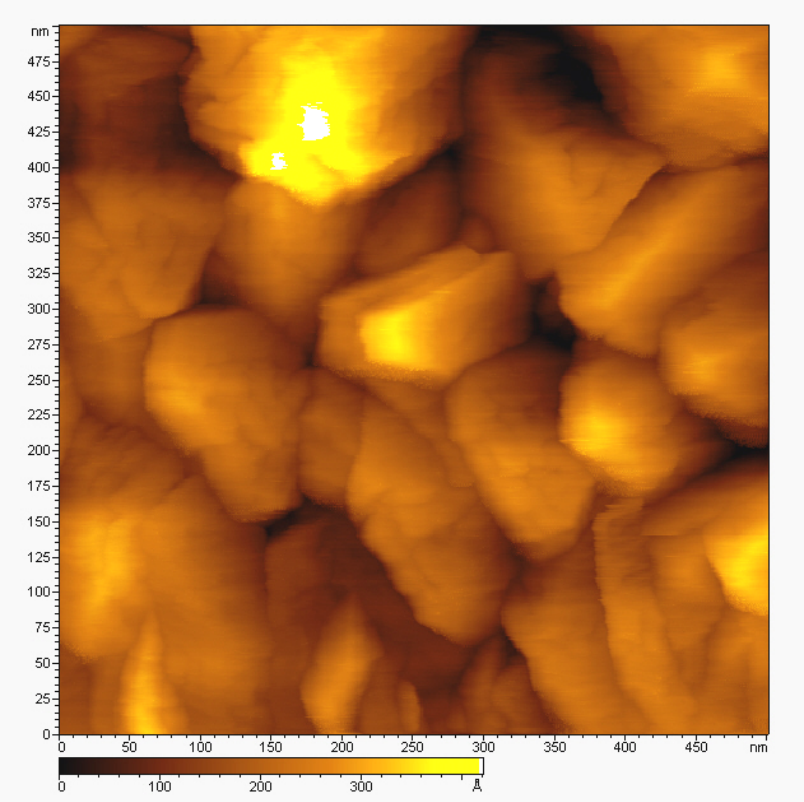

Fig. 5.5. *STM image shows the topography of an aluminium layer on Au (111) in the upper phase of the biphasic mixture of $AlCl_3$ / [BMP] Tf_2N at E = –2.0 V vs. Al/Al(III), E_{tip} = – 1.7 V, I_{tun}= 2 nA, 2 Hz scan rate.*

This is surprising as bulk deposits have grain sizes of about 20 nm under these conditions. This might be due to the slow growth near equilibrium conditions.

It can be concluded that nanocrystalline Al can be obtained from [BMP] Tf_2N ionic liquid and the electrodeposition process is highly irreversible. The cyclic voltammogram at room temperature is characterized by presence of two small reduction peaks at –1.0 and –1.3 V before the bulk Al deposition which are correlated to Tf_2N breakdown. The Au (111) substrate is subject to restructuring / reconstruction. There are no clear hints for underpotential deposition (UPD) of Al.

5.2 In situ STM measurements of electrodeposition of Al in [EMIm] Tf_2N

In this section in situ STM results on the initial stages of the aluminium electrodeposition in the underpotential (UPD) and overpotential (OPD) regime are presented. It was reported that UPD refers to a phenomenon by which an element electrodeposits on another one at a potential positive to its Nernst equilibrium potential **[254]**. UPD results from the difference in energetics of inter- vs. intraelemental bonding. That is, UPD can be thought of as the formation of a surface compound, with the accompanying heat of formation. As a consequence, UPD stops when the surface is covered; thus it is a surface limited reaction, providing atomic layer control. For systems where the elements show a good miscibility, the interaction of the adsorbate with the substrate may not stop with a single atomic layer, and a surface alloy can be formed as in our case.

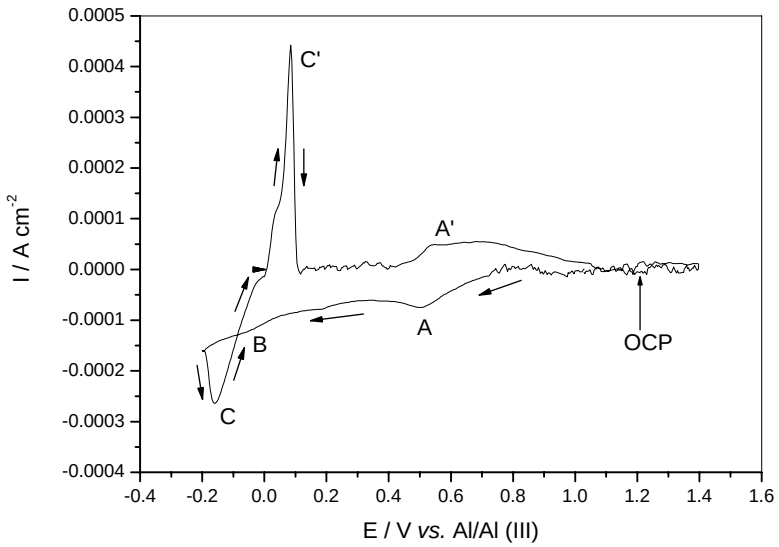

Fig. 4.7 *a typical cyclic voltammogram for aluminium deposition and stripping on Au(111) in the upper phase of the biphasic mixture of $AlCl_3$ / [EMIm] Tf_2N at room temperature (25 ^oC) showing the Al UPD process. Scan rate: 10 mVs^{-1}.*

The initial stages of the aluminium deposition process were investigated by stepwise decreasing the potential from 0.93 V *vs.* Al/Al (III) until the bulk deposition started. For potentials between 0.93 and 0.7 V *vs.* Al/Al (III) we clearly observe the typical terrace like structure of Au (111). Fig. (5.6) shows a sequence of STM images recorded *in situ* during aluminium UPD process on Au (111) from the upper phase of the biphasic mixture of $AlCl_3$ /

[EMIm] Tf_2N. Images (a-f) show the sequence of deposition of the first aluminium monolayer onto Au (111). Fig. 5.6a shows the pure Au (111) surface with terraces of an average step height of the typical 250 pm, i.e, the steps are monoatomically high, at E = 0.7 V *vs.* Al/Al(III).

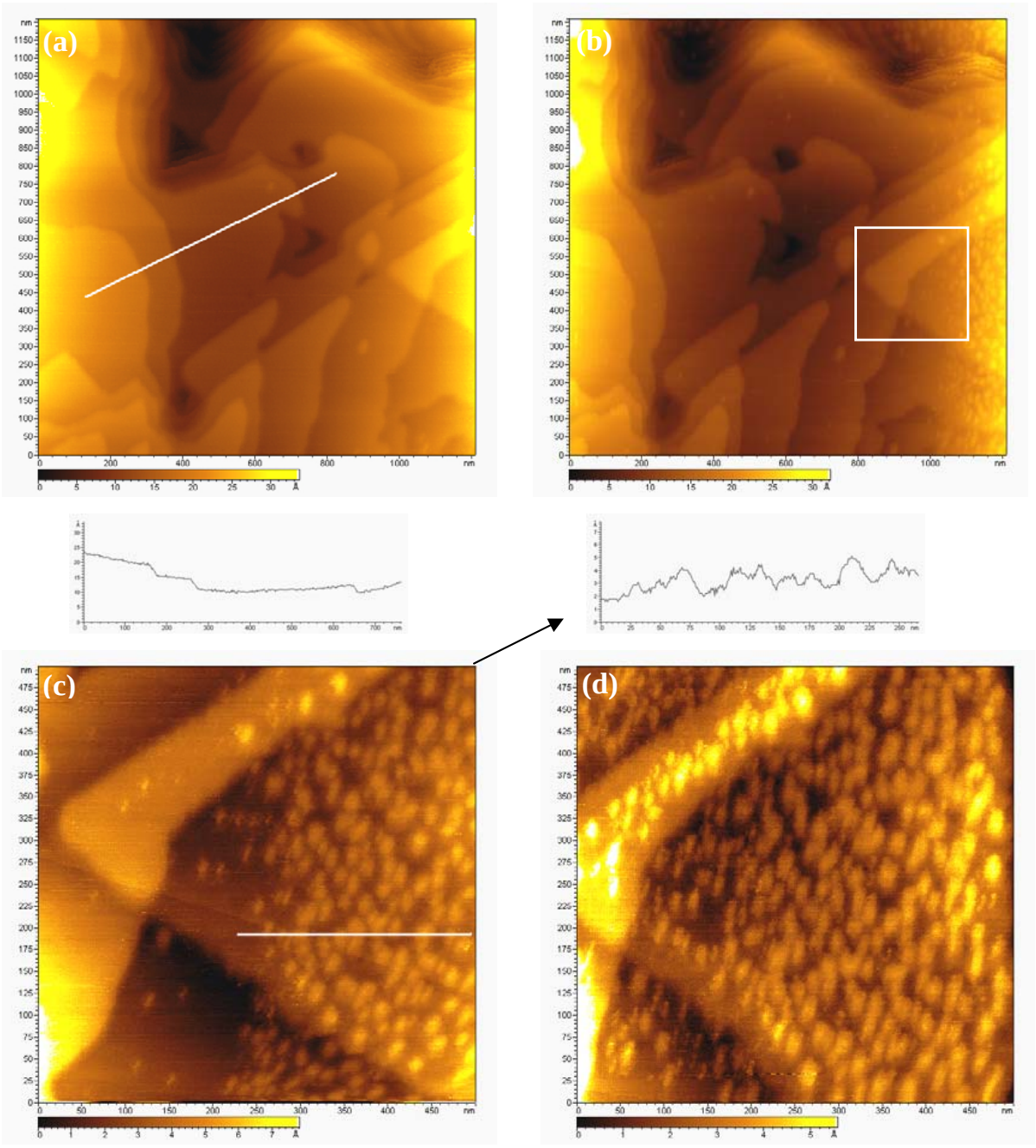

Fig. 5.6. *Sequence of STM pictures recorded in situ during aluminium UPD process on Au(111) from the upper phase of the biphasic mixture of $AlCl_3$ / [EMIm] Tf_2N. Images (a-f) show the deposition of the first aluminium monolayer onto Au (111), I_{tun}= 2 nA, 2 Hz scan rate. (a) STM image of monoatomic terraces on the Au(111) surface acquired at E = 0.7 V vs. Al/Al(III), E_{tip} = 1.0 V. (b) STM image of Al islands formed at E = 0.6 V vs. Al/ Al(III), E_{tip} = 0.9 V. (c) 500X500 nm^2 area from fig. 5.6b. (d) E = 0.5 V vs. Al/ Al (III), E_{tip} = 0.8 V.*

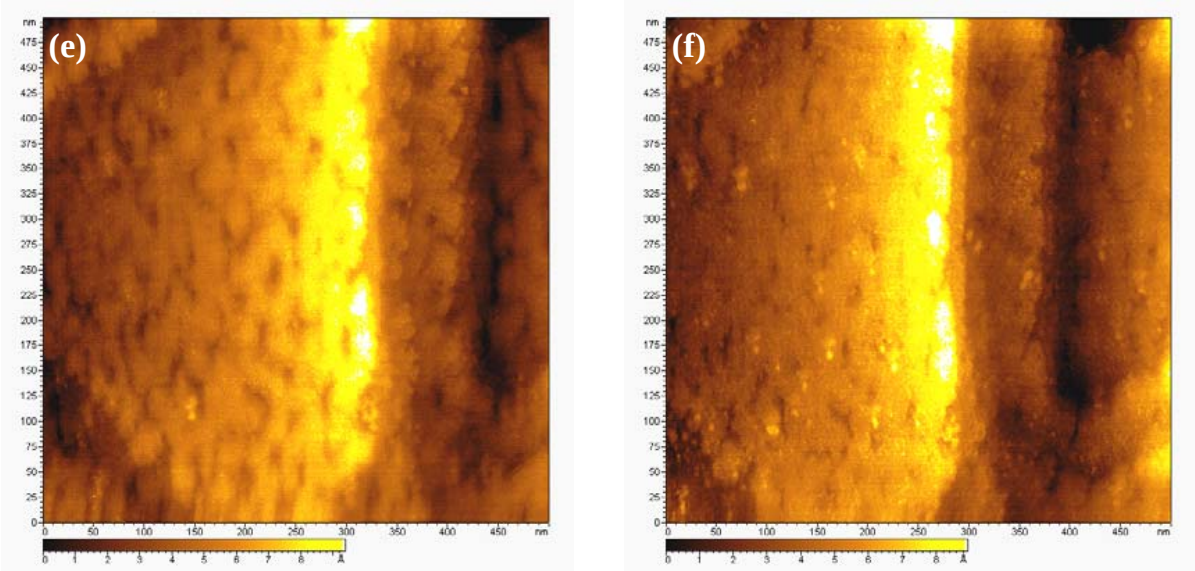

Fig. 5.6 *(continued) (e) E = 0.4 V vs. Al/ Al(III), E_{tip} = 0.7 V. (f) E = 0.3 V vs. Al/ Al(III), E_{tip} = 0.6 V.*

After switching the potential to 0.6 V, aluminium starts to deposit by forming 2D islands as shown in fig. 5.6b. A magnification of the area determined by the white rectangle in fig. 5.6b is shown in fig. 5.6c. The height of these 2D islands is between 200 and 250 pm which is – within the experimental error – in agreement with the monoatomic height of aluminium as shown from a typical height profile of fig. 5.6c. There are no such islands at this electrode potential in the pure ionic liquid. The number and size of such islands increases with further aluminium deposition by decreasing the potential to 0.5 V (fig. 5.6d). If the potential is decreased further to 0.4 V, the number of aluminium islands still rises until – with the exception of few vacancies – one aluminium monolayer is formed (fig. 5.6e). These vacancies are still present even by further shifting the potential to 0.3 V, at which a second aluminium layer starts to grow by forming 2D aluminium islands on top of the first monolayer (fig 5.6f).

With ongoing time (about 25 minutes) the number and size of these islands increase (see fig. 5.7a). Fig. (5.7) shows a series of STM images after the first aluminium monolayer has been formed. The pictures show the formation of a second and third aluminium layer before 3D crystallites start growing. As shown in Fig.5.7a, the number and size of 2D aluminium islands on top of the first monolayer increase with time (25 minutes between figures 5.6f and 5.7a). By switching the electrode potential to + 0.2 V and with ongoing time a complete second

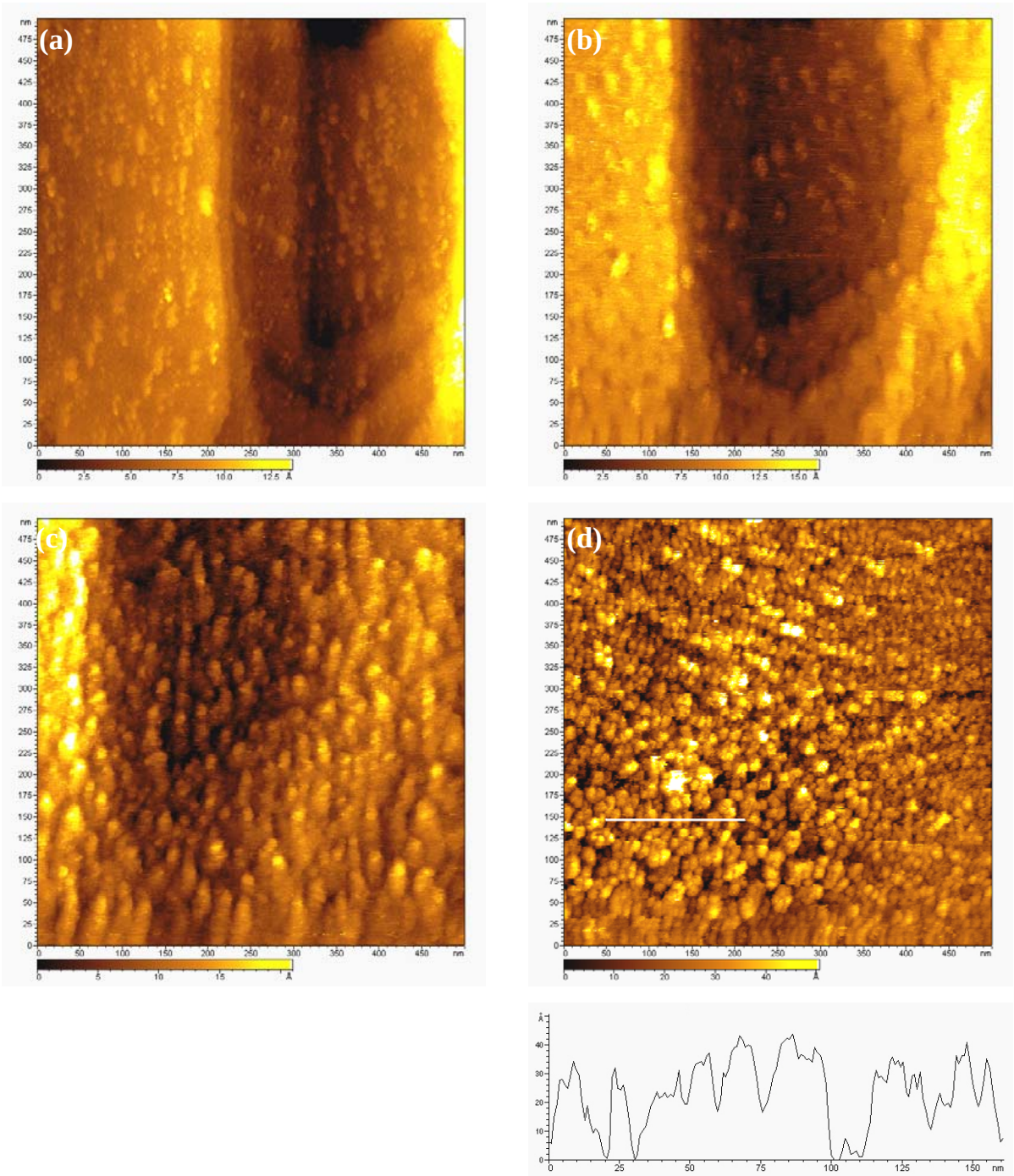

Fig. 5.7. *A series of STM images recorded on the first aluminium monolayer with* I_{tun} *= 2 nA, 2 Hz scan rate. Images (a-d) show the formation of a second and a third aluminium layer followed by the formation of 3D crystallites. (a) At E = 0.3 V vs. Al/Al(III),* E_{tip} *= 0.6 V, the number and size of 2D aluminium islands increase with time (25 minutes between the two images 5.6f and 5.7a). (b) At E = 0.2 V vs.* Al/Al^{3+}*,* E_{tip} *= 0.5 V, a complete second aluminium layer with some vacancy islands is formed, a third aluminium layer starts to grow before completion of the second layer. (c) At E = 0.1 V vs. Al/Al(III),* E_{tip} *= 0.4 V. (d) Aluminium deposit exhibits a granular structure at E = – 0.1 V vs. Al/Al(III),* E_{tip} *= 0.2 V, the given crystallites have an average diameter of about 15 nm as shown from the given height profile.*

aluminium layer with some vacancies forms. The first monoatomic aluminium layer is not yet completely closed, before a third aluminium layer starts to grow still in the UPD regime (see fig 5.7b). When the electrode potential is further reduced to 0.1 V, for several minutes, the number of deposited crystallites rapidly increases and a 3D growth sets in (see fig. 5.7c). Reducing the electrode potential to – 0.1 V leads to a crystal growth and the initial aluminium deposit exhibits a granular structure as shown in fig. 5.7d. This picture shows that the cystallites are homogeneously spread with an average diameter of about 15 nm of crystallites in the height profile. Nevertheless, when a bulk deposit is made in this liquid the obtained deposit is clearly microcrystalline.

The results in the UPD regime can be summarized as follows: firstly, monoatomically high Al islands grow on the Au (111) terraces to form the first monoatomic aluminium layer followed by a second one in the UPD regime. On top of the second Al monolayer, crystallites start growing, which at the onset of overpotential deposition get 3-dimensional.

Similar to the electrodeposition process we have investigated *in situ* the dissolution of formerly deposited aluminium on Au (111). First an aluminium layer was deposited on Au (111) in the bulk deposition regime at a potential of – 0.1V. Then it is dissolved by stepwise switching of the potential to the anodic regime.

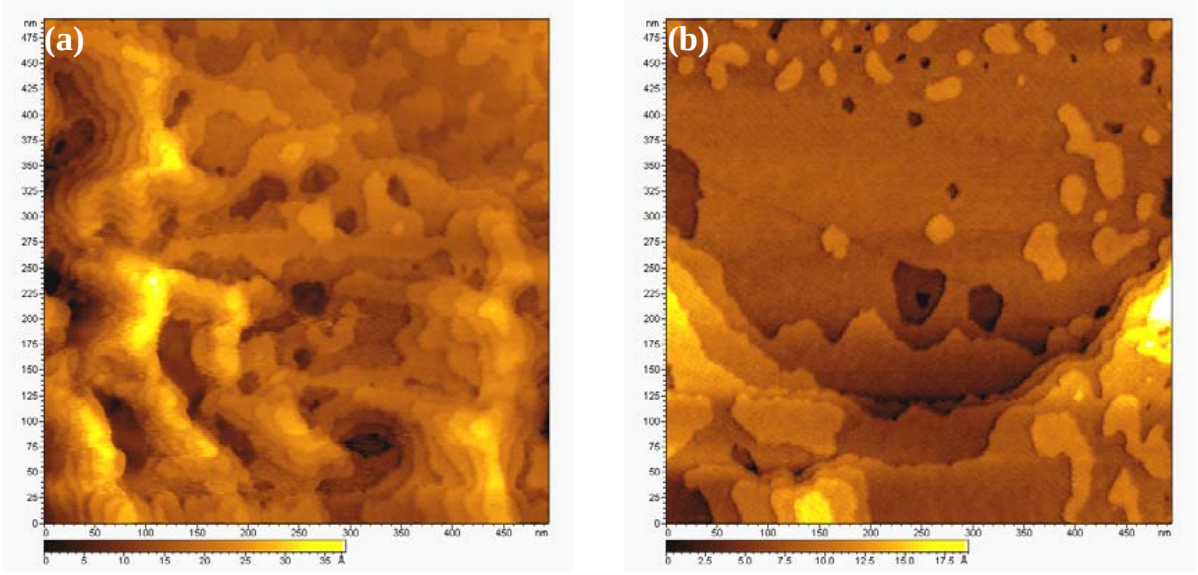

Fig. 5.8. *A sequence of STM images (a-f) acquired during the dissolution of bulk aluminium with I_{tun}= 2 nA and 2 Hz scan rate. (a) At E =0.3 V vs. Al/Al(III), E_{tip} = 0.6 V. (b) At E = 0.5 V vs. Al/Al(III), E_{tip} = 0.8 V.*

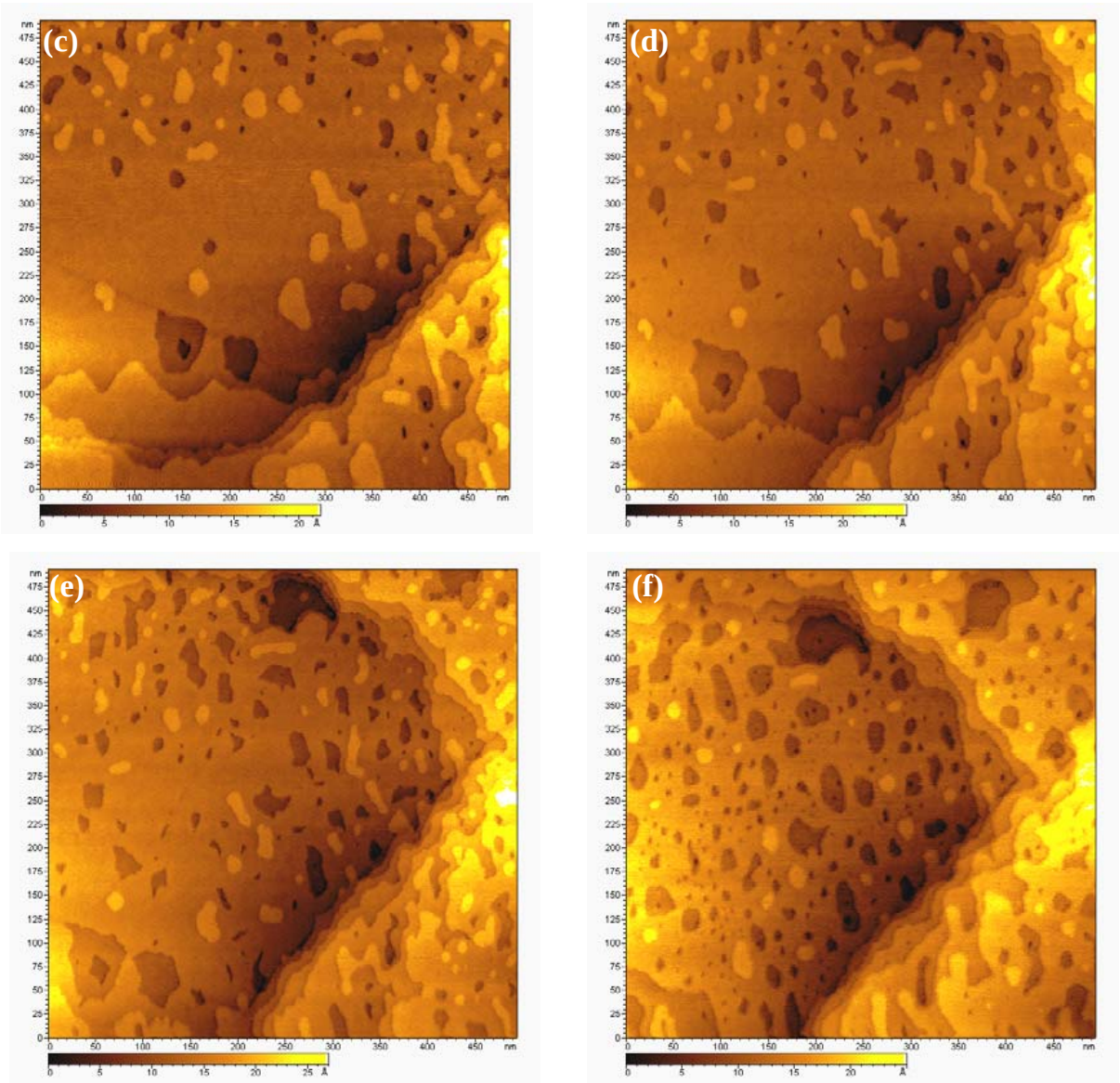

Fig. 5.8. *(continued) (c) At E = 0.6 V vs. Al/Al^{3+}, E_{tip} = 0.9 V. (d) At E = 0.7 V vs. Al/Al(III), E_{tip} = 1.0 V. (e) 8 minutes after image d, at E = 0.7 V vs. Al/Al(III), E_{tip} = 1.0 V. (f) At E = 0.82 V vs. Al/Al(III), E_{tip} = 1.12 V.*

Fig. 5.8 shows STM images acquired during the dissolution of such a bulk aluminium layer. At a potential of 0.0 V the as deposited aluminium layer starts to dissolve. By further increasing of the potential to 0.3 V the surface morphology (see fig. 5.8a) is completely different to the one observed before any deposition (see fig. 5.6a). It can happen at this electrode potential that again 2D Al islands deposit. When the electrode potential is set to 0.5 V, still some aluminium islands are left over on the surface, furthermore some vacancy islands are formed on Au (111) surface as shown in fig 5.8b. When the dissolution process is continued

by switching the potential to 0.6 V, a further pitting of the Au surface is observed as a result of stripping of Al from the Au lattice **[255, 256]**. The number and size of pits increase (pictures 5.8c–5.8f) and the original surface of Au (111) becomes visible. However, the whole of the Au (111) surface presented in fig. 5.8f shows a large number of vacancy islands. This is indicative of surface alloying of Al with Au at the early stage of deposition.

By means of STM investigations we can conclude that the electrodeposition process is in this ionic liquid is completely reversible and exhibit Al UPD at a potential of 0.55 V *vs.* Al/Al (III). Also there is a clear evidence for surface alloying of Al with Au at the early stages of deposition.

5.3 In situ STM measurements of electrodeposition of Al in $[P_{14,6,6,6}]$ Tf_2N

In this section, the initial stages of aluminium deposition onto Au (111) substrate in the mixture of $AlCl_3$ / $[P_{14,6,6,6}]$ Tf_2N ionic liquid at 25 °C was investigated by in situ scanning tunneling microscopy (STM). It should be mentioned that the liquid is pretty viscous, which has a certain impact on the STM picture quality.

Figure 5.9 shows STM pictures of the Au (111) surface in the mixture of $AlCl_3$ / $[P_{14,6,6,6}]$ Tf_2N with $AlCl_3$ concentration of 4.0 M at room temperature (25 °C). In the beginning of the STM experiment, at the open circuit potential (OCP), 1.0 V *vs.* Al / Al(III), a rough Au(111) surface was observed. The surface is characterized by the presence of tiny pits with a measurable depth of about 280 pm which is typical for monoatomic defects as shown from typical depth profile of figure 5.9a).

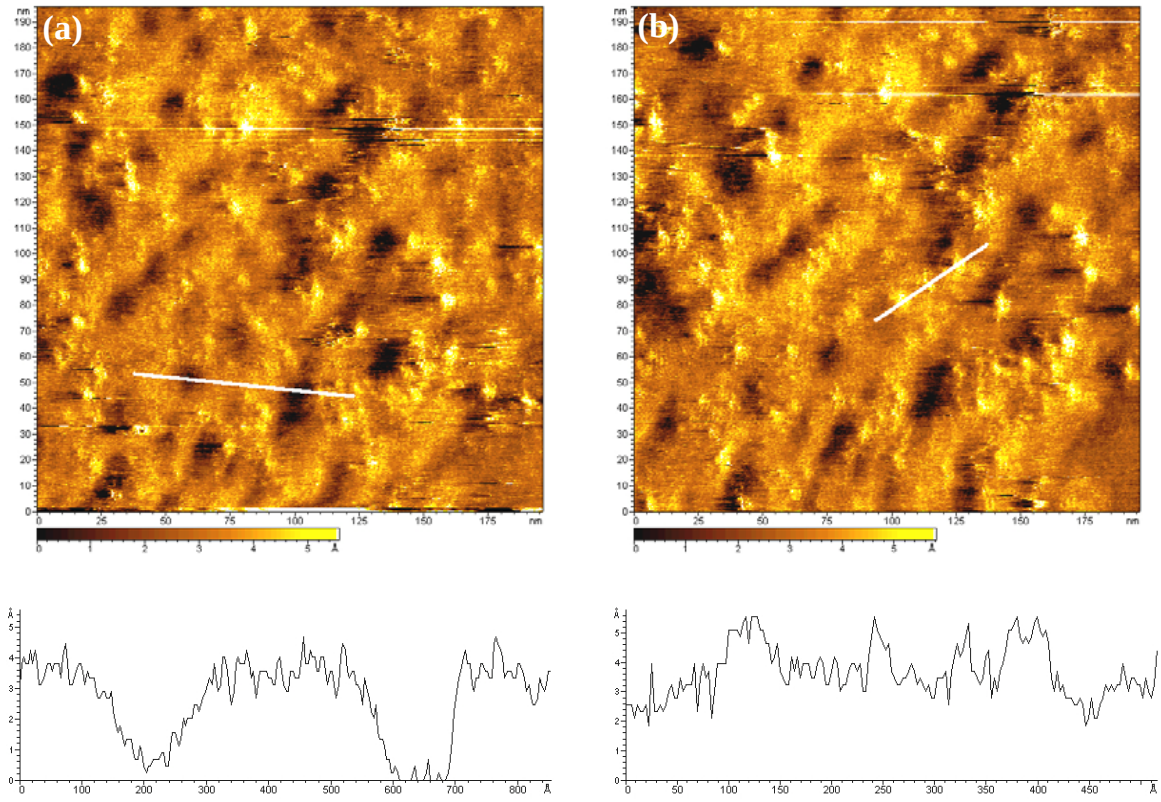

Fig. 5.9. *Two STM images of Au (111) in the mixture of $AlCl_3$ / $[P_{14,6,6,6}]$ Tf_2N at room temperature (25 °C) at 1.0 V vs. Al/Al(III) E_{tip} = 1.3 V, I_{tun}= 2 nA and 2 Hz scan rate. (a) Surface restructuring with tiny pits of depth of about 280 pm as shown from the typical depth profile. (b) The ejected gold atoms can nucleate on the gold terraces sites and form new gold islands of height about 250 pm as shown from the typical height profile.*

Therefore, we can conclude that the Au (111) surface is also subject to a certain restructuring in the mixture of $AlCl_3$ / $[P_{14,6,6,6}]$ Tf_2N at room temperature (25 °C). Such effects are known and may be attributed to an adsorption of ions leading to the formation of vacancies and tiny pits as a result of their interaction with Au surface atoms **[234, 248-251]**. This interaction increases the mobility of gold surface atoms, which can be ejected from the gold surface. The ejected gold atoms can nucleate on the gold terraces sites and form new gold islands of height about 250 pm (see fig. 5.9b and a typical height profile).

By switching the electrode potential to 0.9 V, the roughness of the surface decreases remarkably (fig. 5.10a – 5.10d). At 0.7 V we finally observe the typical Au (111) surface with monoatomically high terraces (see fig. 5.10e, fig. 5.10f and the respective height profile). It should be mentioned clearly that in the potential regime from 1.0 to – 0.1 V *vs.* Al / Al (III) we do not see clear evidence for the deposition of Al. However, it should be mentioned that in this pretty viscous ionic liquid the usual quality can hardly be obtained. Consequently the pictures are noisy.

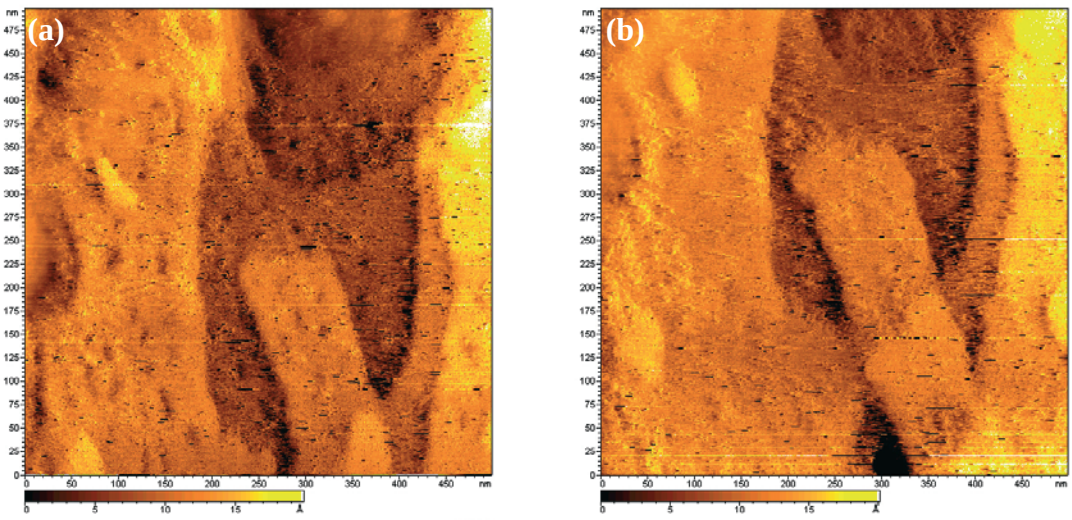

Fig. 5.10. *Sequence of STM images of Au (111) in the mixture of $AlCl_3$ / $[P_{14,6,6,6}]$ Tf_2N at room temperature (25°C), I_{tun}= 2 nA and 2 Hz scan rate. (a) At E = 1.0 V vs. Al/Al(III), E_{tip} = 1.3 V. Images (b-d) at E = 0.9 V vs. Al/Al(III), E_{tip} = 1.2 V, (b) After 20 minutes.*

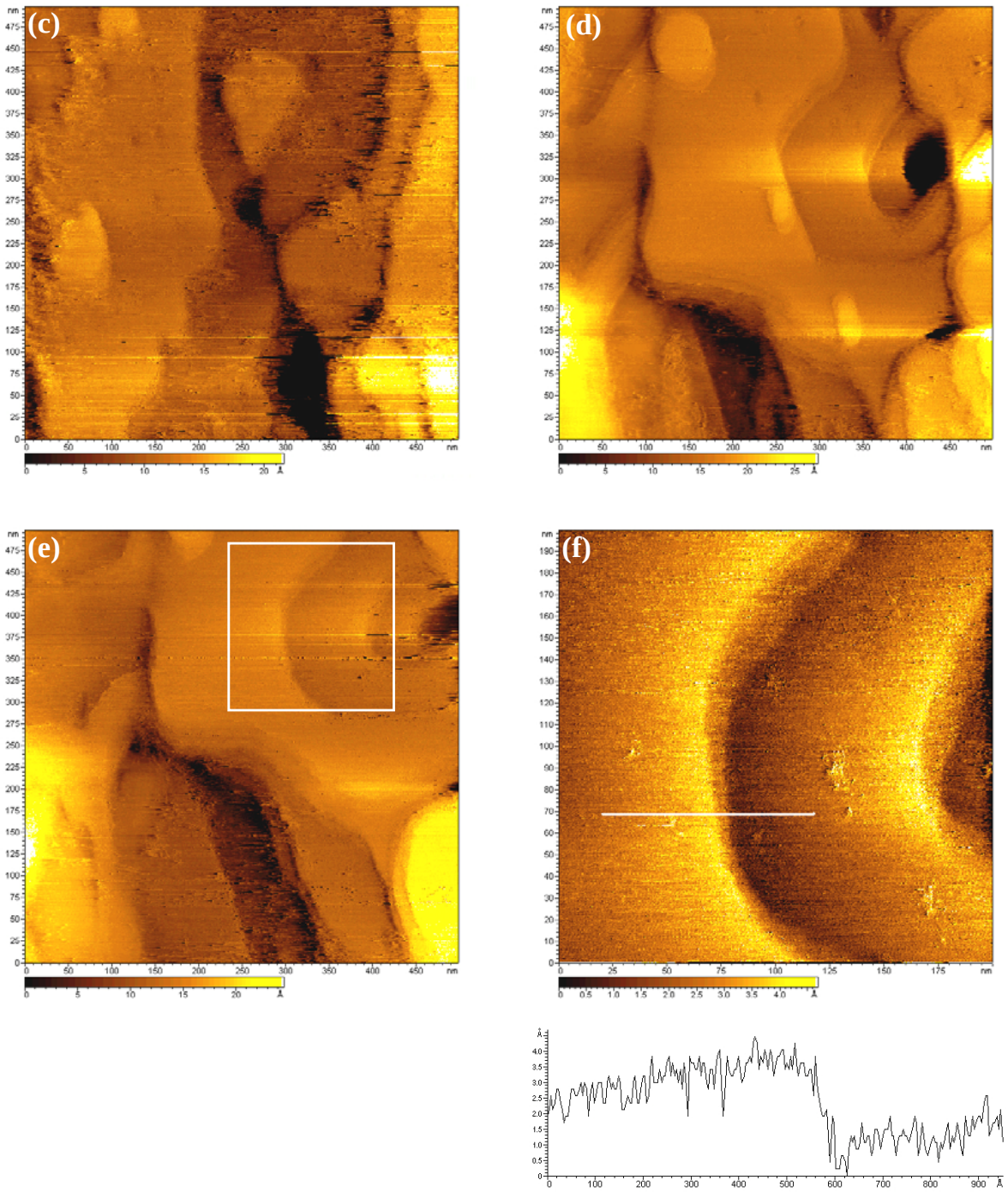

Fig. 5.10 *(continued) (c) After 36 minutes. (d) After 96 minutes. (e) At E = 0.7 V vs. Al/Al(III), E_{tip} = 1.0 V. (f) 200X200 nm2 area from image (e), as shown, the gold surface is reconstructed showing the typical Au (111) terraces of monoatomic height as shown from the typical height profile.*

Fig. (5.11) shows a sequence of STM images recorded *in situ* during the initial stages of aluminium deposition on Au(111) in the mixture of $AlCl_3$ / $[P_{14,6,6,6}]$ Tf_2N at room temperature (25 °C). At a potential of 0.7 V, one can see a typical Au (111) surface with

terraces of an average step height of the typical 250 pm i.e the steps are within the resolution of this experiment monoatomically high as shown in fig. 5.11a and its typical height profile. From the acquired STM pictures, there are no clear hints for aluminium deposition down to a potential of – 0.2 V at which 2D aluminium islands of 200-250 pm height are formed which is – within the experimental error – in agreement with the monoatomic height of aluminium, as shown in fig. 5.11b and in the respective height profile. With going time the size of 2D aluminium islands increases (fig.5.11c - 5.11d). If the potential is further decreased to – 0.3 V, the aluminium islands grow until they merge to form an aluminium layer (figs. 5.11e - 5.11f). By switching the electrode potential to more negative values, the bulk aluminium deposition sets in.

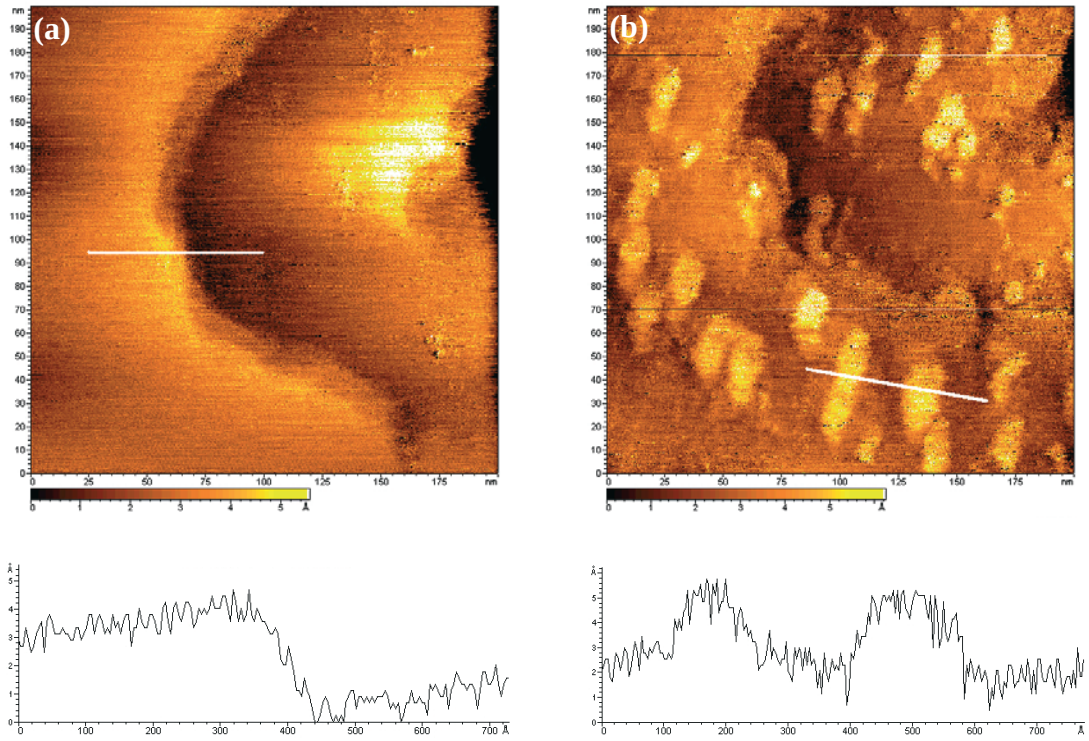

Fig. 5.11. *The initial stages of aluminium electrodeposition in the mixture of $AlCl_3$ / $[P_{14,6,6,6}]$ Tf_2N with 4.0 M $AlCl_3$ on Au (111) at room temperature (25 ºC), I_{tun}= 2 nA and 2 Hz scan rate. (a) A typical Au (111) terraces with monoatomic height is obtained at E = 0.4 V vs. Al/Al(III), E_{tip} = 0.7 V. (b) 2D aluminium islands of 250 pm height are formed as shown from the typical height profile at E = – 0.2 V vs. Al/Al(III), E_{tip} = 0.1 V.*

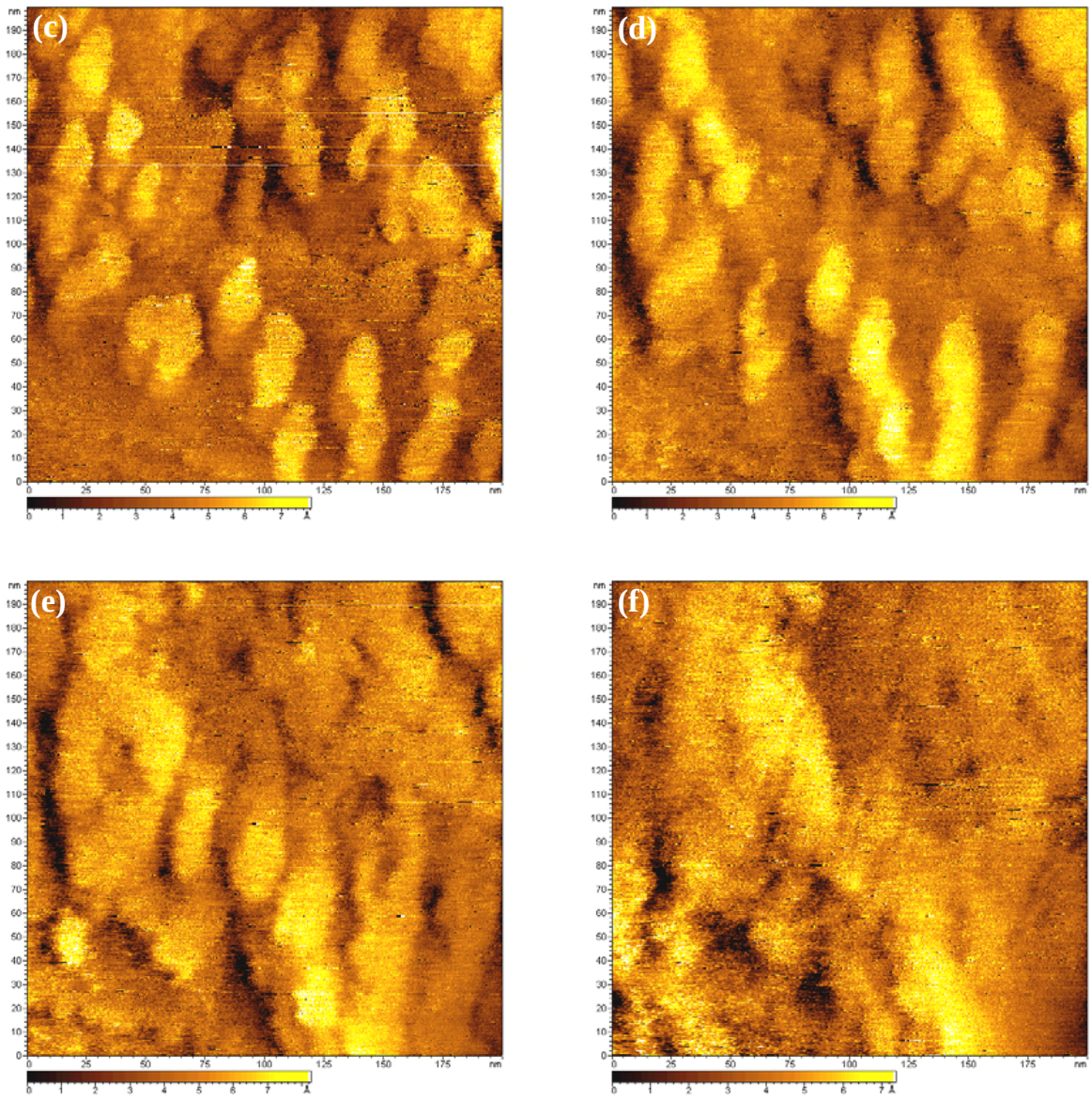

Fig. 5.11 *(continued) (c) After 4 minutes. (d) After 8 minutes. (e) At E = – 0.3 V vs. Al/Al(III),* E_{tip} *= 0.0 V. (f) 8 minutes between two images (e) and (f).*

The STM results obtained in this part can be summarized as in this ionic liquid $[P_{14,6,6,6}]$ Tf_2N, the Au (111) is also subject to restructuring / reconstruction process and there is no clear evidence for Al UPD. At a potential of – 0.2 V, 2D aluminium islands of 200-250 pm height are formed which is in agreement with the monoatomic height of aluminium. With going time the size of 2D aluminium islands increases. If the potential is further decreased to – 0.3 V, the aluminium islands grow until they merge to form an aluminium layer. By switching the electrode potential to more negative values, the bulk aluminium deposition sets in.

SUMMARY

In this thesis, the electrodeposition of aluminium from different air and water stable ionic liquids (3rd generation ionic liquids) was investigated. This type of ionic liquids is water and air stable, it is also easy to purify and in most cases easy to dry to water contents below 1 ppm. The employed ionic liquids are 1-butyl-1-methylpyrrolidinium bis(trifluoromethylsulfonyl) amide [BMP] Tf_2N, 1-ethyl-3-methylimidazolium bis(trifluoromethylsulfonyl) amide [EMIm] Tf_2N and trihexyl-tetradecyl phosphonium bis(trifluoromethylsulfonyl) amide [$P_{14,6,6,6}$] Tf_2N.

Electrodeposition of Al in [BMP] Tf_2N ionic liquid

The ionic liquid [BMP] Tf_2N exhibits a biphasic behaviour in the $AlCl_3$ concentration range from 1.6 to 2.5 M. The lower phase is colourless while the upper one is pale and more viscous. The two phases merge to one phase at temperatures above 80 ^oC. It was surprising that only the upper phase allows Al electrodeposition due to the presence of reducible aluminium containing species in this phase. The electrodeposition process is highly irreversible and the obtained deposits are shiny, dense and adherent with very fine crystallites in the nanometer regime (less than 50 nm). The cyclic voltammogram recorded at room temperature is characterized by the presence of a nucleation loop. Similarly, the cyclic voltammograms recorded at 50 and 75 ^oC exhibit the same behaviour as that obtained at room temperature, that is, in all cases there is a nucleation loop while at 100 ^oC there is no evidence for nucleation. Steep rising of cathodic currents in all cyclic voltammograms recorded at different temperatures (25, 50, 75 and 100 ^oC) are correlated to Al deposition. In the anodic scan, the cyclic voltammograms recorded at 50, 75, 100 ^oC are characterized by the presence of small oxidation peaks at 0.0 V *vs.* Al/Al (III) while at room temperature the small oxidation peak appeared at potential below 0.0 V *vs.* Al/Al (III). These oxidation peaks are due to the partial stripping of the electrodeposits, as the ratio of anodic/cathodic charge is far below 1. The electrodeposition of Al in this ionic liquid is highly irreversible as was evidenced also by in situ STM results. The Al electrodeposits obtained at different temperatures were investigated by means of high-resolution field–emission scanning electron microscopy (SEM). From the high-resolution SEM micrographs of Al layers electrodeposited potentiostatically on gold

substrates at 25, 50, 75 and 100 ^{o}C at potentials of –1.7, –1.0, –0.8 and –0.5 V *vs.* Al/Al (III), respectively, for 2 hours, the electrodeposited layers consist of fine crystallites in the nanometer regime. The electrodeposits obtained at 25, 50 and 75 ^{o}C are stressed. Interestingly, the quality of the Al deposit was improved by increasing the operating temperature to 100 ^{o}C, i.e., the crystallites became finer and the small cracks due to internal stress have disappeared. The XRD patterns of the electrodeposits obtained at 50, 75 and 100 ^{o}C show the characteristic peaks of crystalline Al. The peaks are broad, indicating the small crystal size of the electrodeposited Al and the width of the peaks slightly decreases as the temperature increases upon electrodeposition. The average grain size of Al determined from Scherrer's equation is 40 and 34 nm at 50 and 100 °C, respectively. From the data obtained from Warren-Averbach analysis, the sizes of Al crystallites prepared at 50 ^{o}C range from 5 to 60 nm and most of the crystallites have sizes of about 20 nm. At 100 ^{o}C, the average sizes of the crystallites range between 20 and 65 nm with a maximum around 40 nm. This analysis shows that the temperature in the electrodeposition does not seem to play a significant role, as the grain size distributions are similar. Typical thicknesses of the samples are between 2 and 5 μm. In order to shed more light on this pretty complicated aluminium electrochemistry in this system, the electrodeposition of Al on flame annealed Au (111) in [BMP] Tf_2N ionic liquid has been investigated by in situ scanning tunneling microscopy (STM). In this system, the Au (111) surface is subject to a restructuring / reconstruction as shown from in situ STM results. There is no clear evidence for the underpotential deposition of Al on Au (111) in this ionic liquid, and as one explanation the breakdown of the Tf_2N anion interferes with Al UPD. At –2.0 V vs. Al/Al(III), a deposited aluminium layer of about 100 nm thickness with aluminium nanocrystals is formed.

Electrodeposition of Al in [EMIm] Tf_2N

Similar to the $AlCl_3$/[BMP] Tf_2N mixture, $AlCl_3$/[EMIm] Tf_2N shows also a biphasic behaviour in the $AlCl_3$ concentration range from 2.5 to 5.5 M. It is not possible to deposit Al at concentrations below 2.5 M, which implies that the Tf_2N anion reacts with $AlCl_3$ to form a stable complex that is not reduced within the liquid electrochemical window. In contrast to the mixture $AlCl_3$ / [BMP] Tf_2N, the upper phase of the mixture $AlCl_3$ / [EMIm] Tf_2N is clear and colourless while the lower one

is pale and more viscous. The lower phase can be solidified by further addition of $AlCl_3$. Similar to the $AlCl_3$ / [BMP] Tf_2N mixture, only the upper phase of biphasic mixture of $AlCl_3$/[EMIm] Tf_2N allows Al electrodeposition. Also, the two phases become monophasic by heating up to a temperature of about 80 ^oC. The electrodeposition process is completely reversible and coarse cubic-shaped aluminium particles in the micrometer range are obtained in this ionic liquid. The cyclic voltammogram recorded at room temperature on Au (111) is characterized by presence of two chathodic waves at potentials of 0.55 V and – 0.02 V *vs.* Al/Al (III) followed by a steep increase of cathodic current indicating to bulk Al deposition. The two cathodic waves are correlated to aluminium UPD and 3D aluminium cluster formation in the beginning of the OPD regime, respectively. On the anodic scan, the strong anodic peak is corresponding to complete stripping of bulk aluminium and the small anodic wave at potential of about 0.55 V is correlated to the dissolution of aluminium deposited in the UPD regime. The deposition potential slightly shifts to less negative values on increasing the temperature. Furthermore, the peak currents of both deposition and stripping peaks significantly increase with rising temperature due to increasing of the mobility of the electroactive species towards the electrode surface, which, in turn, leads to accelerating the reaction rate of both reduction and oxidation reactions. The SEM micrographs recorded at different temperatures on gold surfaces showed that the deposits are compact, dense and contain coarse cubic-shaped microcrystallites with thichness ranges from 1 to 5 μm. The sizes of the cystallites are strongly dependent on temperature. The size of the crystallites increases with increasing temperature. The XRD patterns of a thick Al film electrodeposited potentiostatically on glassy carbon substrates at different temperatures show the characteristic peaks of aluminium. To shed more light to the electrodeposition process in this ionic liquid, in-situ STM investigations have been performed. In this system, the STM pictures show that the electrodeposition process is completely reversible and exhibit Al UPD at a potential of 0.55 V *vs.* Al/Al (III). Also there is a clear evidence for surface alloying of Al with Au at the early stages of deposition.

Electrodeposition of Al in [$P_{14,6,6,6}$] Tf_2N

The ionic liquid [(tri-hexyl-tetradecyl) phosphonium] Tf_2N does not show a biphasic behaviour on addition of $AlCl_3$. Here, $AlCl_3$ dissolves homogeneously up to a

concentration of 1.5 M at 25 ^{o}C and the colour of the liquid changes on addition of $AlCl_3$, from colourless to yellow, turning to red at a concentration of 1.5 M $AlCl_3$. The electrodeposition of aluminium is investigated in this ionic liquid with 1.5 M $AlCl_3$ at different temperatures. Unfortunately aluminium cannot be deposited even at elevated temperatures. Further additions of $AlCl_3$, up to a concentration of 4.0 M, can only be dissolved by increasing the temperature up to 150 ^{o}C forming a dark red more viscous liquid. In this mixture aluminium can be deposited even if the liquid is cooled down to room temperature. The cyclic voltammogram of the ionic liquid [$P_{14,6,6,6}$] Tf_2N containing 4.0 M $AlCl_3$ made at 150 ^{o}C and cooled down to 25 ^{o}C on gold substrate at 25 ^{o}C show that at a potential of – 0.3 V the cathodic current increases gradually, not sharply as in the case of [EMIm] Tf_2N ionic liquid, and this may be attributed to the high viscosity of [$P_{14,6,6,6}$] Tf_2N ionic liquid. The increasing of cathodic current at that potential (–0.3 V) is due to the bulk Al electrodeposition. The recorded anodic peak is correlated to the complete stripping of the electrodeposited aluminium. The temperature has a significant effect on the deposition potentials. The deposition potentials of aluminium decrease as the temperature increases. A rise of temperature also enhances the diffusion rate of reducible aluminium ions species to the cathode surface. The both cathodic and anodic currents increase as the temperature increases. A very thin, mirror-like aluminium film containing very fine crystallites of about 20 nm is obtained in this ionic liquid ([$P_{14,6,6,6}$] Tf_2N) at 25 ^{o}C. The XRD patterns of electrodeposited Al films obtained potentiostatically at –0.4 V in this ionic liquid containing 4.0 M $AlCl_3$ on glassy carbon substrate at 150 ^{o}C show the characteristic peaks of crystalline Al and the peaks are broad indicating a small crystal size of the electrodeposit. The average grain size calculated from the Scherrer's equation is about 34 nm. Warren-Averbach analysis indicates that the sizes of Al crystallites range from 10 to 80 nm and most of the crystallites have sizes of about 35 nm. Similar to the observations in [BMP] Tf_2N, the temperature does not play a dominant role on the particle sizes. In this ionic liquid, the Au (111) is also subject to restructuring / reconstruction process and there is no clear evidence for Al UPD. At a potential of –0.2 V, 2D aluminium islands of 200-250 pm height are formed which is in agreement with the monoatomic height of aluminium. With going time the size of 2D aluminium islands increases. If the potential is further decreased to – 0.3 V, the

aluminium islands grow until they merge to form an aluminium layer. By switching the electrode potential to more negative values, the bulk aluminium deposition sets in.

Therefore it can be concluded that under the applied conditions aluminium is deposited as a nanocrystalline metal from the two ionic liquids [BMP] Tf_2N and [$P_{14,6,6,6}$] Tf_2N. This nanocrystalline aluminium in the bulk phase or as coating is an interesting material because by decreasing the particle size an increase in hardness is usually observed. A hard aluminium coating on reactive substrates such as mild steel is interesting for corrosion protection. Furthermore, nano-Al (or nano aluminium alloys) is a precursor to nano-Al_2O_3. However, coarse cubic-shaped aluminium particles in the micrometer regime are obtained in the ionic liquid [EMIm] Tf_2N. Unlikely, these observations are not due to viscosity alone. These results can be interpreted on the basis of cation adsorption on growing Al nuclei in the case of [BMP] Tf_2N, which seems to play a role in the liquid with the pyrrolidinium cation. By using phosphonium cation based ionic liquid we can get nanocrystalline Al even at 150 ^{o}C. In contrast to ionic liquids based on the pyrrolidinium cation the process is reversible, in a possible future technical process to make nano-Al by electrochemical means, an Al sacrificial anode might be employed. Our results emply that similar to the observations in [BMP] Tf_2N, the temperature does not play a dominant role on the particle sizes.

References

[1] P. Walden, Molecular weights and electrical conductivity of several fused salts. Bull. Acad. Imper. Sci. (St. Petersburg) (1914) 405.

[2] F.N. Hurley, T. P Wier, J. Electrochem. Soc. **98** (1951) 207.

[3] H. L. Chum, V. R. Koch, L. L. Miller and R. A. Osteryoung, J. Am. Chem. Soc., **97** (1975) 3264.

[4] J. Robinson and R. A. Osteryoung, J. Am. Chem. Soc., **101** (1979) 323.

[5] J. S.Wilkes, J. A. Levisky, R. A. Wilson and C. L. Hussey, Inorg. Chem., **21** (1982) 1263.

[6] T. B. Scheffler, C. L. Hussey, K. R. Seddon, C. M. Kear and P. D. Armitage, Inorg. Chem., **22** (1983) 2099.

[7] D. Appleby, C. L. Hussey, K. R. Seddon and J. E. Turp, Nature, **323** (1986) 614.

[8] S.E. Fry, N.J. Pienta, J. Am. Chem. Soc. **107** (1986) 6399.

[9] J.A. Boon, J.A. Levisky, J.L. Pflug, J.S. Wilkes, J. Org. Chem. **51** (1986) 480.

[10] J. S. Wilkes and M. J. Zaworotko, J. Chem. Soc., Chem. Commun., (1992) 965.

[11] F. Endres, Phys. Chem. Chem. Phys., **3** (2001) 3165.

[12] P. Bonhôte, A. Dias, N. Papageorgiou, K. Kalyanasundaram and M. Grätzel, Inorg. Chem., **35** (1996) 1168.

[13] J. Fuller and R. T. Carlin, in Molten Salts, ed. P. C. Trulove, H. C. De Long, G. R. Stafford and S. Deki, PV 98-11, The Electrochemical Society Proceedings Series, Pennington, NJ, (1998) p. 227.

[14] D. R. MacFarlane, P. Meakin, J. Sun, N. Amini and M. Forsyth, J. Phys. Chem. B, **103** (1999) 4164.

[15] H. Ohno, "Electrochemical Aspects ionic liquids", John Wiley& Sons, Inc., New Jersy, (2005).

[16] F. Endres and S.Z. El Abedin, Phys. Chem. Chem. Phys., **8** (2006) 2101.

[17] M.J. Earle, K.R. Seddon, Pure Appl. Chem. **72** (2000) 1391.

[18] P. C. Trulove and R. A. Mantz, in Ionic Liquids in Synthesis, ed. P. Wasserscheid and T. Welton, Wiley-VCH, Weinheim, (2003), pp. 103–126.

[19] Q. Y., D. D. Dionysiou., J. Photochemistry and photobiology A: Chemistry **165** (2004) 229.

[20] J.S. Wilkes, Green Chem. **4** (2002) 73.

[21] J.G. Huddleston, A.E. Visser, W.M. Reichert, H.D. Willauer, G.A. Broker, R.D. Rogers, Green Chem. **3** (2001) 156.

[22] P. A. Z. Suarez, S. Einloft, J. E. L. Dullius, R. F. De Souza, J. Dupont, J. Chim. Phys. **95** (1998) 1626.

[23] A. B. McEwen, E. L. Ngo, K. LeCompte, J. L. Goldman, J. Electrochem. Soc. **146** (1999) 1687.

[24] D. R. McFarlane, J. Sun, J. Golding, P. Meakin, M. Forsyth, Electrochim. Acta. **45** (2000) 1271.

[25] U. Schröder, J. D. Wadhawan, R. G. Compton, F. Marken, P. A. Z. Suarez, C. S. Consorti, R. F. de Souza and J. Dupont, New J. Chem. **24** (2000) 1009.

[26] V. M. Hultgren, A. W. A. Mariotti, A. M. Bond, A. G. Wedd, Anal. Chem. **74** (2002) 3151.

[27] R. G. Evans, O. V. Klymenko, C. Hardacre, K. R. Seddon, R. G. Compton, J. Electroanal. Chem. **556** (2003) 179.

[28] M. C. Buzzeo, O. V. Klymenko, J. D. Wadhawan, C. Hardacre, K. R. Seddon, R. G. Compton, J. Phys. Chem. A **107** (2003) 8872.

[29] D. L. Boxall, J. J. O'Dea, R. A. Osteryoung, J. Electrochem. Soc. **149** (2002) E468.

[30] D. L. Boxall, R. A. Osteryoung, J. Electrochem. Soc. **149** (2002) E185.

[31] B. M. Quinn, Z. Ding, R. Moulton, A. J. Bard, Langmuir, **18** (2002) 1734.

[32] J. Zhang, A. M. Bond, W. J. Belcher, K. J. Wallace, J. W. Steed, J. Phys. Chem. B **107** (2003) 5777.

[33] P. Wasserscheid and W. Keim, Angew. Chem., Int. Ed., **39** (2000) 3772.

[34] M. E. Van Valkenburg, R. L. Vaughn, M. Williams and J. S. Wilkes, 15th Symposium on Thermophysical Properties, 2003.

[35] C. Nanjundiah, S. F. McDevitt, V. R. Koch, J. Electrochem. Soc. **144** (1997) 3392.

[36] M. Ue, M. Takeda, A. Toriumi, A. Kominato, R. Hagiwara, Y. Ito, J. Electrochem. Soc. **150** (2003) A499.

[37] A. B. McEwen, S. F. McDevitt, V. R. Koch, J. Electrochem. Soc. **144** (1997) L84.

[38] D. W. Armstrong, L. He, Y.-S. Liu, Anal. Chem. **71** (1999) 3873.

[39] J. G. Huddleston, R. D. Rogers, Chem. Commun. 1998, 1765.

[40] J. G. Huddleston, A. E. Visser, W. M. Reichert, H. D. Willauer, G. A.

Broker, R. D. Rogers, Green Chem. **3** (2001) 156.

[41] P.-Y. Chen, I. W. Sun, Electrochim. Acta **45** (1999) 441.

[42] K. R. Seddon, A. Stark, M.-J. Torres, Pure Appl. Chem. **72** (2000) 2275.

[43] U. Schröder, J. D. Wadhawan, R. G. Compton, F. Marken, P. A. Z. Suarez, C. S. Consorti, R. F. de Souza, J. Dupont, New J. Chem. **24** (2000) 1009.

[44] I. M. Al Nashef, M. L. Leonard, M. C. Kittle, M. A. Matthews, J. W. Weidner, Electrochem. Solid-State Lett. **4** (2001) D16.

[45] I. M. Al Nashef, M. L. Leonard, M. A. Matthews, J. W. Weidner, Ind. Eng. Chem. Res. **41** (2002) 4475.

[46] J. Fuller, R. T. Carlin, R. A. Osteryoung, J. Electrochem. Soc. **144** (1997) 3881.

[47]Y. Katayama, S. Dan, T. Miura, T. Kishi, J. Electrochem. Soc. **148** (2001) C102.

[48] A. M. Leone, S. C. Weatherly, M. E. Williams, H. H. Thorp, R. W. Murray, J. Am. Chem. Soc. **123** (2001) 218.

[49] T. Hatazawa, R. H. Terrill, R. W. Murray, Anal. Chem. **68** (1996) 597.

[50] B. K. Sweeny, D. G. Peters, Electrochem. Commun. **3** (2001) 712.

[51] S.A. Forsyth, D.R. MacFarlane, R.J. Thompson, M. von Itzstein, Chem. Commun. (2002) 714.

[52] Z. Yang and W. Pan, Enzyme and Microbial Technology, **37** (2005) 19.

[53] J. Fuller, A.C. Breda, R.T. Carlin, J. Electroanal. Chem. **459** (1998) 29.

[54] M.J. Earle, K.R. Seddon, Pure Appl. Chem. **72** (2000) 1391.

[55] G.-T. Wei, Z. Yang and C.-J. Chen, Analytica Chimica Acta **488** (2003) 183.

[56] A.N. Visser, R.P. Swatloski, W.M. Reichert, R. Mayton, S. Sheff, A. Wierzbicki, J.H. Davis Jr., R.D. Rogers, Chem. Commun. (2001) 135.

[57] C.M. Gordon, A.J. McLean, Chem. Commun. (2000) 1395.

[58] Q. Yang, D.D. Dionysiou . Journal of Photochemistry and Photobiology A: Chemistry **165** (2004) 229.

[59] D. Allen, G. Baston, A.E. Bradley, T. Gorman, A. Haile, I. Hamblett, J.E. Hatter, M.J.F. Healey, B. Hodgson, R. Lewin, K.V. Lovell, B. Newton, W.R. Pitner, D.W. Rooney, D. Sanders, K.R. Seddon, H.E. Sims, R.C. Thied, Green Chem. **4** (2002) 152.

[60] M. Matsunaga, Electrochemistry **70** (2002) 126.

[61] R. Hagiwara, Electrochemistry **70** (2002) 130.

[62] H. Ohno, Y. Yoshizawa, Electrochemistry **70** (2002) 136.

[63] A. Noda, M. Watanabe, Electrochemistry **70** (2002) 140.

[64] H. Matsumoto, T. Matsuda, Electrochemistry **70** (2002) 190.

[65] M. Ue, M. Takeda, Electrochemistry **70** (2002) 194.

[66] S. Tobishima, Electrochemistry **70** (2002) 198.

[67] N. Koura, Y. Suzuki, F. Matsumoto, Electrochemistry **70** (2002) 203.

[68] F. Endres, Electrochemical and Solid State Letters, **5(3)** (2002) C38.

[69] F. Endres and S. Zein El Abedin, Chem. Commun. (2002) 892.

[70] F. Endres and S. Zein El Abedin, Phys.Chem.Chem.Phys., **4** (2002) 1649.

[71] S. Zein El Abedin, N. Borissenko and F. Endres, Electrochem. Commun. **6** (2004) 510

[72] N. Borissenko, S. Zein El Abedin and F. Endres, J. Phys. Chem. B **110** (2006) 6250.

[73] M.-H. Yang, M.-C. Yang and I.-W. Sun, J. Electrochem. Soc., 150 (2003) C544.

[74] S.-I. Hsiu and I.-W. Sun, J. Appl. Electrochem., 34 (2004) 1057.

[75] Ping He, Hongtao Liu, Zhiying Li, Yang Liu, Xiudong Xu, and Jinghong Li Langmuir 20 (2004) 10260.

[76] Chia-Cheng Tai, Fan-Yin Su and I-W. Sun Electrochim. Acta **50** (2005) 5504.

[77] P. Y. Chen and I. W. Sun, Electrochim. Acta **44** (1999) 441.

[78] P.Y. Chen, Mei-Chen Lin and I-W. Sun, J. Electrochem. Soc. **147 (9)** (2000) 3350.

[79] P.Y. Chen and I-W. Sun, Electrochim. Acta **45** (2000) 3163.

[80] M. H. Yang and I.-W. Sun, J. Appl. Electrochem., **33** (2003) 1077.

[81] M. Schlesinger, M. Paunovic (Eds.), Modern Electroplating, Wiley & Sons, New York, 2000, p. 483.

[82] A.A. Tikhonov, P.M. Vyacheslavov, G.K. Burkat, Zh. Prikl. Khim. **54** (1981) 364.

[83] F.M. Dzhandubaeva, G.K. Burkat, P.M. Vyacheslavov, Zh. Prikl. Khim. **54** (1981) 2331.

[84] F.M. Dzhandubaeva, G.K. Burkat, P.M. Vyacheslavov, Zh. Prikl. Khim. **54** (1981) 2334.

[85] N.F. Reshetnikova, K.S. Pedan, Zh. Prikl. Khim. **55** (1982) 1996.

[86] P.M. Vyacheslavov, G.K. Burkat, A.A. Tikhonov, F.M. Dzhandubaeva, Zh. Prikl. Khim. **63** (1990) 436.

[87] S.-I. Hsiu , C.-C. Tai and I.-W. Sun, Electrochim. Acta **51** (2006) 2607.

[88] J. F. Huang and I.-W. Sun, Adv. Funct. Mater., **15** (2005) 989.

[89] J. F. Huang and I.-W. Sun, Chem. Mater., **16** (2004) 1829.

[90] H. Y. Hsu and C. C. Yang, Z. Naturforsch., B, **58b** (2003) 1055.

[91] J. F. Huang and I.-W. Sun, Electrochim. Acta, **49** (2004) 3251.

[92] J. F. Huang and I.-W. Sun, J. Electrochem. Soc., **151** (2004) C8.

[93] J. F. Huang and I.-W. Sun, J. Electrochem. Soc., **150** (2003) E299.

[94] J. F. Huang and I.-W. Sun, J. Electrochem. Soc., **149** (2002) E348.

[95] K. Koyama, T. Iwagishi, H. Yamamoto, H. Shirai and H. Kobayashi, Electrochemistry **70 (3)** (2002) 178.

[96] K. Y. Chan, J. Ding, J. W. Ren, S. A. Cheng, and K. Y. Tsang, J. Mater. Chem., **14** (2004) 505.

[97] P. He, H. Liu, Z. Li and J. Li, J. Electrochem. Soc., **152 (4)** (2005) E146.

[98] J. F. Huang and I. W. Sun, Chem. Mater., **16** (2004) 1829.

[99] Frontiers in Surface and Interface Science, ed. C. B. Duke and E. W. Plummer, Elsevier, Amsterdam, 2002.

[100] C. L. Aravinda and W. Freyland, Chem . Commun. (2004) 2754.

[101] A. P. Abbott, C. A. Eardley, N. R. S. Farley, G. A. Griffith, and A. Pratt, J. Appl. Electrochem., **31** (2001) 1345.

[102] S. Zein El Abedin, H. K. Farag, E. M. Moustafa, U. Welz-Biermann and F. Endres, Phys. Chem. Chem. Phys., **7** (2005) 2333.

[103] I. Mukhopadhyay, C.L. Aravinda, D. Borissov and W. Freyland, Electrochim. Acta **50** (2005) 1275.

[104] I. Mukhopadhyay and W. Freyland Langmuir , **19** (2003) 1951.

[105] A. P. Abbott, G. Capper, D. L. Davies, H. L. Munro, R. K. Rasheed and V. Tambyrajah, Chem. Commun., **7** (2001)1010.

[106] A. P. Abbott, G. Capper, D. L. Davies and R. K. Rasheed, Chem.-Eur. J., **10** (2004) 3769.

[107] A. P. Abbott, G. Capper, D. L. Davies, R. K. Rasheed, J. Archer and C. John, Trans. Inst. Met. Finish., **82** (2004) 14.

[108] A. R. Brukin, *Production of Aluminium and Alumina, Critical reports in Applied Chemistry*, Vol. 20. John Wiley, Chichester, U.K. (1987).

[109] Y.Zhao and T. J. VanderNoot, Electrochim. Acta, **42 (1)** (1997) 3.

[110] M. Galova, Surface Technology, **11** (1980) 357.

[111] M. W. M. Great, J. Electrochem. Soc. **132** (1985) 1308.

[112] T. Garai, Mater. Chem. Phys. **8** (1983) 399.

[113] M. I. Konovalov and V. A. Plotnikov, J. Russ. Phys. Chem. Soc., **31** (1899) 1020.

[114] V. A. Plotnikov, J. Russ. Phys. Chem. Soc., **34** (1902) 466.

[115] S. Simanavicius, Chemija **178** (1990) 3.

[116] D.E. Couch and A. Brenner, J. Electrochem. Soc. **99** (1952) 234.

[117] A. Brenner and D.E. Couch, U. S. patent 2,651, 608 (1953).

[118] A. Brenner, in Advances in Electrochemistry and Electrochemical Engineering (Edited by C. W. Tobias), vol. 5, p. 217. Interscience, New York (1967).

[119] A. Brenner, J. Electrochem. Soc., **106** (1959) 148.

[120] D. E. Couch and A. Brenner, J. Electrochem. Soc. **103** (1956) 657.

[121] M. Galova, Surface Technology, **11** (1980) 357.

[122] F.J. Schmidt and I. J. Hess, Electroforming aluminum for solar energy concentrators, NASA Tech. Rep. CR-197, 1965.

[123] A.G. Buschow, I. J. Hess and F. J. Schmidt, Electroforming aluminium composites for solar energy concentrators, NASA Tech. Rep. CR-66322, 1967.

[124] F.J. Schmidt and I. J. Hess, Plating, **53** (1966) 229.

[125] W.C. Schickner, Steel, **133** (1953) 125.

[126] R.N. Hanson, D. G. Du Pree and K. Lui, Plating, **55** (1968) 347.

[127] J.C. Withers and E. F. Abrams, Plating, **55** (1968) 605.

[128] F.A. Clay, W. B. Harding and C. J. Stimetz, Plating, **56** (1969) 1027.

[129] A.L. Levinskas and J. J. Sinius, Elektrokhimiya, **8** (1972) 1053.

[130] B.I. Ingaunite and A. L. Levinskas, Issled. Obl. Elektroosazhd. Met., **2** (1973) 140.

[131] A.G. Buschov and C. H. Esola, Plating, **55** (1968) 931.

[132] A. Levinskas and J. Sinius, C. A. **72** (1970) 62161y.

[133] J. Hess and J. F. Betz, Metal Finish **69** (1971) 38.

[134] N. Ishibashi and M. Yoshio, Electrochim. Acta, **17** (1972) 1343.

[135] M. Yoshio and N. Ishibashi, J. Appl. Electrochem., **3** (1973) 321.

[136] H.J. Eckert and H. Kslling, Wiss. Z. Tech. Univ. Dresden, **24** (1975) 19.

[137] T. Kurata, R. Kawabata, K. Katayama and E. Takeshima., Jpn. Patent 73 44,608 (1973).

[138] T. Kurata, R. Kawabata, K. Katayama and E. Takeshima., dpn. Patent 73 44,609 (1973).

[139] T. Kurata, R. Kawabata, K. Katayama and E. Takeshima., Jpn. Patent 74 00,018 (1974).

[140] M. Yoshio, Mat. Finish. **7** (1987) 33.

[141] S.P. Sidelnikova, V. N. Sherstkina and A. N. Jakubetz, Izv. Akad. Nauk Mold. SSR, Ser. Fiz.-Tekh. Mat. Nauk, **1** (1979) 69.

[142] M. W. M. Graef, J. Electrochem. Soc., **132 (5)** (1985) 1038.

[143] E. Eckert, Dechema-Monographien, Vol. 125, p. 425, VCH Verlagsgesellschaft, Winheim, (1992).

[144] M. C. Lefebvre and B. E. Conway, J. Electroanal. Chem. **480** (2000) 34.

[145] M. C. Lefebvre and B. E. Conway, J. Electroanal. Chem. **480** (2000) 46.

[146] F.H. Hurley and T. P. Wier, J. Electrochem. Soc., **98** (1951) 207.

[147] W. Safranek, W. Schickfier and C. Faust, J. Electrochem. Soc., **99** (1952) 53.

[148] L.E. Simanavicius and P. P. Dobrovolskis, Issled. Obl. Elektroosazhd. Met., **1** (1971) 192.

[149] L. E. Simanavicius and P. P. Dobrovolskis, USSR Patent 382,761 (1972).

[150] L.E. Simanavicius and P. P. Dobrovolskis, Issled. Obl. Elektroosazhd. Met., **2** (1973) 131.

[151] E. Peled and E. Gileadi, J. Electrochem. Soc., **123** (1976) 15.

[152] E. Peled and E. Gileadi, Plating, **62** (1975) 342.

[153] L. Simanavicius, A. Stakenas and A. Sarkis, Electrochim. Acta **46** (2000) 499.

[154] G.A. Capuano and W. G. Davenport, J. Electrochem. Soc., **118** (1971) 1688.

[155] G.A. Capuano and W. G. Davenport, Plating, **60** (1973) 251.

[156] W.G. Davenport and G. A. Capuano, in J. H. E. Jeff and R. J~ Tait (eds.), Proc. Richardson Conf. on the Physical Chemistry of Process Metallurgy, London, 1973, Institution of Mining and Metallurgy, London, 1973, p. 77.

[157] G. A. Capuano and W. G. Davenport , Can. Patent 4375 (1971).

[158] L.E. Simanavicius and A. M. Levinskiene, Elektrokhimiya, **2** (1966) 353.

[159] L.E. Simanavicius and A. Karpavicius, Issled. Obl. Elektroosazhd. Met., **1** (1968) 164.

[160] L.E. Simanavicius and A. P. Karpavicius, Nauchn. Tr. Vyssh. Uchebn. Zaved. Lit. SSR, Ser. B, **4** (1970) 139.

[161] L.E. Simanavicius and A. M. Levinskiene, Tr. Akad. Nauk Litov. SSR, Set. B, **4** (1966) 39.

[162] V.A. Kazakov, V. N. Titova and N. V. Petrova, Elektrokhimija, **12** (1976) 576.

[163] V.A. Larchenko, V. A. Kazakov, V. N. Titova and V. F. Chuvajev, Elektrokhimija, **14** (1978) 588.

[164] E. Bokor, Proc. 29th Meet. of ISE, Budapest, 1978. MTA Kozponti Kemiai Kutato Intezet, Budapest, 1978, p. 1182.

[165] S. P. Shavkunov and T. L. Strugova, Russ. J. Electrochem. **39** (2003) 642.

[166] G. A. Capuano, J. Electrochem. Soc., **138** (1991) 484.

[167] H. Lehmkuhl, Dissertation, Rheinisch-Westfalische Technische Hochschule, Achen (1954).

[168] K. Ziegler and H. Lehmkuhl, Z. Anorg. Allg. Chem., **283** (1956) 414.

[169] K. Ziegler and H. Lehmkuhl, C. A. **52** (1958) 19619d.

[170] R. Dötzer, Chem.-Ing.-Tech., **45** (1973) 653.

[171] G. Iwantscheff and R. Dötzer, Werkstattstechnik, **9** (1972) 10.

[172] R. Dötzer, E. Todt and H. G. Hauschildt Ger. Offen, Patent 2553830 (1976).

[173] J. P. Pereira-Ramos, Dissertation, University of Paris 12 (1988).

[174] T.R. Griffiths, J. Chem. Soc. Comm. 1222 (1967).

[175] J. Hennion and J. Nicole, J. Bull. Soc. Chim. Fr. 426 (1978).

[176] J. P. Pereira-Ramos, R. Messina and J. Perichon, J. Electrochem. Chem. **209** (1986) 283.

[177] L. Legrand, A. Tranchant and R. Messina, Electrochim. Acta **39** (1994) 1427.

[178] L. Legrand, A. Tranchant and R. Messina, J. Electrochem. Soc. **141** (1994) 378.

[179] L. Legrand, A. Tranchant, R. Messina, F. Romain and M. Lautie, Inorg. Chem. **35** (1996) 1310.

[180] J. Fransaer, E. Leunis, T. Hirato and J-P. Celis, J. Appl. Electrochem. **32** (2002) 123.

[181] G. R. Stafford, J. Electrochem. Soc., **136** (1989) 635.

[182] R. Bunsen, Poggendorf's Ann., **97** (1854) 648.

[183] V. A. Plotnikov, V. P. Mashovets and N. S. Fortunatov, Zhur. Khim. Prom., **7** (1930) 1476.

[184] V. A. Plotnikov and N. N. Gratsianskii, Zhur. Khim. Prom., **8** (1931) 829.

[185] V. A. Plotnikov and N. N. Gratsianskii, Legkie Metally, **No 2-3** (1933) 47.

[186] Y. F. Chittum, U.S. 1,927,772, 19 Sept. 1933.

[187] S. N. Orleva and V. I. Lainer, Legkie Metally, **No 12**, (1935) 9.

[188] W. H. Wade, G. 0. Tellmeyer and L. F. Yntema, Trans. Electrochem. Sot., **78** (1940) 77.

[189] R. Wehrmann and L. F. Yntema, J. Phys. Chem., **48** (1944) 259.

[190] R. G. Verdieck and L. F. Yntema, J. Phys. Chem., **48** (1944) 268.

[191] Yu. K. Delimarskii, A. V. Chetverikov and V. F. Makogon, USSR, No 178 257, 8 Jan. 1966.

[192] A. V. Chetverikov, Yu. K. Deiimarskii and V. F. Makogon, Dopovidi Akad. Nauk SSSR - S.B. **2** (1967) 447.

[193] A. V. Chetverikov, V. F. Makogon and Yu. K. Delimarskii, Fizicheskaya khimia I elektrokhimia rasplavlennykh solei i shlakov, Khimia, Moscow (1968).

[194] A. Miyata, H. Okubo, Ch. Tomito and A. Suzuki, U.S. 3,470,073, 30 Sept. 1969.

[195] Japan Steel and Tube Corp., Fr. 1,549,879, 13 Dec. 1968.

[196] V. V. Kuzmovich, V. F. Makogon and Yu. B. Kazakov, Ukr. Khim. Zhur., **34** (1968) 344.

[197] V. V. Kuzmovich, V. F. Makogon and Yu. B. Kazakov, Ukr. Khim. Zhur., **35** (1969) 258.

[198]Yu. K. Delimarskii, V. F. Makogon and V. V. Kuzmovich, Zashchita Metallov, **4** (1968) 743.

[199] Yu. K. Deiimarskii and V. V. Kuzmovich, Ukr. Khim. Zhur., 36 (1970) 776.

[200] L. W. Austin, M. G. Vucich and E. J. Smith, Electrochem. Technology, **1** (1963) 267.

[201] Yu. K. Delimarskii and V. V. Kuzmovich, Zhur. Fiz. Khim., **46** (1972) 2567.

[202] C. S. Charlton and N. F. Murphy, U.S. 2,807,575, 24 Sept. 1957.

[203] M. Paucirova and K. Matiasovsky, Electrodeposition and Surface Treatment, **3** (1975) 121.

[204] G. R. Stafford, J. Electrochem. Soc., **141** (1994) 945.

[205] R.J. Gale and R.A. Osteryoung, Inorg. Chem.,**18** (1979) 1603.

[206] J. Robinson and R. A. Osteryoung, J. Electrochem. Soc. **127** (1980) 122.

[207] C. L. Hussey, G. Mamantov and A. I. Popov, Editors, p. 227, VCH Publishers, New York (1994).

[208] T. Tsuda, C. L. Hussey and G. R. Stafford, J. Electrochem. Soc. 151, **6** (2004) C379.

[209] T. Tsuda, C. L. Hussey, G. R. Stafford and J. E. Bonevich, J. Electrochem. Soc. **150, 4** (2003) C234.

[210] T. Tsuda, C. L. Hussey, G. R. Stafford and O. Kongstein, J. Electrochem. Soc. **151, 7** (2004) C447.

[211] Q. Zhu, C. L. Hussey and G. R. Stafford, J. Electrochem. Soc. **148, 2** (2001) C88.

[212] T. Tsuda, C. L. Hussey and G. R. Stafford, J. Electrochem. Soc. **152, 9** (2005) C620.

[213] T. Jiang, M. J. C. Brym, G. Dube, A. Lasia and G. M. Brisard, Surface and Coatings Technology, **201, 1-2** (2006) 1.

[214] Q.X. Liu, S. Z. El Abedin and F. Endres, Surface and Coatings Technology, **201, 3-4** (2006) 1352.

[215] Q. Zhu and C. L. Hussey, J. Electrochem. Soc. **148, 5** (2001) C395.

[216] Q. Zhu and C. L. Hussey, J. Electrochem. Soc. **149, 5** (2002) C268.

[217] F. Endres, M. Bukowski, R. Hempelmann and H. Natter, Angew. Chem. Int. Ed. **42** (2003) 3428.

[218] D. FIoreani, D. Stech, J. Wilkes, J. Williams, B. Piersma, L. King and R. Vaughn, Proc. Power Sources Symp., **30** (1982) 84.

[219] P. K. Lai and M. Skyllas-Kazacos, J. Electroanal. Chem., **248** (1988) 413.

[220] R. T. Carlin, W. Crawford and M. Bersch, J. Electrochem. Soc., **139, 10,** (1992) 2720.

[221] G. R. Stafford, J. Electrochem. Soc., **144,3** (1997) 936.

[222] J. Robinson and R.A. Osteryoung, J. Am. Chem. Soc **101**(1979)323.

[223] P. K. Lai and M. Skyllas-Kazacos, Electrochim. Acta, **32,10** (1987) 1443.

[224] Qi-Xian Qin and M. Skyllas-Kazacos, J. Electroanal. Chem., **168** (1984) 193.

[225] J. Robinson and R. A. Osteryoung, J. Electrochem. Soc. **127,1** (1980) 122.

[226] Chao-Cheng Yang, Materials Chemistry and Physics, **37** (1994) 355.

[227] M. R. Ali, A. Nishikata and T. Tsuru, Electrochim. Acta, **42,12** (1997) 1819.

[228] M. R. Ali, A. Nishikata and T. Tsuru, Electrochim. Acta, **42,15** (1997) 2347.

[229] G. Binnig and H. Rohrer, Helv. Phys. Acta **55** (1982) 726.

[230] A. A. Gewirth and B. K. Niece, Chem. Rev. **97** (1997) 1129.

[231] R. Sonnenfeld and P. K. Hansma, Science (1986) 232.

[232] R. Hoyer, L.A. Kibler and D.M. Kolb, Electrochim. Acta, **49** (2003) 63.

[233] S.G. Garcia, D. R. Salinas, C. E. Mayer, W. J. Lorenz and G. Staikov, Electrochim. Acta, **48** (2003) 1279.

[234] D. M. Kolb, Prog. Surf. Sci. **51** (1996) 109.

[235] F. Endres and W. Freyland, J. Phys. Chem. B, **102** (1998) 10229.

[236]L. G. Lin, Y. Wang, J. W. Yan, Y. Z. Yuan, J. Xiang and B. W. Mao, Electrochem. Commun. **5** (2003) 995.

[237]C. A. Zell, F. Endres and W. Freyland, Phys. Chem. Chem. Phys. **1** (1999) 697.

[238]C. A. Zell and W. Freyland, Langmuir **19** (2000) 7445.

[239]F. Endres, ChemPhysChem **3** (2002) 144.

[240] F. Endres, in "Ionic Liquids in Synthesis", by P. Wasserscheid and T. Welton (Eds.), Wiley- VCH (2002) p. 294.

[241] "Scanning tunnelling Microscopy and spectroscopy: Theory, Techniques and Applications" (D. A. Bonnell ed.), John Wiley& Sons, 2000, ISBN: 0-471-24824-X.

[242] P. Scherrer, Göttinger Nachrichten, **2** (1918) 98.

[243] B. E. Warren, L. E. Averbach, J. Appl. Phys. **21** (1950) 595, **23** (1952) 497.

[244] N. Brausch, A. Metlen, P. Wasserscheid, Chem. Commun. **13** (2004) 1552.

[245] F. Czerwinski, J. Electrochem. Soc., **143** (1996) 3327.

[246] O. O. Okoturo, T. J. VanderNoot, J. Electroanal. Chem. **568** (2004) 167.

[247] G.A. Baker, S. Pandey, S. Pandey and S.N. Baker, Analyst, **129** (2004) 890.

[248] G. E. Poirier. Chem. Rev. **97** (1997) 1117.

[249] G. E. Poirier & E. D. Pylant. Science **272** (1996) 1145.

[250] G. E. Poirier. Langmuir **13** (1997) 2026.

[251] O. Chailapakul, L. Sun, C. Xu & R. M. Crooks. J. Am. Chem. Soc., **115** (1993) 12459.

[252] F. Endres, S. Zein El Abedin, N. Borissenko, Z. Phys. Chem., 220 (2006) 1377.

[253] P.C. Howlett, E. Izgorodina, M. Forsyth, D.R. MacFarlane, Z. Phys. Chem. 220 (2006) 1483.

[254] E. Budevski, G. Staikov and W. J. Lorenz (Ed), "Electrochemical phase formation and growth", Wiley-VCH, Weinheim, (1996).

[255] M.P. Green, M. Richter, X. Xing, D. Scherson, K.J. Hanson, P.N. Ross, R. Carr, I. Lindau, J. Microscopy-Oxford, **152** (1988) 823.

[256] Marcus D. Lay, Kris Varazo, Nattapong Srisook and John L. Stickney, J. Electroanal.Chem. **554-555** (2003) 221.

Curriculum Vitae

Personal Data:

Name: Essam Mohamed Moustafa
Family Name: Moustafa
Nationality: Egyptian
Marital Status: Married with two children
Sex: Male
Date of Birth: 30th. Oct. 1973
E.mail: ess1073@hotmail.com
Tel.: (0049) 174 40 566 15 or (0049) 5323 715 495
Current Address: Institut für Metallurgie der Technischen Universität Clausthal (Prof. F. Endres) Robert-Koch Straße 42 38678 Clausthal-Zellerfeld, Germany.
Permanent Address: Department of Physical Chemistry, National Research Centre (NRC),Cairo, Egypt.

Eductional Background:

1. M.Sc. (Physical Chemistry), 2003, M.Sc. Thesis examined *"Electroplating of nickel and iron from environmentally friendly gluconate baths"* Ain Shams University, Egypt.

2. B.Sc. (Chemistry & Physics) May 1995 with general estimation of "Very Good", Cairo University, Egypt.

Professional Experience:

1998-2003: Assistant Researcher, Physical Chemistry Department, National Research Centre (NRC), Cairo, Egypt.

2003-present: Ph.D. Student, Clausthal University of Technology, Institute of Metallurgy, Robert –Koch Str. 42, Clausthal-Zellerfeld, Germany.

Research Experience:

- Electrodeposition of metals, alloys and metal matrix composites in both aqueous and ionic liquids.
- Corrosion of metals and alloys.
- Analytical assessments by SEM, EDX and XRD.
- In situ STM measurements.

List of Publications:

- "Electroplating of Nickel from Aqueous Gluconate Baths" E.A.Abd El Meguid, S.S.Abd El Rehim, and E.M.Moustafa, Trans.IMF, **77** (1999)188.

- "Effect of some additives on nickel electrodeposition from gluconate bath" E.A.Abd El Meguid, S.S.Abd El Rehim, and E.M.Moustafa, Egypt. J. Chem., **43** (2000) 1.

- Electrodeposition of Iron Films on Copper Surfaces from Iron (III) Gluconate Solutions" S.S.Abd El Rehim E.A.Abd El Meguid, and E.M.Moustafa, Trans.IMF, **81**(2003) 79.

- "Electroplating of Iron from Alkaline Gluconate Baths" E.A.Abd El Meguid, S.S.Abd El Rehim, and E.M.Moustafa, Thin Solid Films, **443** (2003) 53.

- " Electroreduction of tantalum fluoride in a room temperature ionic liquid at variable temperatures" S. Zein El Abedin, H. K. Farag, E. M. Moustafa, U. W.-Biermann and F. Endres, Phys. Chem. Chem. Phys., **7** (2005) 2333.

- "Additive free electrodeposition of nanocrystalline aluminium in a water and air stable ionic liquid" S. Zein El Abedin, E. M. Moustafa, R. Hempelmann, H. Natter and F. Endres, Electrochem. Commun. **7** (2005) 1111.

- "Electrodeposition of nano- and microcrystalline aluminium in three different air and water stable ionic liquids" S. Zein El Abedin, E. M. Moustafa, R. Hempelmann, H. Natter and F. Endres, Chem Phys. Chem. **7** (2006) 1535.

- " Electrochemical deposition of nanostructured metals and alloys from ionic liquids" H. Natter, M. Bukowski, R. Hempelmann, S. Zein El Abedin, E. M. Moustafa and F. Endres, Z. Phys. Chem. **220** (2006) 1275.

- "Electrodeposition of Al in 1-butyl-1-methylpyrrolidinium bis (trifluoro- methyl-sulfonyl) amide and 1-ethyl-3-methylimidazolium bis (trifluoro- methylsulfonyl) amide ionic liquids: In situ STM and EQCM studies" E. M. Moustafa, S. Zein El Abedin, A. Shkurankov, E. Zschippang, A.Y. Saad, A. Bund and F. Endres, submitted to J. Phys. Chem. B.